Spring 1994

Explicit and Iterative LQG Controller Design

Min-Hung Hsiao
Old Dominion University

EXPLICIT AND ITERATIVE LQG CONTROLLER DESIGN

by

Min-Hung Hsiao

B.S. June 1983, National Cheng Kung University, R.O.C.
M.S. June 1985, National Cheng Kung University, R.O.C.

A Dissertation Submitted to the Faculty of Old Dominion University in partial fulfillment of the requirements for the degree of

Doctor of Philosophy

Engineering Mechanics

Old Dominion University
May, 1994

Approved by:

_____

Dr. Jen-Kuang Huang (director)

_____

Dr. Sebastian Bawab

_____

Dr. Colin Britcher

_____

Dr. Chuh Mei

ACKNOWLEDGMENT

I would like to thank my advisor, Dr. Jen-Kuang Huang, from whom I have received attentive instruction, care, motivation and guidance. The members of my doctoral committee, Dr. Chuh Mei, Dr. Colin Britcher, and Dr. Sebastian Bawab are appreciated for their constructive suggestions in revising the dissertation.

Thanks to late Mr. Lawrence Taylor, who guided me in the work for the NASA SCOLE configuration. Thanks also to Mr. David Cox, research engineer at NASA Langley Research Center, who provided the test data for the NASA LAMSTF system.

This dissertation will not be possible without my parent's love and support. Special acknowledgment goes to my wife, Wen-Yueh Wu, for her constant love, patience and encouragement. It was not easy for her to take care of the family alone during the last few years of my Ph.D. program.

This work was supported partially by NASA Langley Research Center (NAS1-19858, No. 30). This support is gratefully acknowledged.

CONTENTS

LIST OF TABLES

LIST OF FIGURES

LIST OF SYMBOLS

Unless otherwise stated the listed symbols are specified as follows.

A,B,C	open-loop system matrices
A_c,B_c,C_c	closed-loop system matrices
A_d,B_d,C_d,D_d	system matrices of dynamic controller
a_i,b_i	coefficient matrices of ARX model
$E[\ ]$	expectation operator
F	state feedback gain
H	Hankel matrix
I	identify matrix
i,j,k	integer number
K	Kalman filter gain
l	data length
m	number of outputs
N	open-loop Kalman filter Markov parameter
N_c	closed-loop Kalman filter Markov parameter
N_ε	covariance matrix of process noise in modal space
N_η	covariance matrix of measurement noise in modal space
n	number of states
Q	weighting matrix for system state in performance index
q	order of ARX model
R	weighting matrix for system input in performance index
r	reference input

s	Laplace transformations or number of inputs
u	control input
V	covariance matrix of measurement noise
v	measurement noise
W	covariance matrix of process noise
w	process noise
x	system state
Y	open-loop system Markov parameter
Y_c	closed-loop system Markov parameter
Y_d	controller Markov parameter
y	system output
z	z-transformations
$\| \|_2$	2-norm
∞	infinity

Symbols for System Modeling

A	cross sectional area of beam
E	Young's modulus
e	mode shape
f	force
G	shear modulus
g	acceleration of gravity
I_b	moment of inertia of cross sectional area
J	moment of inertia of rigid body
J_b	polar moment of inertia of cross sectional area
K	stiffness matrix
L	length of beam
M	mass matrix

m	rigid body mass
q	generalized force vector
r	distance vector
v	system output
w	linear displacement
x	displacement vector
y	modal coordinate
δ	process noise in modal space
η	measurement noise in modal space
θ	angular displacement
ρ	mass density
τ	torque
ω	modal frequency
ξ	system state in modal space
$[\ ]_i$	transfer matrix of element i
$\{\ \}_i$	displacement and generalized force vector at point i

Greek Letters

ε	residual after filtering
Φ	input/output data matrix
η	augmented state of open-loop system and controller
θ	augmented coefficient matrix of ARX model
ξ	output data

Subscripts

k	k-th time step
x	in x axis
y	in y axis
z	in z axis

Superscripts

T	matrix transpose
-1	matrix inverse
$'$	spatial derivative

Notations above a Symbol

$\wedge$	estimate
$\cdot$	time derivative

Abbreviations

ARX	AutoRegressive with eXogeneous input
LQR	Linear Quadratic Regulator
LQG	Linear Quadratic Gaussian
LAMSTF	Large-Angle Magnetic Suspension Test Facility
NASA	National Aeronautics and Space Administration
SCOLE	Spacecraft COtrol Laboratory Experiment

Chapter 1

INTRODUCTION

1.1 Background and Problem Statement

Control has played a vital role in the advancement of engineering and science. In addition to its extreme importance in space-vehicles, missile-guidance, and aircraft-piloting systems, etc., control has become an important and integral part of modern manufacturing and industrial processes. The essential feature of control is to improve system performance and to stabilize systems if they are unstable.

The main problem of control is how to determine appropriate control inputs so that controlled systems can accomplish prescribed requirements. Mathematically, the solution of the problem is represented by a set of equations called the *control law*. The history of *control theory*, which deals with how to design the control law, can be conveniently divided into three periods. The first, starting in prehistory and ending in the early 1940s, may be termed the *primitive* period. This was followed by a *classical* period, lasting scarcely 20 years, and finally came the *modern* period. The theory in the primitive period consisted of a collection of analyses of specific systems by mathematical methods

appropriate to, and often invented to deal with, the specific systems, rather than an organized body of knowledge that characterizes the classical and modern period. In the classical period some techniques like root locus, Nyquist, and Bode design had been developed to design control laws based on *Laplace transforms* of systems. In the modern control period *state-space models* instead of Laplace transforms are used to represent systems. The essential feature of the state-space models is that the systems are characterized by simultaneous, first-order differential equations. Therefore, it is easier to develop computer code associated with control design in a digital computer by using a state-space model than by using Laplace transforms.

In the modern control period Linear Quadratic Regulator (LQR) control design was first developed to minimize a performance index described by system states and inputs. This controller requires the information of all states for the feedback control law. However, in general, state information cannot be measured directly. In addition, system outputs may be corrupted by system process and measurement noise. State estimation, which is the technique of reconstructing state information from noise-corrupted outputs, is thus required. In 1960 Kalman published his famous method for sequential state estimation of discrete systems, known as the Kalman filter, using state-space formulation[1]. Two years later, a version of the Kalman filter for continuous systems was published[2]. With the Kalman filter, the state estimation can be established and the state feedback from the LQR control design can be thus performed. The technique of combining state feedback and state estimation is called Linear Quadratic Gaussian (LQG) control design.

For state estimation, a priori covariance matrices of system process and measurement noise are required. The covariance matrices and system model are then used to obtain the state estimation gain by solving the corresponding Riccati equation. For state feedback, weighting matrices of state and input in the performance index have to be chosen. The

weighting matrices and system model are then used to obtain the state feedback gain by solving the corresponding Riccati equation. There are several problems in LQG control design. First, numerically solving Riccati equations requires a lot of computational time when the system is very large. Second, choosing the weighting matrices for the state feedback may need trial-and-error approach. Third, detecting the covariance matrices for the state estimation is usually difficult. Fourth, the system model from system analysis usually contains some errors. Fifth, the statistics of the noise may vary with the controller.

For flexible structures, the order of systems is usually large. To avoid numerically solving large dimensional Riccati equations, an explicit solution to the LQG control design for flexible structures with collocated rate sensors has been found[3]. In the derivation of the explicit solution the performance index and the covariance matrices are based on physical state variables. However, the number of the design parameters for either state feedback or state estimation is one regardless of the number of controlled modes. The performance of the controller may be degraded if the desired controlled modes are increased. Some other methods[4,5] without the need to solve Riccati equations are called model-independent controllers, which are viewed as virtual passive damping system. Since the number of the design parameters is very large, it is usually hard to adjust so many design parameters to satisfy a specific performance requirement.

For some systems, it is difficult to obtain an accurate model through system modeling. For a system with some model errors, it is usually required to update the system model through system identification. System identification is the process of constructing a mathematical model from input and output data for a dynamic system under testing, and characterizing the system behaviors. This technique is important in many disciplines such as economics, communication, system dynamics and control. In the past few decades, a great variety of system identification methods have been studied

extensively[6,7]. The choice of an identification method depends on the nature of the system and the purpose of identification. For control of a dynamic system, the state-space model is usually preferred. Recently, a method[8] was introduced to identify a state-space model from a finite difference model. The difference model, called AutoRegressive with eXogeneous input (ARX) model, is derived through Kalman filter theory. However, the method requires an ARX model of large order, which causes intensive computation in the embedded least-squares operation. Another method[9,10] is derived to obtain a state-space model from open-loop input/output data using the notion of state observers. This approach can use an ARX model with an order much smaller than that derived through the Kalman filter, but the derivation is based on a *deterministic* approach. For a stochastic system and an ARX model of a small order, it is not clear what the least-squares identification of the ARX model will converge to in a stochastic sense. In order to solve this problem, projection filters, which were originally derived for deterministic systems[11], are developed for identification of linear *stochastic* systems[12,13].

Those methods, however, deal with system identification when a system is under open-loop excitation with uncorrelated white noise inputs. For an unstable system, the input/output data are not available while it is under open-loop operation. To directly use those methods, we have to design a controller and input signal to the closed-loop system so that the input signal to the open-loop system is almost white. Unfortunately, this is very difficult. On the other hand, some identification methods[14-17] have been proposed recently for identifying a system under closed-loop operation. However, they have several shortcomings. First, the Kalman filter cannot be simultaneously identified because they are applied only for *deterministic* systems. In Reference 16, no recursive form was derived for computing the open-loop system Markov parameters. In Reference 17, the approach is based on system *pulse* response. Generally speaking, random excitation provides better result of identification than pulse input because part of the noise from random excitation response can be removed through least squares method.

Furthermore, the noise statistics may be related to the controller if part of the measurement and process noise are generated by the sensor and actuator amplifiers, respectively. For this reason, iterative control design is required to take into account the interdependence between the system modeling from identification and the applied control input. The need of an iteration is also presented in the literature[18-20]. Several principles regarding modeling error has been found. Arbitrarily small modeling errors can lead to arbitrarily bad closed-loop performance. Large open-loop modeling errors do not necessarily lead to bad closed-loop performance. Open-loop modeling error bounds do not generally constitute enough information for successful control design. Hence, it is concluded that the most appropriate model depends on the controller design. To accurately predict closed-loop behavior, a change in the controller usually requires a change in the model. This motivates the development of iterative control design.

1.2 Objective

The objective of this dissertation is to develop new approaches of LQG control design to overcome some of the problems associated with existing LQG control. First, An explicit LQG control design for large flexible structure systems with collocated rate sensors and actuators is developed. In the derivation the performance index and the covariance matrices are based on modal state variables rather than physical state variables. This results in the number of design parameters for either state feedback or state estimation equals the number of the controlled modes. Each state-feedback design parameter weighs the contribution of actuators to the performance of a specific mode. Similarly, each state-estimation design parameter weighs the contribution of the sensors to the estimate of a specific modal state. The advantages of the control include no need to numerically solve Riccati equations and the ease of choosing design parameters to

achieve a good performance. To illustrate the controller design, the NASA's Spacecraft COntrol Laboratory Experiment (SCOLE) configuration is provided.

Second, a closed-loop identification is developed for simultaneously identifying a system and the corresponding Kalman filter when the system is under closed-loop operation. The relationship between state-space and ARX models is re-derived in a much simpler way through z-transform rather than projection filters. It provides physical interpretation of mapping from closed-loop input/output data to the open-loop state space and the explicit meaning of the ARX parameters. The system model can be updated through this identification. Since the Kalman filter gain can be directly identified, the covariance matrices of system process and measurement noise are no longer required to be detected.

Third, an iterative LQG control design through the closed-loop identification is proposed. This design consists of the closed-loop identification and state feedback redesign cycles. In each cycle the closed-loop identification is performed to obtain the system model and Kalman filter gain. Then the identified system model is used for the state feedback design. The state feedback and the identified Kalman filter are used to form an updated LQG controller for next closed-loop identification. The process continues until the updated LQG controller converges. Since the Kalman filter is obtained directly from the closed-loop identification, it automatically takes into account the effect of the controller on the noise statistics. To validate the iterative LQG control design, the NASA Large-Angle Magnetic Suspension Test Facility (LAMSTF) is applied.

1.3 Dissertation Outline

Chapter 2 introduces some background material about existing LQG control design and Kalman filters. The LQG control design includes continuous-time and discrete-time approaches. The LQG control separates design problems into state feedback and state estimation. The solutions to the state feedback and the state estimation are provided. In the LQG control, the control law from the LQR control design is used for the state feedback and the steady state Kalman filter is used for the state estimation. A filter-innovation model associated with the steady state Kalman filter will be derived and then used in the derivation of the closed-loop identification presented in Chapter 6.

Chapter 3 provides the brief description and system modeling of the NASA's Spacecraft COntrol Laboratory Experiment (SCOLE) configuration. The comparison between finite-element model and distributed-parameter model, which are commonly used for the modeling of a flexible structure, is also discussed. The distributed-parameter model is chosen for modeling the SCOLE configuration by using Holzer's transfer matrix method. The estimation of the system parameter is performed. The analytical model after parameter estimation is used to design the explicit LQG control presented in the next chapter.

Chapter 4 presents the derivation of the explicit LQG control based on modal space. The conditions of the existence of the explicit LQG control are also discussed. The SCOLE configuration satisfies all the conditions and is thus chosen as the example. To demonstrate how to choose the design parameters to achieve prescribed performance, numerical simulations are performed. To validate the feasibility of the explicit LQG control, experiments are also performed.

Chapter 5 provides the description of the NASA's Large-Angle Magnetic Suspension Test Facility (LAMSTF). The system matrices are also provided and used for numerical simulations in the following two chapters. The analytical model shows that the system is highly unstable. Because it is difficult to accurately model the magnetic field and its gradients, the analytical model contains some modeling errors. The model will be updated through the closed-loop identification presented in the next chapter.

Chapter 6 presents the derivation of the closed-loop identification for identifying an open-loop system and Kalman filter gain when the system is under closed-loop identification. There are several adjustable numbers in the closed-loop identification. To understand the effect of these numbers to the identification accuracy, numerical simulations for the LAMSTF configuration are provided. Experiments are also performed to validate the closed-loop identification.

Chapter 7 proposes the iterative LQG control design through the closed-loop identification. The identified Kalman filter is directly used for state estimation. The LQG control design can be reduced to the design of state feedback based on the identified model. The state estimation and state feedback will form a updated LQG controller. Since, a change in the controller usually requires a change in the model, the closed-loop identification is performed for the system under the updated controller. The closed-loop identification and state feedback redesign based on the identified model continues until the updated controller converges. Numerical simulations and experiments for the LAMSTF configuration will be provided to illustrate and validate the iterative LQG control design.

Finally, Chapter 8 provides conclusions and prospects for the extension of this research.

Chapter 2

EXISTING LQG CONTROL AND KALMAN FILTER

2.1 Introduction

This chapter introduces existing Linear Quadratic Gaussian (LQG) control design for both continuous-time and discrete-time domains, and a discrete-time version of Kalman filter for state estimation.

The performance of a closed-loop system can be arbitrarily adjusted only through full state feedback. In more realistic systems, we may not have a sensing system to measure all states. In this case, output feedback control is required. The LQG control design is the most systematic approach to output feedback control design. The LQG control separates the design problem into two problems, namely, state feedback and state estimation. Figure 2.1 shows an LQG control system. The system is disturbed by process noise and the output is corrupted by measurement noise. Such a system is called a *stochastic* system. In the state estimation the optimal estimate of the state is established by using the information of the system output. To accomplish this, one needs the statistics of the process and measurement noises to design a steady state Kalman filter

which is used for the state estimation. The estimate of the state is then used for the state feedback. The state feedback is designed to minimize a performance index described by the system states and inputs with weighting matrices. The LQG control basically uses the output information to accomplish state feedback through state estimation. By choosing proper design parameters of state estimation, the performance of the LQG control can achieve that of a true full state feedback[21-23].

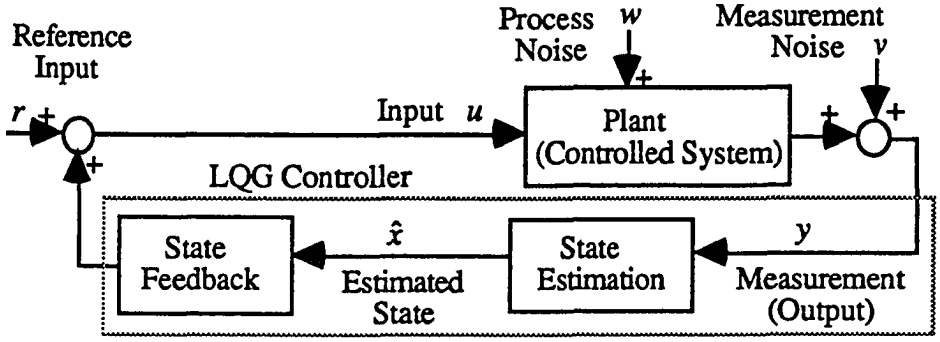

Figure 2.1 LQG control system.

2.2 Continuous-time Approach

A finite-dimensional, linear, continuous-time, time-invariant, stochastic system can be modeled as:

$$\dot{x} = Ax + Bu + w \tag{2.1}$$

$$y = Cx + v. \tag{2.2}$$

where $x \in R^{n\times 1}$, $u \in R^{s\times 1}$, $y \in R^{m\times 1}$ are state, input and output vectors, respectively; w is the process noise, v the measurement noise; $[A, B, C]$ are the state-space parameters. Sequences w and v are assumed gaussian, white, zero-mean, and stationary with covariance matrices W and V, respectively.

For state feedback, LQG control is designed to minimize a performance index associated with state and input vectors

$$\text{P.I.} = \int_0^\infty (x^T Q x + u^T R u) dt \tag{2.3}$$

where Q and R are weighting matrices. Generally speaking, a larger Q , which makes the error more important, provides less state error so that the system has quicker response. A larger R, which makes the input more important, results in less input so that the system has slower response. To insure that the solution to minimize the performance index exists, Q has to be positive semidefinite and R has to be positive definite. The optimal control input can be found from optimal control theory[24] as follows

$$u = -R^{-1} B^T S x \tag{2.4}$$

where S can be solved from the following Riccati equation

$$SA + A^T S + Q - SBR^{-1} B^T S = 0. \tag{2.5}$$

For state estimation, the state estimation law is

$$\dot{\hat{x}} = A\hat{x} + Bu + G(y - C\hat{x}) \tag{2.6}$$

where G is the estimation gain and $\hat{x}$ is the estimated state. The estimated state can be corrected by the measurement output. The estimation gain is designed to minimize $\int_0^\infty E\left[(x - \hat{x})(x - \hat{x})^T\right] dt$ the covariance of the error between the true and estimated states based on the covariance matrices of the process and measurement noises. The optimal estimation gain can be found as[24]

$$G = LC^T V^{-1} \tag{2.7}$$

where L can be solved from the following Riccati equation

$$AL + LA^T + W - LC^T V^{-1} CL = 0. \tag{2.8}$$

With the state estimation (2.6), the estimated state $\hat{x}$ can be established and be used for the state feedback (2.4).

2.3 Discrete-time Approach

The great advances made in large-scale integration of semiconductors, the resulting cost-effective digital computer and data storage devices, and the development of suitable programming techniques are all having increasing influence on the techniques of system identification and control in general. Digital computers provide high flexibility for implementing control laws as compared with analog computers. It is also easier to maintain and modify computer codes in digital computers than wire connections in analog computers. Digital computers, therefore, are more often used to implement control laws than analog computers. However, a sampling rate is required to allow digital computers to process control laws. The sampling rate will affect the closed-loop system performance and stability in general. If a low sampling rate is necessary for the process of more complex control law, one may need to use discrete-time approach for LQG control to maintain the closed-loop system performance and stability. Moreover, most system identification methods are based on discrete-time systems. Therefore, it is necessary to introduce the discrete-time approach of LQG control.

A finite-dimensional, linear, discrete-time, time-invariant, stochastic system can be modeled as:

$$x_{k+1} = Ax_k + Bu_k + w_k \tag{2.9}$$

$$y_k = Cx_k + v_k. \tag{2.10}$$

where $x \in R^{n\times 1}$, $u \in R^{s\times 1}$, $y \in R^{m\times 1}$ are state, input and output vectors, respectively; w_k is the process noise, v_k the measurement noise; $[A, B, C]$ are the state-space parameters.

Sequences w_k and v_k are assumed gaussian, white, zero-mean, and stationary with covariance matrices W and V, respectively. Since everything is similar to the continuous-time approach, only the corresponding items are summarized as follows[25]:

1. Performance index: $\sum_{k=1}^{\infty} x_k^T Q x_k + u_k^T R u_k$. (2.11)

2. Optimal state feedback: $u_k = -(R + B^T S B)^{-1} B^T S A x_k$. (2.12)

3. Riccati equation for state feedback: $S = A^T (S - SBR^{-1}B^T S)A + Q$. (2.13)

4. Optimal state estimation: $\hat{x}_{k+1} = A\hat{x}_k + Bu_k + ALC^T(CLC^T + V)^{-1}(y_k - C\hat{x}_k)$ (2.14)

5. Riccati equation for state estimation: $L = A[L - LC^T(CLC^T + V)^{-1}CL]A^T + W$. (2.15)

2.4 Kalman Filter

The Kalman filter for discrete systems with stationary, white process and measurement noises which are not correlated to each other can be summarized as follows[26]:

a. Initial Conditions:

$$E[x_0] = \hat{x}_0,\ E[(x_0 - \hat{x}_0)(x_0 - \hat{x}_0)^T] = P_0$$

b. Prediction:

$$\hat{x}_k^- = A\hat{x}_{k-1}^+ + Bu_{k-1} \tag{2.16}$$

$$P_k^- = AP_{k-1}^+ A^T + W \tag{2.17}$$

c. Measurement Update:

$$\begin{aligned} \hat{x}_k^+ &= \hat{x}_k^- + K_k(y_k - C\hat{x}_k^-) \\ &= (I_n - K_k C)\hat{x}_k^- + K_k y_k \end{aligned} \tag{2.18}$$

$$P_k^+ = (I_n - K_k C)P_k^- \tag{2.19}$$

$$K_k = P_k^- C^T (CP_k^- C^T + V)^{-1} \tag{2.20}$$

where W and V are the covariance matrices of process and measurement noises, respectively, $\hat{x}$ the estimated state vector, P the corresponding estimation error covariance matrix, I_n the n-dimensional identity matrix, K_k the Kalman filter gain and the superscripts - and + distinguish the estimates before and after taking account of the current measurement data, respectively.

The inner operation of Kalman filtering can be explained as follows. Given the state, x_{k-1} , at time $k-1$ and its corresponding error covariance, P^+_{k-1}, the Kalman filter propagates the state and the error covariance to the next moment k ((2.16) and (2.17)) using the system model, and the results are x^-_k and P^-_k , respectively. This procedure is called prediction or extrapolation, because the current state is calculated based on previous data. Upon the arrival of the measurement y_k at time k , there are two sources of information about the state at time k: the propagated state with its error covariance and the new measurement with measurement noise covariance. The measurement is related to the state through measurement equation (2.15). Using a minimum-mean-square estimation error criterion, the Kalman filter provides a method of combining these two sources of information into an optimal estimate of state x_k . This is done by adding a modifying term to the predicted value, where the modifying term is computed by pre-multiplying the output prediction error (the difference between the real and the predicted measurements) with a weighting matrix. This weighting matrix is called the optimal Kalman filter gain, and is given by (2.20). This procedure is called measurement update. After measurement update, the next prediction can be made, and so on. By this method the Kalman filter can use data recursively to yield the optimal estimated state. There is no need to keep a record of previous data.

To combine the prediction and measurement update, one can substitute (2.18) into (2.16) and (2.19) into (2.17) by changing k to $k-1$ in (2.18) and (2.19). This results in a

alternative filter formulation which produces the a priori estimated state $\hat{x}_k^-$ and error covariance P_{k-1}^- as follows

$$\hat{x}_k^- = A\hat{x}_{k-1}^- + Bu_{k-1} + AK_{k-1}(y_{k-1} - C\hat{x}_{k-1}^-) \tag{2.21}$$

$$P_k^- = A(P_{k-1}^- - K_{k-1}CP_{k-1}^-)A^T + W. \tag{2.22}$$

Substituting (2.20) into (2.22) by changing k to $k-1$ in (2.20) yields

$$P_k^- = A[P_{k-1}^- - P_{k-1}^-C^T(CP_{k-1}^-C^T + V)^{-1}CP_{k-1}^-]A^T + W. \tag{2.23}$$

Comparing (2.23) and (2.15), one can have

$$\lim_{k\to\infty} P_{k-1}^- = L. \tag{2.24}$$

Substituting (2.24) into (2.20) yields

$$\lim_{k\to\infty} K_{k-1} = K = LC^T(CLC^T + V)^{-1}. \tag{2.25}$$

This means that the steady state Kalman filter gain exists and is used for the state estimation in the LQG control. One can rewrite (2.21) with the steady state Kalman filter gain as follows

$$\hat{x}_{k+1} = A\hat{x}_k + Bu_k + AK(y_k - C\hat{x}_k). \tag{2.26}$$

If one defines the error between the actual output y_k and the estimated output $C\hat{x}_k$ as residual ε_k, one can have

$$\hat{x}_{k+1} = A\hat{x}_k + Bu_k + AK\varepsilon_k \tag{2.27}$$

$$y_k = C\hat{x}_k + \varepsilon_k. \tag{2.28}$$

In a Kalman filter sense, (2.27) and (2.28) are the best description of a stochastic system whose state-space model is shown in (2.9) and (2.10). The model using the presentation of (2.27) and (2.28) is called a filter-innovation model. This model will be used in the derivation of the closed-loop identification.

Chapter 3

NASA SCOLE CONFIGURATION

3.1 Introduction

In this chapter the NASA's Spacecraft COntrol Laboratory Experiment (SCOLE) configuration (see Figure 3.1) is introduced. This configuration is used as the example of the explicit LQG controller design presented in the next chapter. The system modeling for this configuration by using the Holzer's transfer matrix method is also derived for the controller design. The estimation of the system parameters are then obtained by adjusting few parameters to match the first five modal frequencies from the analytical model with those from test data.

Many space programs such as communications, radar and laser systems require the use of flexible structures to minimize weight so that they can be easily launched into the space. The light and flexible materials, however, provide very low damping and thus cause vibration problem during operation. For this reason, active or passive control is required to enhance the system damping so that the vibration can be damped out more quickly. For certain future missions in space, it seems that adequate structural damping enhancement can be

obtained only through active control. Usually, control system design for large flexible structures is a challenging problem because of their special dynamic characteristics, which include a large number of significant elastic modes with very small inherent damping, and inaccuracies in the knowledge of the modal parameters. The SCOLE facility is one of the facilities designed for investigating system modeling, parameter estimation, and controller design for large flexible structural systems[27].

The SCOLE facility consists of a dynamic model of the Space Shuttle orbiter to which is attached a reflector by a flexible mast. The dynamic model is extensively instrumented by sensing devices for measurement and force and torque generating devices for control and for disturbance generation. A single, flexible tether is used to suspend the dynamic model, allowing complete angular freedom in yaw and limited freedom in pitch and roll. The reflector is put downward in ground test so that the gravity effects on mast bending will be minimized. This facility can simulate the vibration problem of the reflector whenever the space shuttle changes its speed. Therefore, the primary control objective is to damp the structural vibrations to the degree for precise pointing of the reflector. For the tests of the explicit LQG controller design proposed in the next chapter, the Space Shuttle orbiter is assumed fixed to simplify the controller design problem. The flexible mast is slender enough and is thus assumed to be an Euler beam. To simplify the system modeling problem, the reflector is assumed to be a rigid body because it is much more rigid than the mast. Therefore, the simplified version of the SCOLE configuration is like a cantilever beam with a rigid body at the free end in three dimensional motion. Three reaction wheels and one three-axis rate gyro are used as torque actuators and rate sensors. Both actuators and rate sensors are mounted on the attachment point of the mast and the reflector and are thus collocated.

For system modeling of large flexible structures, finite-element and distributed-parameter formulations are commonly used. A satisfactory finite-element model for a

flexible structure may require a large number of degrees of freedom (>50), so that more effort is needed in solving the eigenvalue problem and for model reduction for further controller design. Compared with the finite element model, the distributed parameter model offers the advantage of comprehensive dynamics description of flexible structures with a minimal number of modal parameters. Thus, it is easier to identify the modal parameters by using the distributed parameter model than by using the finite element model[28-30]. The main advantage of the finite element method over distributed parameter modeling is the ease at which computer models can be generated for various structural geometry. Recently, a computer code[31] has been developing to derive distributed parameter models for relatively complex geometry structures by using the Holzer's transfer matrix method[32-34]. Therefore, Holzer's transfer matrix method is used to derive the distributed-parameter model for the SCOLE configuration.

From open-loop tests of the SCOLE, it is known that the sixth modal excitation will free decay 95 % in about 2 seconds with more than 10 Hz frequency. The sixth mode is the third bending mode in the X'Z plane. Therefore, only the first five modes are chosen as the controlled modes. The design challenge arises not only because of very low damping and plant uncertainties but also few available actuators (three actuators used to control five modes). The control objective is to damp out system vibration as quickly as possible. In other word, it is to enhance system damping. A control design proposed in Reference 35 has been applied to the SCOLE configuration. The number of the design parameter are only two no matter how many controlled modes are considered. It is so hard to adjust two design parameters to enhance damping for each mode that the performance of the control is not good. As shown in the control result, the vibration amplitude of the first mode decays about 50 % in 30 seconds. The first two modes are believed to be the most difficult to control.

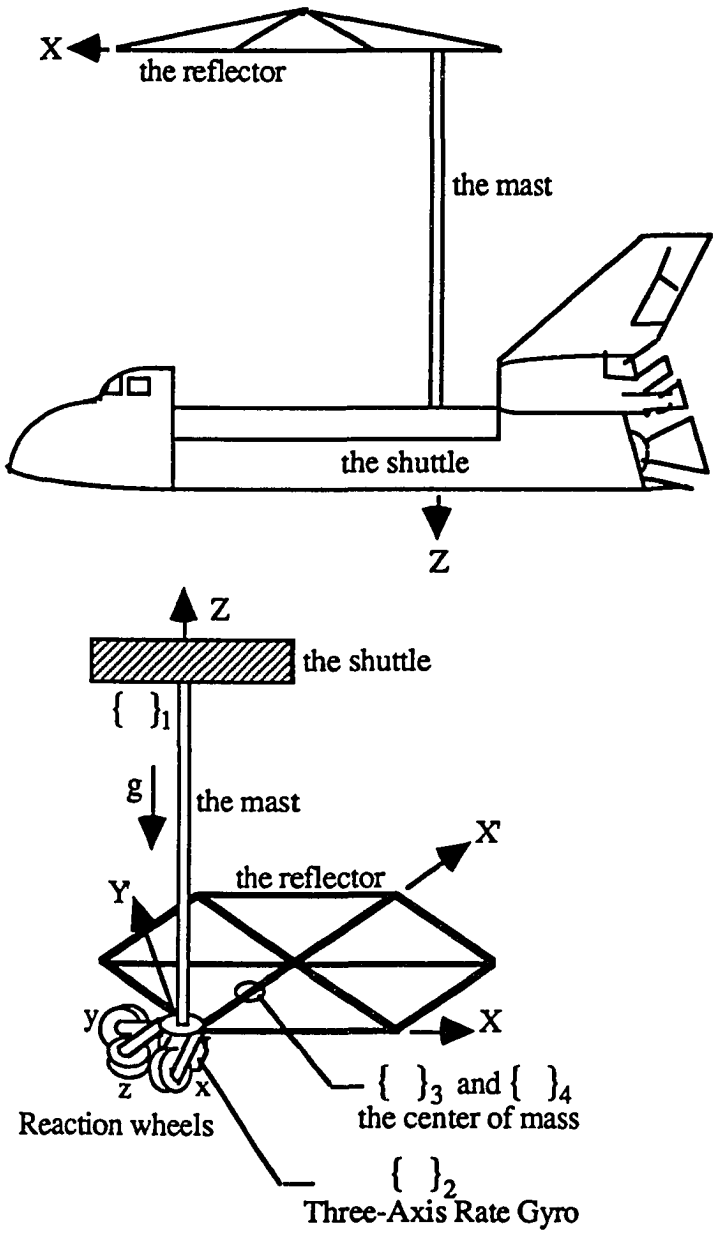

Figure 3.1 The NASA SCOLE configuration.

3.2 System Modeling

In sections 3.3 to 3.6, a distributed parameter model for the SCOLE configuration is first derived by using Holzer's transfer matrix method. The distributed parameter model can be used to estimate system parameters presented in section 3.7. Then the distributed parameter model is reduced to a finite-dimensional model for the further controller design.

In this section Holzer's transfer matrix method is introduced. Any large flexible structures can be broken down into sub-structures with simple elastic and dynamic properties. For each single element, such as beam, tether, or rigid body, one can derive the corresponding transfer matrix. The transfer matrix represents the relationship between two ends of each element by taking Laplace transformation for each dynamic equation and solving each differential equation with respect to spatial coordinate. Combining these elements' matrices enables the solution of the global system equations.

Consider a cascaded beam-body system shown in figure 3.2 where $\oplus$ indicates mass center and points i and i+1 are located at the mass center of the element i. The variables for each point include displacement and force. There are three different kinds of elements, namely, rigid body dynamics, force system transformation, and beam dynamics. For example, one can relate points i and i+1 through rigid body dynamics, points i+1 and i+2 through force system transformation, and points i+2 and i+3 through beam dynamics.

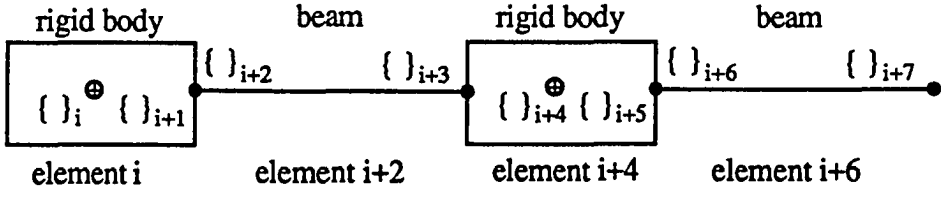

Figure 3.2 A cascaded beam-body system.

A simplified version of the SCOLE model (see Figure 3.1) is considered as a flexible mast clamped at one end (the shuttle end) and an offset reflector attached to the other end of the mast. Thus the mast is modeled by an equivalent uniform Euler beam of length L along the z-axis extending from 0, the clamped end, to L, the reflector end. The reflector is treated as a rigid body with small motions. The corresponding transfer matrices for rigid body dynamics, force system transformation, and beam dynamics are derived as follows.

3.3 Rigid Body Dynamics

Considering a rigid body subjected to two forces $-f_i$ and f_{i+1} at its center of mass, the side force of gravity f_g, and two torques $-\tau_i$ and τ_{i+1}, the force and the torque balance equations yield

$$m_i \ddot{w}_i = f_{i+1} - f_i + f_g, \tag{3.1}$$

$$J_i \ddot{\theta}_i = \tau_{i+1} - \tau_i, \tag{3.2}$$

where m is the rigid body mass, w the linear displacement vector, J the moment of inertia matrix of the rigid body, and θ the angular displacement vector. The subscript represents the acting point. Because both i-th and $(i+1)$-th points are located at the center of mass of the rigid body, one has

$$w_{i+1} = w_i, \tag{3.3}$$

$$\theta_{i+1} = \theta_i. \tag{3.4}$$

For small motions, the side force of gravity is

$$f_g = G_i \theta_i, \tag{3.5}$$

where $G_i = \begin{bmatrix} 0 & mg & 0 \\ -mg & 0 & 0 \\ 0 & 0 & 0 \end{bmatrix}$. After taking Laplace transformation for the above equations, one can derive

$$\begin{Bmatrix} x \\ q \end{Bmatrix}_{i+1} = \begin{bmatrix} I & 0 \\ s^2\overline{M} + \overline{G} & I \end{bmatrix}_i \begin{Bmatrix} x \\ q \end{Bmatrix}_i \tag{3.6}$$

where $x = \begin{Bmatrix} w \\ \theta \end{Bmatrix}$ is the displacement vector, $q = \begin{Bmatrix} f \\ \tau \end{Bmatrix}$ the generalized force vector, $\overline{M} = \begin{bmatrix} mI & 0 \\ 0 & J \end{bmatrix}$, $\overline{G} = \begin{bmatrix} 0 & G \\ 0 & 0 \end{bmatrix}$, and I an identity matrix. This equation represents the rigid body dynamics subjected to two force systems located at the center of the mass and the side force of gravity.

3.4 Force System Transformation

Let r_i denote the distance vector $\{r_x, r_y, r_z\}_i^T$ from the i-th point to the $(i+1)$-th point, then one can relate the displacement vectors between the i-th and the $(i+1)$-th points on the same rigid body for small motion by

$$w_{i+1} = w_i + \theta_i \times r_i = w_i - R_i\theta_i, \tag{3.7}$$

$$\theta_{i+1} = \theta_i. \tag{3.8}$$

where $R_i = \begin{bmatrix} 0 & -r_z & r_y \\ r_z & 0 & -r_x \\ -r_y & r_x & 0 \end{bmatrix}_i$. Besides, one can transform the force system from the i-th point to the $(i+1)$-th point to get

$$f_{i+1} = f_i, \tag{3.9}$$

$$\tau_{i+1} = \tau_i - r_i \times f_i = \tau_i - R_i f_i. \tag{3.10}$$

Combining (3.7)-(3.10), one has

$$\begin{Bmatrix} x \\ q \end{Bmatrix}_{i+1} = \begin{bmatrix} T_1 & 0 \\ 0 & T_2 \end{bmatrix}_i \begin{Bmatrix} x \\ q \end{Bmatrix}_i, \tag{3.11}$$

where $T_1 = \begin{bmatrix} I & -R \\ 0 & I \end{bmatrix}$, $T_2 = \begin{bmatrix} I & 0 \\ -R & I \end{bmatrix}$. As one transforms the force system from the i-th point to the $(i+1)$-th point, equation (11) relates the generalized force vector q as well as the displacement vector x at these two points.

3.5 Beam Dynamics

The beam dynamics in three dimension includes one elongation, one torsion, and two bending motions. Each motion is assumed to be uncoupled to another since the effects of Poisson's ratio is insignificant for a slender beam. The transfer matrix for each motion is first derived and then augmented to form a transfer matrix of a beam dynamics.

3.5.1 Elongation

First, considering the elongational motion of a beam i with length L, cross section area A, Young's modulus E and mass density ρ, one has the equation of motion

$$E_i A_i w'' = \rho_i A_i s^2 w \tag{3.12}$$

where s denotes the time derivative and w is the displacement of the beam in elongation and the solution is

$$w = a_i \sin \alpha_i^e z + b_i \cos \alpha_i^e z, \tag{3.13}$$

where $\alpha_i^e = j\sqrt{\frac{\rho_i}{E_i}}s$. At one end of the beam (z=0), the displacement $w(0)$ and the normal force $f(0)$ can be expressed as

$$w_i = w(0) = b_i,$$

$$f_i = f(0) = -E_i A_i w'(0) = -E_i A_i \alpha_i^e a_i,$$

or

$$\begin{Bmatrix} a \\ b \end{Bmatrix}_i = \begin{bmatrix} 0 & -\dfrac{1}{EA\alpha^e} \\ 1 & 0 \end{bmatrix}_i \begin{Bmatrix} w \\ f \end{Bmatrix}_i, \tag{3.14}$$

where the displacement and the normal force use the same sign definition of the direction. Similarly, at the other end of the beam ($z = L$), the corresponding quantities are

$$w_{i+1} = w(L_i) = a_i \sin \alpha_i^e L_i + b_i \cos \alpha_i^e L_i,$$
$$f_{i+1} = f(L_i) = E_i A_i w'(L_i) = E_i A_i \alpha_i^e (a_i \cos \alpha_i^e L_i - b_i \sin \alpha_i^e L_i),$$

or

$$\begin{Bmatrix} w \\ f \end{Bmatrix}_{i+1} = \begin{bmatrix} \sin \alpha^e L & \cos \alpha^e L \\ EA\alpha^e \cos \alpha^e L & -EA\alpha^e \sin \alpha^e L \end{bmatrix}_i \begin{Bmatrix} a \\ b \end{Bmatrix}_i. \tag{3.15}$$

From (3.14) and (3.15), one obtains

$$\begin{Bmatrix} w \\ f \end{Bmatrix}_{i+1} = [FE]_i \begin{Bmatrix} w \\ f \end{Bmatrix}_i, \tag{3.16}$$

where the transfer matrix $[FE]_i$ for the motion in elongation is

$$[FE]_i = \begin{bmatrix} \cos \alpha^e L & -\dfrac{\sin \alpha^e L}{EA\alpha^e} \\ -EA\alpha^e \sin \alpha^e L & -\cos \alpha^e L \end{bmatrix}_i = \begin{bmatrix} e_{11} & e_{12} \\ e_{21} & e_{22} \end{bmatrix}_i.$$

3.5.2 Torsion

Next, for the motion of the beam in torsion, the equation of motion is

$$G_i J_{bi} \theta'' = \rho_i J_{bi} s^2 \theta, \tag{3.17}$$

where J_b is the moment of inertia of cross section area, G the shear modulus and θ the angular displacement due to torsion. Similarly, one can derive

$$\begin{Bmatrix}\theta\\ \tau\end{Bmatrix}_{i+1} = [FT]_i \begin{Bmatrix}\theta\\ \tau\end{Bmatrix}_i, \tag{3.18}$$

where τ is the applied torque which has the same sign definition of the direction with the angular displacement and the transfer matrix for the motion in torsion is

$$[FT]_i = \begin{bmatrix} \cos\alpha^t L & -\dfrac{\sin\alpha^t L}{GJ\alpha^t} \\ -GJ\alpha^t \sin\alpha^t L & -\cos\alpha^t L \end{bmatrix}_i = \begin{bmatrix} t_{11} & t_{12} \\ t_{21} & t_{22} \end{bmatrix}_i, \text{ with } \alpha_i^t = j\sqrt{\frac{\rho_i}{G_i}}s.$$

3.5.3 Bending

Finally, for the bending motion of the beam, the equation of motion is

$$E_i I_{bi} w'''' - \rho_i I_{bi} s^2 w'' + \rho_i A_i s^2 w = 0 \tag{3.19}$$

where I_b is the moment of inertia of cross section area and w is the deflection due to bending. Similarly, one can derive

$$\begin{Bmatrix} w\\ \theta\\ f\\ \tau \end{Bmatrix}_{i+1} = [FB]_i \begin{Bmatrix} w\\ \theta\\ f\\ \tau \end{Bmatrix}_i, \tag{3.20}$$

where θ , f and τ are the slope (i.e. w'), shear force, and bending moment respectively, and the transfer matrix for the bending motion is

$$[FB]_i = \frac{1}{2}\begin{bmatrix} cn+ch & \dfrac{sn}{\beta_1}+\dfrac{sh}{\beta_2} & -\dfrac{sn}{h_1}+\dfrac{sh}{h_2} & -\dfrac{cn}{h_3}+\dfrac{ch}{h_4} \\ -\beta_1 sn+\beta_2 sh & cn+ch & -\dfrac{\beta_1}{h_1}cn+\dfrac{\beta_2}{h_2}ch & \dfrac{\beta_1}{h_3}sn+\dfrac{\beta_2}{h_4}sh \\ -h_1 sn-h_2 sh & \dfrac{h_1}{\beta_1}cn-\dfrac{h_2}{\beta_2}ch & -cn-ch & \dfrac{h_1}{h_3}sn-\dfrac{h_2}{h_4}sh \\ h_3 cn-h_4 ch & \dfrac{h_3}{\beta_1}sn-\dfrac{h_4}{\beta_2}sh & -\dfrac{h_3}{h_1}sn-\dfrac{h_4}{h_2}sh & -cn-ch \end{bmatrix}_i$$

$$= \begin{bmatrix} b_{11} & b_{12} & b_{13} & b_{14} \\ b_{21} & b_{22} & b_{23} & b_{24} \\ b_{31} & b_{32} & b_{33} & b_{34} \\ b_{41} & b_{42} & b_{43} & b_{44} \end{bmatrix}_i,$$

where $\beta_1^2 = \dfrac{-\rho I s^2 + s\sqrt{(\rho I s)^2 - 4\rho AEI}}{2EI}, \beta_2^2 = \dfrac{\rho I s^2 + s\sqrt{(\rho I s)^2 - 4\rho AEI}}{2EI},$

$k_1 = EI,\ k_2 = \rho I,$

$h_1 = k_1\beta_1^3 + k_2\beta_1 s^2,\ h_2 = k_1\beta_2^3 - k_2\beta_2 s^2,\ h_3 = \mathrm{k}_1\beta_1^2,\ h_4 = \mathrm{k}_1\beta_2^2,$

and $sn = \sin\beta_1 L,\ cn = \cos\beta_1 L,\ sh = \sinh\beta_2 L,\ ch = \cosh\beta_2 L.$

The deflection and shear force have the same sign definition of the direction but the slope and bending moment have the opposite sign definition of the direction.

3.5.4 Sign Change of the Direction of Variables

It is noted that the deflection and shear force have the same sign definition of the direction but the slope and bending moment have the opposite sign definition of the direction. If the sign definition of the direction for any variable is changed, one needs to modify the transfer matrix. For example, changing the sign definition of the direction for θ, one has

$$\begin{Bmatrix} w \\ -\theta \\ f \\ \tau \end{Bmatrix}_{i+1} = \begin{bmatrix} b_{11} & b_{12} & b_{13} & b_{14} \\ b_{21} & b_{22} & b_{23} & b_{24} \\ b_{31} & b_{32} & b_{33} & b_{34} \\ b_{41} & b_{42} & b_{43} & b_{44} \end{bmatrix}_i \begin{Bmatrix} w \\ -\theta \\ f \\ \tau \end{Bmatrix}_i,$$

$$\text{or} \begin{Bmatrix} w \\ \theta \\ f \\ \tau \end{Bmatrix}_{i+1} = \begin{bmatrix} b_{11} & -b_{12} & b_{13} & b_{14} \\ -b_{21} & b_{22} & -b_{23} & -b_{24} \\ b_{31} & b_{32} & b_{33} & b_{34} \\ b_{41} & b_{42} & b_{43} & b_{44} \end{bmatrix}_i \begin{Bmatrix} w \\ \theta \\ f \\ \tau \end{Bmatrix}_i. \qquad (3.21)$$

3.5.5 Overall Dynamics of a Beam

From (3.16), (3.18), (3.20) and (3.21), one can obtain the relationship between two ends of an Euler beam

$$\begin{Bmatrix} w_x \\ w_y \\ w_z \\ \theta_x \\ \theta_y \\ \theta_z \\ f_x \\ f_y \\ f_z \\ \tau_x \\ \tau_y \\ \tau_z \end{Bmatrix}_{i+1} = \begin{bmatrix} b_{11} & 0 & 0 & 0 & -b_{12} & 0 & b_{13} & 0 & 0 & 0 & b_{14} & 0 \\ 0 & b_{11} & 0 & b_{12} & 0 & 0 & 0 & b_{13} & 0 & -b_{14} & 0 & 0 \\ 0 & 0 & e_{11} & 0 & 0 & 0 & 0 & 0 & e_{12} & 0 & 0 & 0 \\ 0 & b_{21} & 0 & b_{22} & 0 & 0 & 0 & b_{23} & 0 & -b_{24} & 0 & 0 \\ -b_{21} & 0 & 0 & 0 & b_{22} & 0 & -b_{23} & 0 & 0 & 0 & -b_{24} & 0 \\ 0 & 0 & 0 & 0 & 0 & t_{11} & 0 & 0 & 0 & 0 & 0 & t_{12} \\ b_{31} & 0 & 0 & 0 & -b_{32} & 0 & b_{33} & 0 & 0 & 0 & b_{34} & 0 \\ 0 & b_{31} & 0 & b_{32} & 0 & 0 & 0 & b_{33} & 0 & -b_{34} & 0 & 0 \\ 0 & 0 & e_{21} & 0 & 0 & 0 & 0 & 0 & e_{22} & 0 & 0 & 0 \\ 0 & -b_{41} & 0 & -b_{42} & 0 & 0 & 0 & -b_{43} & 0 & b_{44} & 0 & 0 \\ b_{41} & 0 & 0 & 0 & -b_{42} & 0 & b_{43} & 0 & 0 & 0 & b_{44} & 0 \\ 0 & 0 & 0 & 0 & 0 & t_{21} & 0 & 0 & 0 & 0 & 0 & t_{22} \end{bmatrix}_i \begin{Bmatrix} w_x \\ w_y \\ w_z \\ \theta_x \\ \theta_y \\ \theta_z \\ f_x \\ f_y \\ f_z \\ \tau_x \\ \tau_y \\ \tau_z \end{Bmatrix}_i ,$$

or in short

$$\begin{Bmatrix} x \\ q \end{Bmatrix}_{i+1} = \begin{bmatrix} F_1 & F_2 \\ F_3 & F_4 \end{bmatrix}_i \begin{Bmatrix} x \\ q \end{Bmatrix}_i . \tag{3.22}$$

3.6 Overall System Dynamics

Now as shown in Figure 3.1, one can define the shuttle end of the mast as point 1, the reflector end of the mast as point 2, and the center of mass of the reflector as point 3 or point 4. The relationship between point 1 and point 2 can be obtained from the beam dynamics (3.22)

$$\begin{Bmatrix} x \\ q \end{Bmatrix}_2 = \begin{bmatrix} F_1 & F_2 \\ F_3 & F_4 \end{bmatrix}_1 \begin{Bmatrix} x \\ q \end{Bmatrix}_1 . \tag{3.23}$$

Transforming the force system from point 2 to point 3, as shown in (3.11), yields

$$\begin{Bmatrix} x \\ q \end{Bmatrix}_3 = \begin{bmatrix} T_1 & 0 \\ 0 & T_2 \end{bmatrix}_2 \begin{Bmatrix} x \\ q \end{Bmatrix}_2. \tag{3.24}$$

The rigid body dynamics (3.6) gives the relationship between point 3 and 4

$$\begin{Bmatrix} x \\ q \end{Bmatrix}_4 = \begin{bmatrix} I & 0 \\ s^2\overline{M} + \overline{G} & I \end{bmatrix}_3 \begin{Bmatrix} x \\ q \end{Bmatrix}_3. \tag{3.25}$$

From (3.23) to (3.25), one can obtain the relationship between point 1 and 4

$$\begin{Bmatrix} x \\ q \end{Bmatrix}_4 = \begin{bmatrix} I & 0 \\ s^2\overline{M} + \overline{G} & I \end{bmatrix}_3 \begin{bmatrix} T_1 & 0 \\ 0 & T_2 \end{bmatrix}_2 \begin{bmatrix} F_1 & F_2 \\ F_3 & F_4 \end{bmatrix}_1 \begin{Bmatrix} x \\ q \end{Bmatrix}_1. \tag{3.26}$$

Because point 1 is clamped, $\{x\}_1=0$, so one can obtain

$$\{x\}_4 = [T_1]_2[F_2]_1\{q\}_1, \tag{3.27}$$

and

$$\{q\}_4 = ((s^2[\overline{M}]_3 + [\overline{G}]_3)[T_1]_2[F_2]_1 + [T_2]_2[F_4]_1)\{q\}_1. \tag{3.28}$$

Recall that the displacement vector $\{x\}_4$ and the generalized force $\{q\}_4$ are applied at the center of mass of the reflector. Let $x=\{x\}_4$ and $q=\{q\}_4$. After eliminating $\{q\}_1$ from (3.27) and (3.28), one can derive

$$M_r s^2 x + A(s)x = q, \tag{3.29}$$

where $M_r = [\overline{M}]_3$, $A(s) = [\overline{G}]_3 + [T_2]_2[F_4]_1([T_1]_2[F_2]_1)^{-1}$. Because three reaction wheels and one collocated three-axis rate gyro are used to provide the control input u and the measurement v respectively, the system becomes

$$M_r s^2 x + A(s)x = Bu \tag{3.30}$$

$$v = B^T s x \tag{3.31}$$

where $B = \begin{bmatrix} 0_{3x3} \\ I_{3x3} \end{bmatrix}$, $u = \{\tau_x \quad \tau_y \quad \tau_z\}^T$, and $v = \{\dot{\theta}_x \quad \dot{\theta}_y \quad \dot{\theta}_z\}^T$. It is noted that M_r is constant and the matrix $A(s)$ contains sinusoidal functions and hyperbolic functions of s.

One may perform parameter estimation based on this distributed model. For further controller design, this model needs to be transformed to a reduced finite-dimensional model.

Now taking the first two terms of Taylor's serial expansion of $A(s)$ yields a reduced-order model

$$M\ddot{x} + Kx = Bu \tag{3.32}$$

$$v = B^{T}\dot{x} \tag{3.33}$$

where $M = M_r + \frac{1}{2}A''(0)$, $K = A(0)$. This model can also be derived using the finite element method.

3.7 Parameter Estimation

After obtaining the system model, one needs to estimate system parameters. All system parameters for the SCOLE configuration are listed in Table 3.1. Among them, the length, area, mass, and density can be accurately measured and hence can not be adjusted. The moment of inertia of cross sectional area and the mass center of the reflector can be calculated. Only the Young's modulus, shear modulus, and moment of inertia of the reflector are adjusted to match the first five modal frequencies from the analytical model with those from test data. The analytical modal frequencies can be obtained by solving the roots of

$$\det(-M_r\omega^2 + A(j\omega)) = 0 \tag{3.34}$$

where ω is the modal frequency. The estimated parameters are listed in Table 3.1. As shown in Table 3.2, the identified modal frequencies match fairly well with measured ones.

Figure 3.3 shows the first five mode shapes obtained by solving the corresponding eigenvectors of (3.34).

3.8 Concluding Remarks

The NASA SCOLE facility has been introduced. This facility is designed for investigating system modeling, parameter estimation or system identification, and control design for large structural flexible systems. The distributed parameter model for the simplified version of the SCOLE configuration has been derived by using Holzer's transfer matrix method. This method provides a useful means to simplify and standardize the procedure for obtaining a distributed parameter model of a large structural flexible system. The parameter estimation based on the distributed parameter model has been performed by matching the first five modal frequencies from the analytical model with those from test data. The advantage of using a distributed parameter model in parameter estimation is that there is no model reduction like a finite element model. Therefore, it is expected that a distributed parameter model will provide a more accurate model than a finite element model. The result shows that the identified modal frequencies match fairly well with measured ones. There are two features of this configuration which are the required conditions of the explicit LQG controller design presented in the next chapter. First, the control objective is structural vibration suppression. Second, the rate sensors and the actuators are collocated. The controller design and performance are demonstrated in the next chapter.

Table 3.1 Estimated parameters of the SCOLE configuration.

the mast:		the reflector:
L=125.5 in	E=30 Mpsi	$r = \{r_x, r_y, r_z\}^T = \{1.795, 4.319, 0.\}^T$ in
A=0.108 in^2	G=13.3 Mpsi	m = 0.864 slug
I_b=6.66x10^{-3} in		$J = \begin{bmatrix} 110 & -28 & -0.7 \\ -28 & 74 & -1.6 \\ -0.7 & -1.6 & 184 \end{bmatrix}$ slug - in^2
J_b=2I_b=1.33x10^{-2} in^4		
ρ=0.0205 slug/in^3		

Table 3.2 Identified modal frequencies of the SCOLE configuration.

mode #	mode shape	measured (Hz)	identified (Hz)
1	first bending in X'Z	0.4512	0.4514
2	first bending in Y'Z	0.4567	0.4524
3	first torsion	1.5223	1.5250
4	second bending in X'Z	3.1333	3.2264
5	second bending in Y'Z	4.3926	4.4019

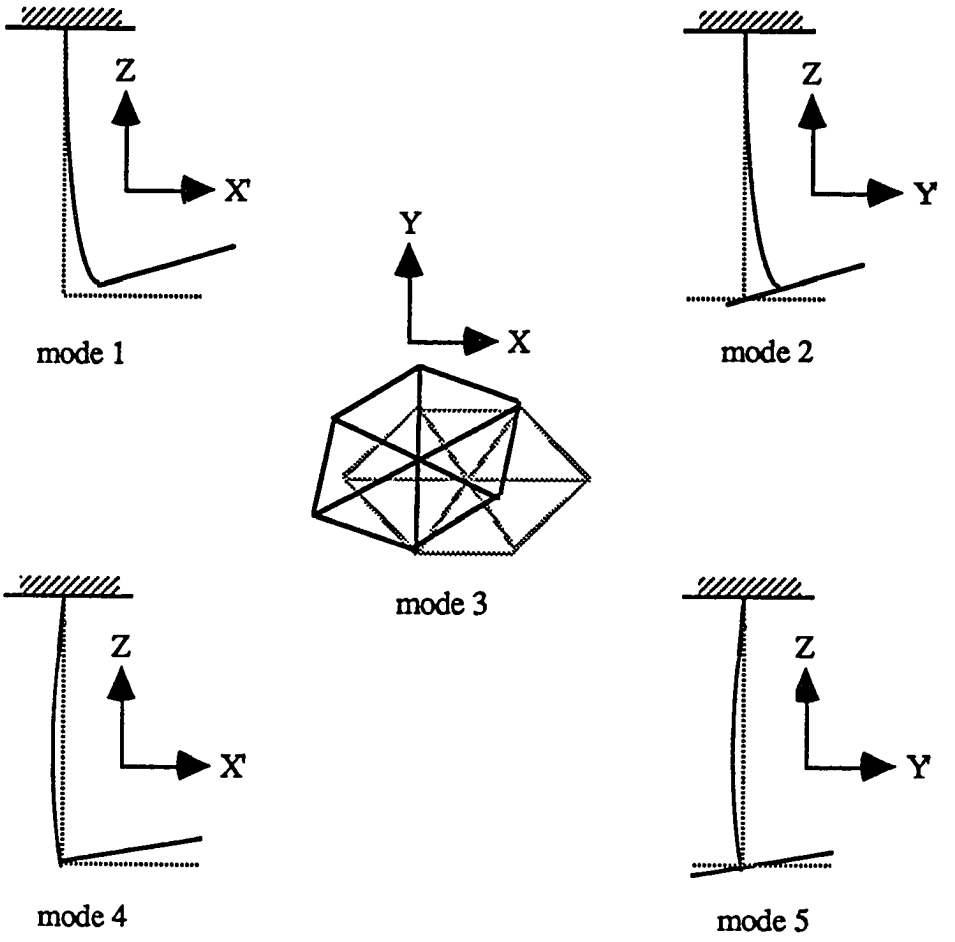

Figure 3.3 The first five mode shapes of the SCOLE configuration.

Chapter 4

EXPLICIT LQG CONTROLLER DESIGN

4.1 Introduction

In this chapter the explicit LQG controller design and performance are presented. The existence of the explicit LQG controller requires three features. First, the control objective is structural vibration suppression. Second, the measurement is from rate sensors collocated with actuators. Third, the performance index for state feedback and the noise covariance matrices are defined on a modal-space model. The transformation between a finite-dimensional model and a modal-space model for a structural system with collocated rate sensors and actuators is first presented. The explicit solutions of the Riccati equations associated with state feedback and state estimation are then derived. Then the explicit LQG controller is applied to the NASA SCOLE configuration. Numerical simulations are provided to demonstrate how to choose the design parameters. Experiments are performed to validate this controller design.

4.2 Modal-Space Model

In this section the transformation between a finite-dimensional model and a modal-space model will be presented. Any finite-dimensional model can be transformed into a modal space so that all the modes are internally decoupled. Recall a finite-dimensional model for a structural system with collocated rate sensors and actuators

$$M\ddot{x} + Kx = Bu, \tag{4.1}$$

$$v = B^{\mathrm{T}}\dot{x}, \tag{4.2}$$

where M, K, and B are the mass, stiffness, and input influence matrices, respectively, x the displacement, u the input, and v the measurement. The modal frequency ω_k and the mode shape e_k for the k-th mode can be obtained by solving an eigenvalue problem

$$(-\omega^2 I + M^{-1}K)x = 0, \tag{4.3}$$

where the mode shapes are orthonormalized with the mass matrix M. Thus, one can have

$$M\omega_k^2 e_k = Ke_k, \text{ and } e_j^T M e_k = \delta_{jk}, \tag{4.4}$$

where δ is the Kronecker delta. One can choose any N modes, not necessarily the first N modes, for further model reduction. Substituting $x = \sum_1^N e_k y_k$ into (4.1), one has

$$\sum_1^N Me_k\ddot{y}_k + Ke_k y_k = Bu, \tag{4.5}$$

where y_k is the k-th modal coordinate. Multiplying e_j^{T} on both sides, one obtains

$$\sum_1^N e_j^{\mathrm{T}} Me_k\ddot{y}_k + e_j^{\mathrm{T}} Ke_k y_k = e_j^{\mathrm{T}} Bu, \qquad j = 1,2,\cdots,N \tag{4.6}$$

Applying (4.4) to (4.6) yields

$$\ddot{y}_j + \omega_j^2 y_j = e_j^{\mathrm{T}} Bu, \qquad j = 1,2,\cdots,N \tag{4.7}$$

or in matrix form

$$\ddot{y} + \Lambda_N y = B_N u \qquad (4.8)$$

where $y = \{y_1, \cdots, y_N\}^T$, $\Lambda_N = \text{diag}[\omega_1^2, \cdots, \omega_N^2]$, and $B_N = \begin{bmatrix} e_1^T B \\ \vdots \\ e_N^T B \end{bmatrix}$. Similarly, the output equation (4.2) becomes

$$v = \sum_1^N B^T e_k \dot{y}_k = B_N^T \dot{y}. \qquad (4.9)$$

Equations (4.8) and (4.9) are the modal-space model derived for the control design presented in the next two sections.

4.3 Explicit Solution of Riccati Equation for State Estimation

In this section the explicit solutions for the corresponding Riccati equations of the optimal state estimation is derived. This starts with transforming the dynamic model from the modal space to a state space. Let

$$\xi = \{\xi_1 \quad \xi_2 \quad \cdots \quad \xi_{2N-1} \quad \xi_{2N}\}^T = \{y_1 \quad \dot{y}_1/\omega_1 \quad \cdots \quad y_N \quad \dot{y}_N/\omega_N\}^T \qquad (4.10)$$

and the model becomes

$$\dot{\xi} = \mathcal{A}\xi + \mathcal{B}u + \delta \qquad (4.11)$$

$$v = C\xi + \eta \qquad (4.12)$$

where

$$\mathcal{A} = \text{diag}\left[\begin{bmatrix} 0 & \omega_1 \\ -\omega_1 & 0 \end{bmatrix} \cdots \begin{bmatrix} 0 & \omega_N \\ -\omega_N & 0 \end{bmatrix}\right], \mathcal{B} = \begin{bmatrix} 0 \\ e_1^T B/\omega_1 \\ \vdots \\ 0 \\ e_N^T B/\omega_N \end{bmatrix},$$

$$\text{and } C = \begin{bmatrix} 0 & B^T e_1 \omega_1 & \cdots & 0 & B^T e_N \omega_N \end{bmatrix}.$$

Here it is assumed that the transformed state-space model is subjected to additive process noise δ and measurement noise η. Both are assumed to be gaussian, zero-mean and white with constant covariance matrices N_δ and N_η, respectively. They are also assumed statistically uncorrelated with each other. Since the system dynamics and the measurements are corrupted by the noises, this problem becomes an LQG problem.

For the linear time-invariant dynamic system (4.11) and (4.12), the optimal state estimation is[24]

$$\dot{\hat{\xi}} = \mathcal{A}\hat{\xi} + \mathcal{B}u + LC^{\mathrm{T}}N_\eta^{-1}(v - C\hat{\xi}) \tag{4.13}$$

where $\hat{\xi}$ is the estimate of the state ξ and the matrix L has to satisfy the Riccati equation

$$\mathcal{A}L + L\mathcal{A}^{\mathrm{T}} + N_\delta - LC^{\mathrm{T}}N_\eta^{-1}C\,L = 0 \tag{4.14}$$

Next, the closed form solution of this Riccati equation can be found by choosing $N_\eta = d_\eta I$, $N_\delta = S\mathcal{B}\mathcal{B}^{\mathrm{T}}S^{\mathrm{T}}$ where $S = \mathrm{diag}[s_1 \quad s_1 \quad \cdots \quad s_N \quad s_N]$. Since $N_\delta = S\mathcal{B}\mathcal{B}^{\mathrm{T}}S^{\mathrm{T}} = (S\mathcal{B})(S\mathcal{B})^{\mathrm{T}}$, one can easily prove that N_δ is semi-positive definite. From the process noise covariance N_δ, it can be seen that the effect of the process noise to the i-th mode can be adjusted by choosing a suitable parameter s_i directly. It is expected that s_i also affects the estimation gain for the i-th mode. To obtain the closed form solution of the Riccati equation, a diagonal L is investigated and denoted by

$$L = \mathrm{diag}[l_1 \quad l_1 \quad \cdots \quad l_N \quad l_N]. \tag{4.15}$$

One can easily prove that

$$\mathcal{A}L + L\mathcal{A}^{\mathrm{T}} = 0\,, \tag{4.16}$$

$$N_\delta = \begin{bmatrix} 0 & 0 & \cdots & 0 & 0 \\ 0 & e_1^{\mathrm{T}}BB^{\mathrm{T}}e_1 s_1^2/\omega_1^2 & \cdots & 0 & e_1^{\mathrm{T}}BB^{\mathrm{T}}e_N s_1 s_N/\omega_1\omega_N \\ \vdots & \vdots & \vdots & \vdots & \vdots \\ 0 & 0 & \cdots & 0 & 0 \\ 0 & e_1^{\mathrm{T}}BB^{\mathrm{T}}e_N s_1 s_N/\omega_1\omega_N & \cdots & 0 & e_N^{\mathrm{T}}BB^{\mathrm{T}}e_N s_N^2/\omega_N^2 \end{bmatrix}, \tag{4.17}$$

$$\text{and } LC^{\mathrm{T}}N_{\eta}^{-1}C\,L=\frac{1}{d_{\eta}}\begin{bmatrix}0 & 0 & \cdots & 0 & 0\\ 0 & e_1^{\mathrm{T}}BB^{\mathrm{T}}e_1l_1^2\omega_1^2 & \cdots & 0 & e_1^{\mathrm{T}}BB^{\mathrm{T}}e_Nl_1l_N\omega_1\omega_N\\ \vdots & \vdots & \vdots & \vdots & \vdots\\ 0 & 0 & \cdots & 0 & 0\\ 0 & e_1^{\mathrm{T}}BB^{\mathrm{T}}e_Nl_1l_N\omega_1\omega_N & \cdots & 0 & e_N^{\mathrm{T}}BB^{\mathrm{T}}e_Nl_N^2\omega_N^2\end{bmatrix}. \tag{4.18}$$

Substituting (4.16)-(4.18) into (4.14) yields

$$L=\sqrt{d_{\eta}}\,\mathrm{diag}\left[s_1/\omega_1^2 \quad s_1/\omega_1^2 \quad \cdots \quad s_N/\omega_N^2 \quad s_N/\omega_N^2\right]. \tag{4.19}$$

This is the explicit solution derived for the optimal estimation (4.13) and s_i weighs the sensor information used for the state estimation for the i-th mode.

4.4 Explicit Solution of Riccati Equation for State Feedback

Next, for the optimal control design with a performance index

$$\text{P.I.}=\frac{1}{2}\mathrm{E}\left[\int_0^{\infty}(\xi^{\mathrm{T}}Q\xi+u^{\mathrm{T}}Ru)dt\right], \tag{4.20}$$

where E[ ] is the expectation operator, the optimal control input is[24]

$$u=-R^{-1}\mathcal{B}^{\mathrm{T}}K\hat{\xi} \tag{4.21}$$

and the matrix K has to satisfy the Riccati equation

$$K\mathcal{A}+\mathcal{A}^{\mathrm{T}}K+Q-K\mathcal{B}^{\mathrm{T}}R^{-1}\mathcal{B}K=0. \tag{4.22}$$

Similarly, the closed form solution of this Riccati equation can be found by choosing $Q=H^{\mathrm{T}}C^{\mathrm{T}}CH$ $(H=\mathrm{diag}[h_1 \quad h_1 \quad \cdots \quad h_N \quad h_N])$ and R to be an identical matrix, respectively. Since $Q=H^{\mathrm{T}}C^{\mathrm{T}}CH=(CH)^{\mathrm{T}}(CH)$, one can easily prove that Q is semi-positive definite. The closed form solution is

$$K=\mathrm{diag}\left[h_1\omega_1^2 \quad h_1\omega_1^2 \quad \cdots \quad h_N\omega_N^2 \quad h_N\omega_N^2\right]. \tag{4.23}$$

This is the explicit solution derived for the optimal state feedback (4.21) and h_i weighs the contribution of the actuators to the i-th mode. From the weighting matrix Q, it can be seen that the weighting of the i-th mode performance can be adjusted by choosing a suitable parameter h_i directly.

Transforming the state estimation (4.13) and the state feedback (4.21) back to the modal space, one has

$$\ddot{\hat{y}} + (UB_N B_N^{\mathrm{T}} + B_N B_N^{\mathrm{T}} P)\dot{\hat{y}} + \Lambda_N \hat{y} = UB_N v \tag{4.24}$$

$$u = -B_N^{\mathrm{T}} P \dot{\hat{y}} \tag{4.25}$$

where

$$U = \sqrt{1/d_\eta}\ \mathrm{diag}[s_1 \quad s_2 \quad \cdots \quad s_N], \qquad P = \mathrm{diag}[h_1 \quad h_2 \quad \cdots \quad h_N],$$

$$\text{and} \qquad \hat{y} = \{\hat{y}_1 \quad \hat{y}_2 \quad \cdots \quad \hat{y}_N\}^{\mathrm{T}} = \left\{\hat{\xi}_1 \quad \hat{\xi}_3 \quad \cdots \quad \hat{\xi}_{2N-1}\right\}^{\mathrm{T}}.$$

Equations (4.24) and (4.25) represent the explicit optimal LQG controller and matrices U and P are the design parameters. It is noted that both the parameter h_i of P and the parameter s_i of U are directly related to the performance of the i-th mode so that it can be easily adjusted by choosing suitable design parameters for that mode. Both design parameters also contribute damping to the controller dynamics. In addition, for N desired controlled modes, one has $2N$ design parameter (N for the optimal estimator and another N for the optimal controller). This provides an easier way for the controller design to achieve a specific performance requirement.

This optimal LQG controller can also be represented by a transfer function. After taking Laplace transformation of (4.24) and (4.25) and eliminating the state of the estimation $\hat{y}$, one has

$$u = \Psi(s)v \tag{4.26}$$

with

$$\Psi(s) = -sB_N^T P(s^2 + (UB_N B_N^T + B_N B_N^T P)s + \Lambda_N)^{-1} UB_N.$$

This explicit LQG optimal controller is obtained based on a finite-dimensional model in the modal space. It is interesting to see that if one chooses P and U to be a scalar times an identity matrix and let N go to infinity, this controller is the same as the explicit LQG optimal controller derived based on the distributed parameter model[3,35,36]. Finally, one can also check any closed-loop pole for the uncontrolled modes by determining the roots of the characteristic equation based on the distributed parameter model (3.29)

$$\det[s^2 M_r + A(s) - sB\Psi(s)B^T] = 0. \tag{4.27}$$

4.5 Numerical Simulations and Experimental Results

The experimental setup basically consists of a digital controller which is sandwiched between A/D and D/A converters. Since the bandwidth of both actuators and sensors is more than 10 times higher than the highest controlled modal frequency, the dynamics of actuators and sensors are ignored. From the experiment, it is found that the sixth modal excitation damps out 95 % within 2 seconds with more than 10 Hz frequency. Therefore, the first five modes are chosen to design the controller. Since the highest controlled modal frequency is about 4.4 Hz, a sampling rate of 50 Hz for the digital controller is sufficiently fast. From the free decay response of the experiment, it can be found that the corresponding damping ratios are 0.19, 0.19, 0.17, 0.30, and 1.07%, respectively. The first two modes are found to be the hardest two to control.

Before the experiment, numerical simulations are performed in order to choose suitable design parameters. Tables 4.1 and 4.2 show the different design parameters used and the corresponding damping ratios, respectively. Cases 1 to 6 are the results from numerical

simulations and the last one (test) is from testing. Let $P=2.5I$, it can be seen that the closed-loop damping ratios are increased as U is increased until $U=P$ (see case 1 and 2). Since the damping ratios are not improved for $U>P$ (case 3), it is decided to use $U=P$ in the experiment. However the damping ratios of the first two modes are still low, so the weighting of the first two modes is increased by using the values shown in case 4 (see table 4.1). Then the damping ratios of the first two modes are significantly increased (see table 4.2). After considering the torque limitation for the actuator (6.3 in-lbs) and the satisfactory damping ratios, it is decided to use $P=U$=diag[13, 13, 2.5, 2.6, 1.9] for the remaining cases.

In the experiment, each mode is individually excited for 40 seconds and then the explicit LQG controller is activated. This procedure is repeated for all the five modes with the same controller. Figures 4.1 to 4.5 show the time responses (with control (solid line) and without control (doted line)) and the corresponding control input for mode 1 to 5 respectively. The results demonstrate that the controller provides sufficient damping, which means approximately 80% of amplitude decay in 10 seconds, for all the controlled modes. However, the damping ratios (see Table 4.2, last column) are less than those predicted in case 5. This may be caused by the modeling error in the controller design. It is assumed that the modal frequencies used in the controller design are 2% higher than those of the actual system. The result shows that the damping ratios from the simulation (case 6) are very close to those of the experiment except the third mode. The reason may be attributed to the control input which saturates at the torque limitation for most of the time (see Figure 4.3, z reaction wheel). Although the performance of the system through the optimal controller design is very sensitive to the modeling error, the damping still can be significantly improved. In summary, both analytical and experimental results show that the proposed explicit LQG controller not only enhance the structural damping effectively but also provide an easy way to choose the design parameters correspondingly.

4.5 Concluding Remarks

We have derived an explicit optimal LQG controller based on modal space for the vibration suppression of large structural systems with collocated rate sensors and actuators. There are two main contributions. First, numerically solving the corresponding Riccati equations for state estimation and feedback is no longer required. It is quite time consuming to solve the corresponding Riccati equations, particularly for large-scale systems. Second, the number of design parameters (i.e. elements of weighting matrices and noise covariances) for either state estimation or state feedback equals the number of the controlled modes and can be easily selected to achieve the desired damping for each mode. This overcomes the problem of choosing suitable weighting matrices and noise covariances in the optimal LQG control design. This proposed controller has been successfully applied to the NASA SCOLE configuration. Both numerical simulations and experimental results demonstrate that this proposed controller is easy to design and implement. It can also suppress vibrations effectively for large flexible structures.

Table 4.1 Design parameters of the explicit LQG controller.

case #	matrix P	matrix U
1	$2.5I$	I
2	$2.5I$	$2.5I$
3	$2.5I$	$5I$
4	diag[10, 10, 2.5, 2.5, 2.5]	diag[10, 10, 2.5, 2.5, 2.5]
5	diag[13, 13, 2.5, 2.6, 1.9]	diag[13, 13, 2.5, 2.6, 1.9]
6*	diag[13, 13, 2.5, 2.6, 1.9]	diag[13, 13, 2.5, 2.6, 1.9]
test	diag[13, 13, 2.5, 2.6, 1.9]	diag[13, 13, 2.5, 2.6, 1.9]

*assume that each modal frequency has 2% error.

Table 4.2 Comparison of damping ratios (%).

mode #	case 1	case 2	case 3	case 4	case 5	case 6	test
1	0.38	0.96	0.96	3.85	5.01	2.89	2.27
2	0.38	0.95	0.95	3.84	4.95	2.84	2.20
3	4.06	10.14	10.14	10.14	10.14	7.05	2.45
4	1.93	4.82	4.82	4.82	5.01	2.78	2.13
5	2.67	6.66	6.66	6.66	5.06	2.83	2.15

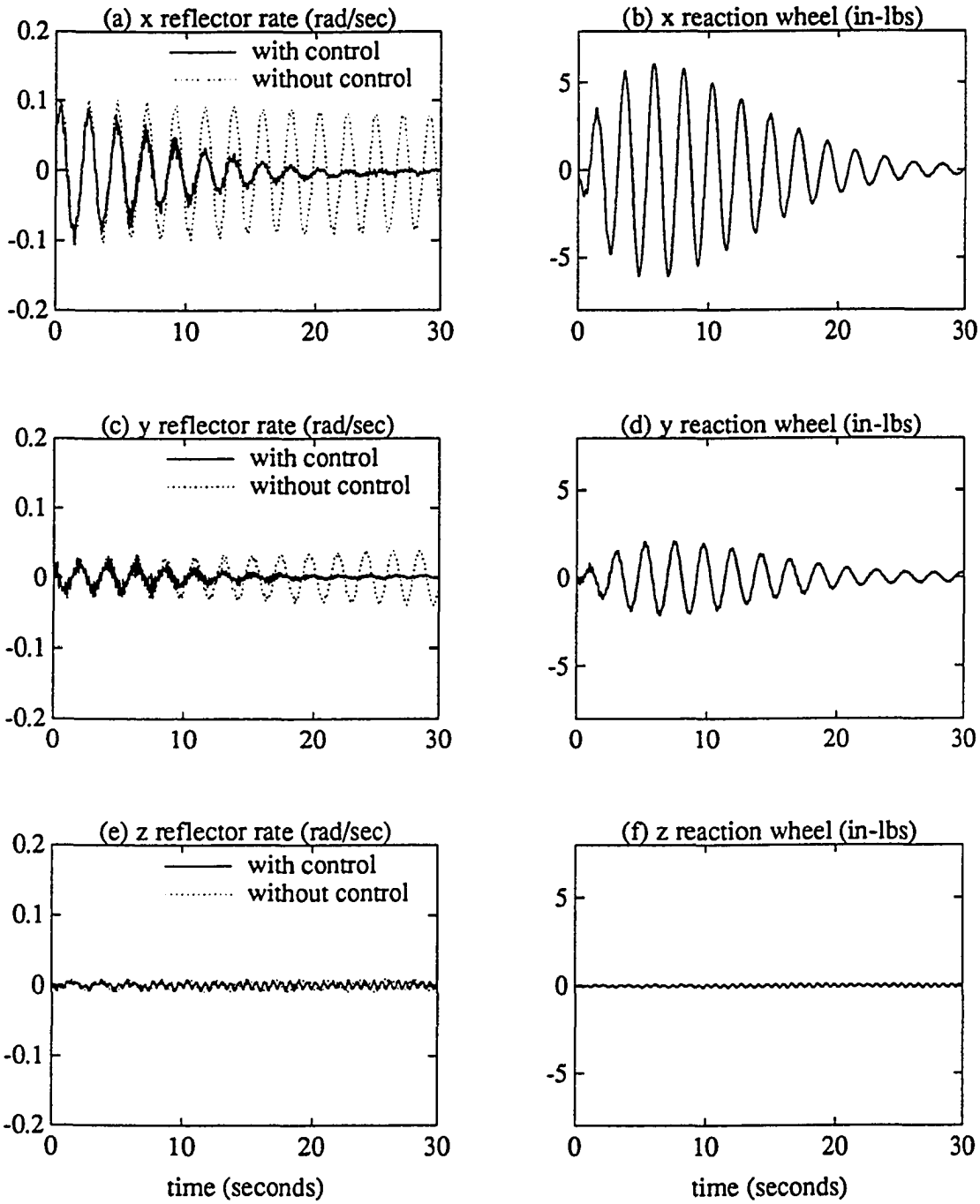

Figure 4.1 Experimental result of mode 1 excitation.

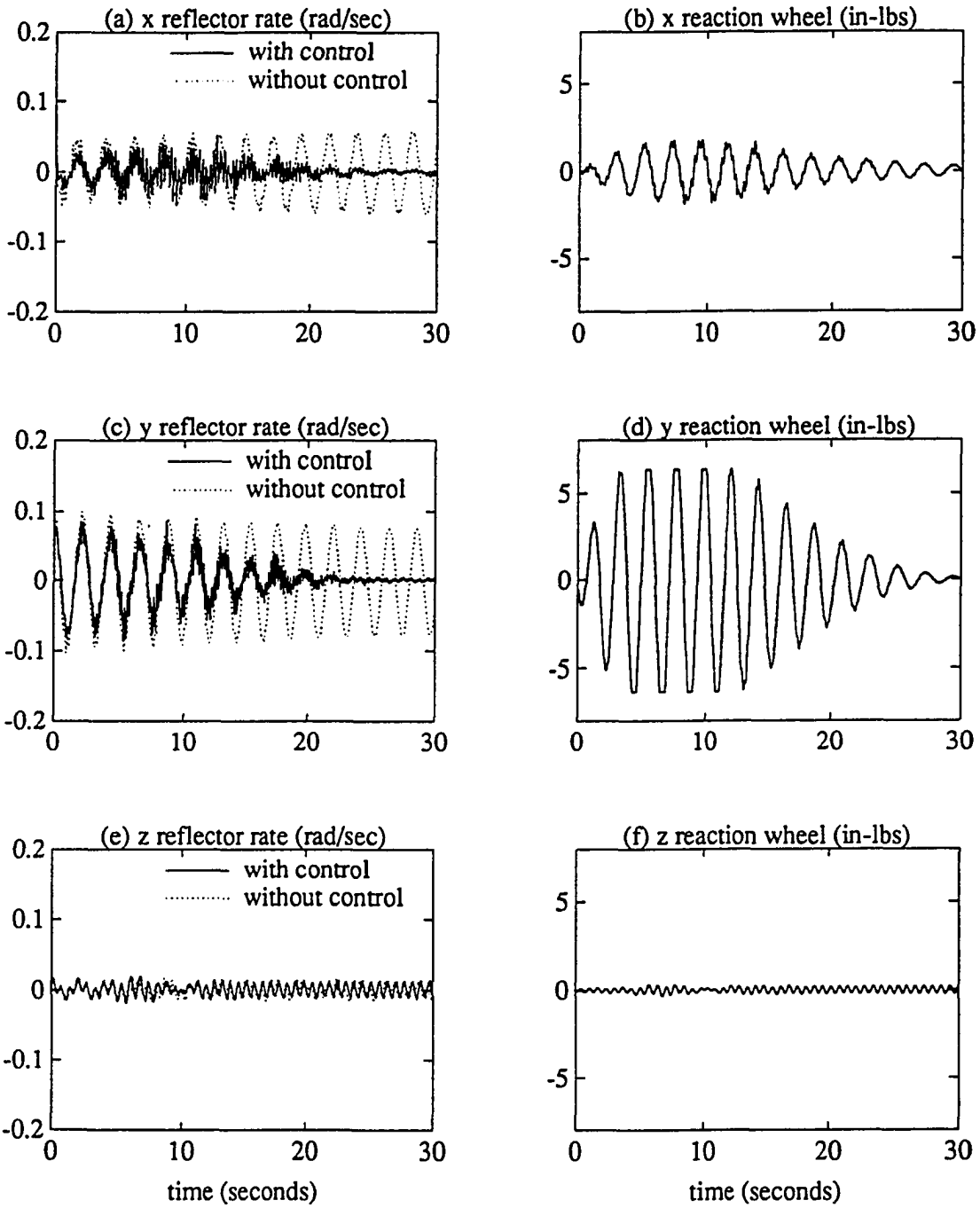

Figure 4.2 Experimental result of mode 2 excitation.

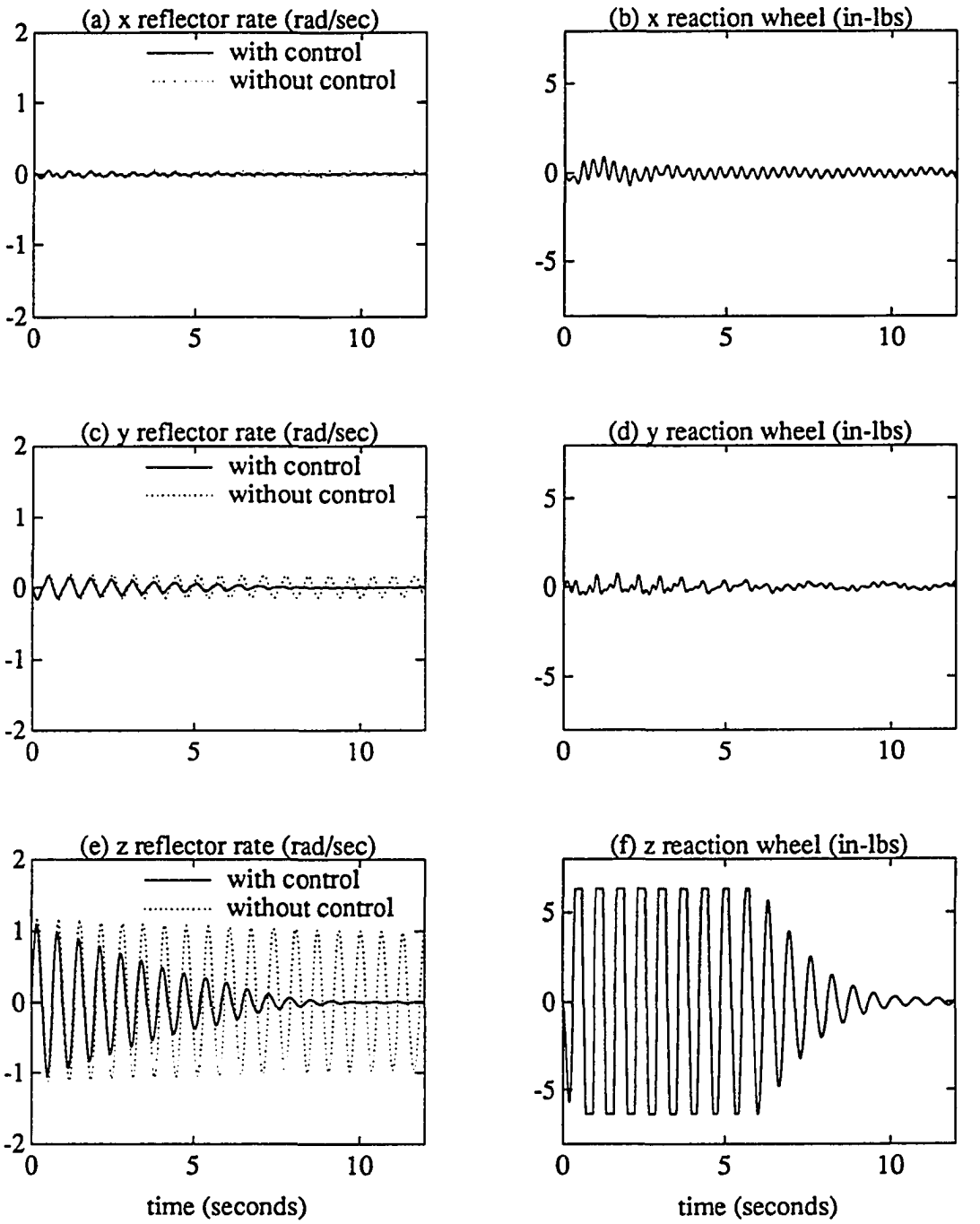

Figure 4.3 Experimental result of mode 3 excitation.

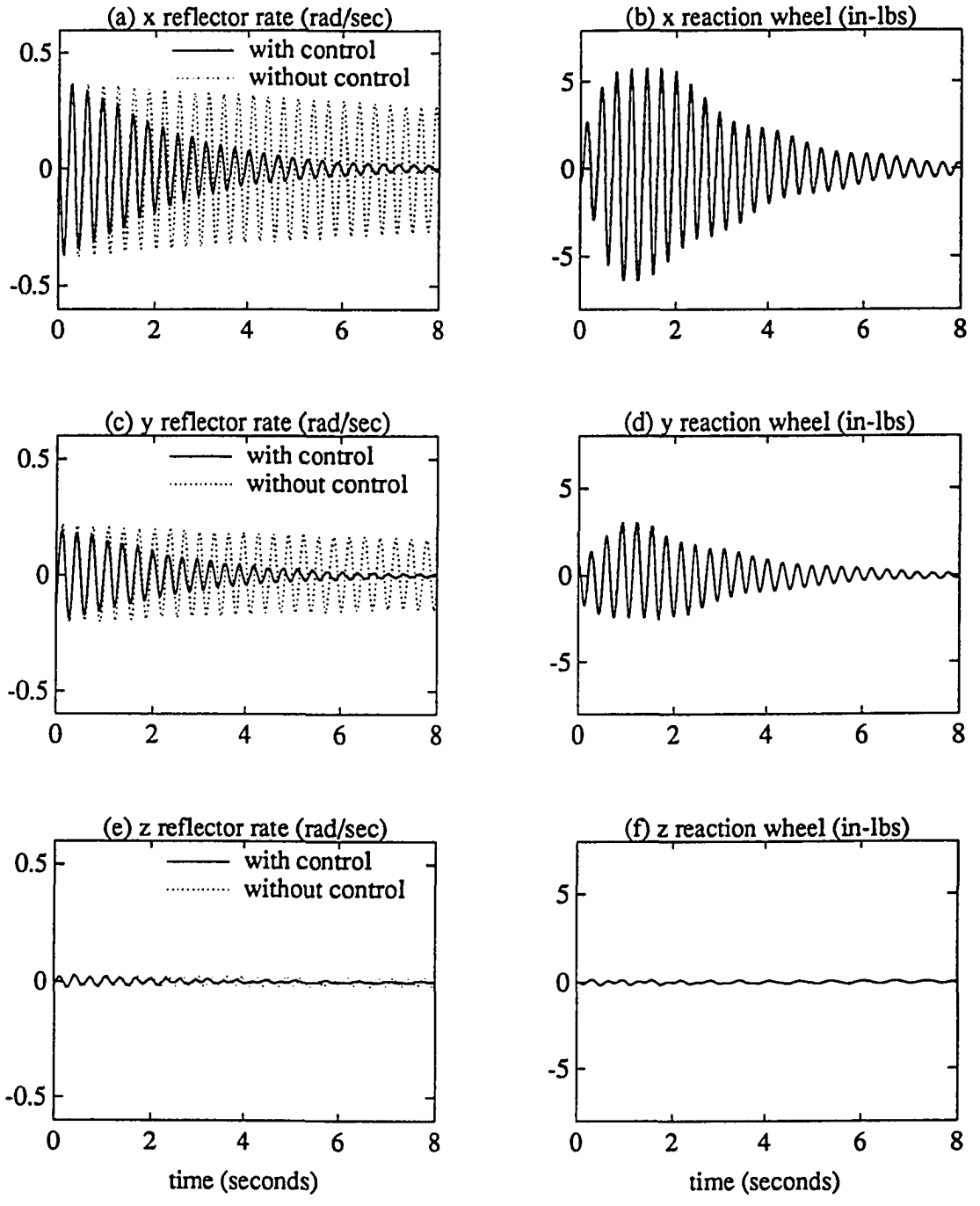

Figure 4.4 Experimental result of mode 4 excitation.

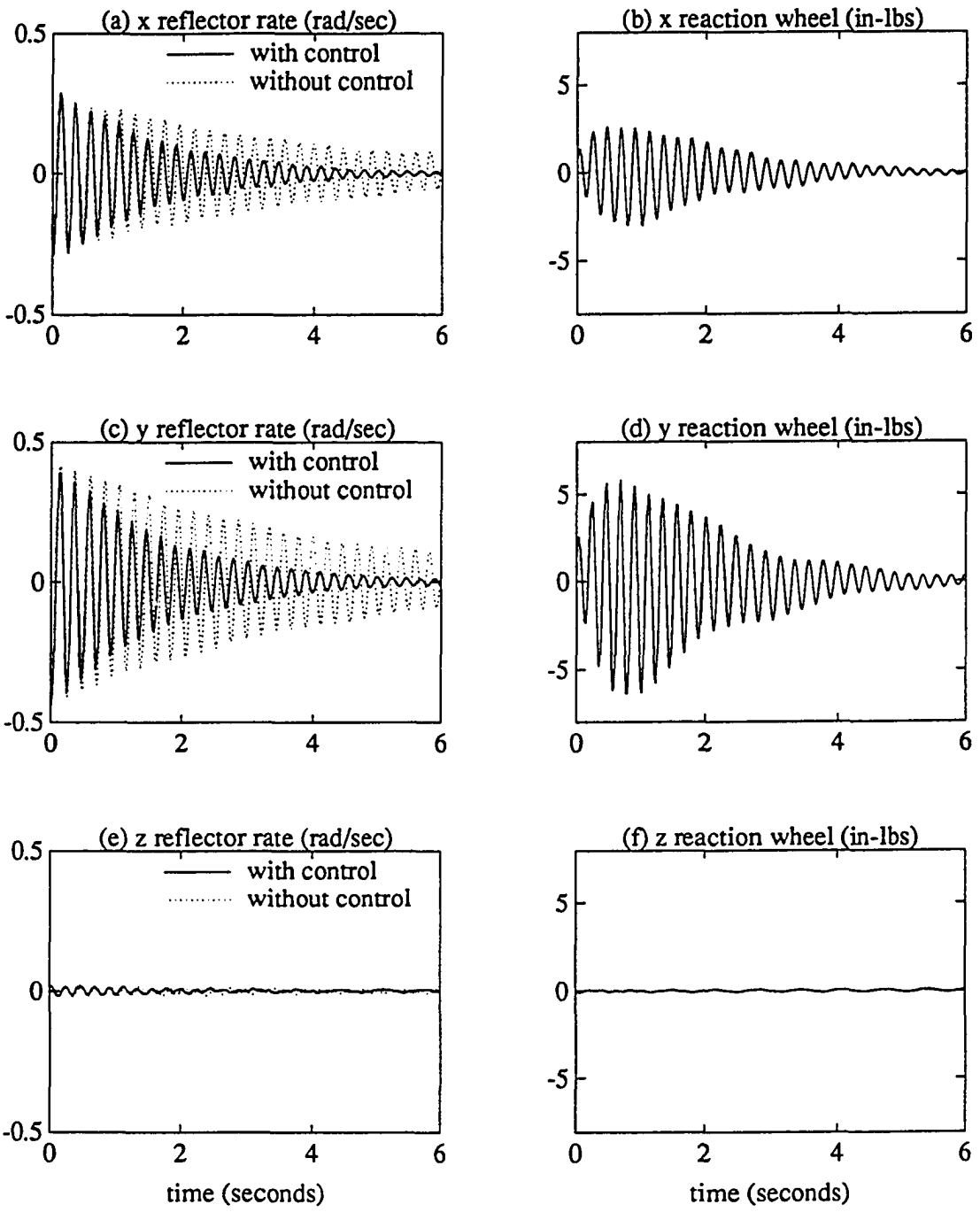

Figure 4.5 Experimental result of mode 5 excitation.

Chapter 5

NASA LAMSTF CONFIGURATION

5.1 Introduction

In this chapter the Large Angle Magnetic Suspension Test Facility (LAMSTF) is introduced and used as the example for the closed-loop identification presented in Chapter 6 and the iterative LQG controller design in Chapter 7. This facility has been assembled by NASA Langley Research Center for a ground-based experiment that can be used to investigate the technology issues associated with magnetic suspension at large gaps, accurate suspended-element control at large gaps, and accurate position sensing at large gaps. This technology is applicable to future efforts that range from magnetic suspension of wind-tunnel models to advanced spacecraft experiment isolation and pointing systems[37].

This facility basically consists of five electromagnets (see Figure 5.1) which actively suspend a small cylindrical permanent magnet. The cylinder is a rigid body and has six independent degrees of freedom, namely, three displacements (x, y and z) and three rotations (pitch, yaw and roll). The roll of the cylinder is uncontrollable and is assumed to be motionless. Five pairs of LEDs and photo detectors are used to indirectly sense the pitch

and yaw angles, and three displacements of the cylinder's centroid. The inputs consist of five currents into five electromagnets and the outputs are five voltage (position) signals from the five photo detectors. Very briefly, the currents into the electromagnets generate a magnetic field which produces a net force and torque on the suspended cylinder.

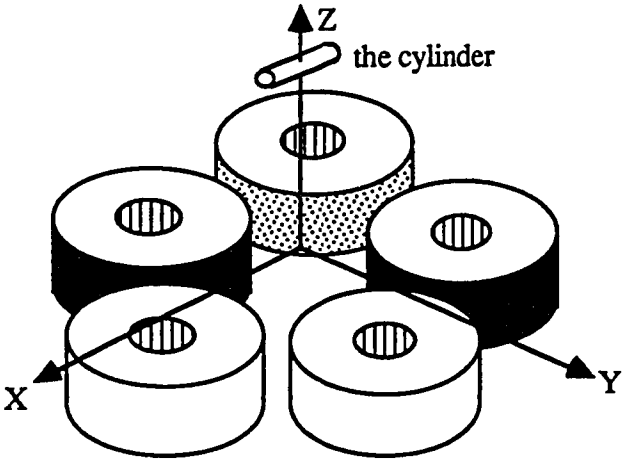

Figure 5.1 Large-Angle Magnetic Suspension Test Facility (LAMSTF) configuration.

The details of the suspended cylinder, the coils, power amplifiers, and the position sensors are described in the following sections[38]. The mathematical model of this system has been derived in detail in References 39 and 40. Only the final system matrices will be provided in the later section.

5.2 Suspended Cylinder

The suspended cylinder is an aluminum tube filled with 16 wafers of Neodymium-Iron-Boron permanent magnet material. The aluminum tube is about 5.32 cm long and 0.525 cm outside diameter. The wafers are arranged in N-S-N-S sequence and are epoxied. Each magnetic wafer is 0.7963 cm in diameter and 0.3135 cm long, having a magnetization of

about 9.5493×10^{-5} A/m. The suspended cylinder will be put at a height of about 10 cm above the coils.

5.3 Coils and Power Amplifiers

There are five coils mounted on the circumference of a circle of about 13.77 cm radius, at a spacing of 72° apart, on a 1/2" thick, square aluminum plate. The coils are made of 509 turns of AWG 10 enameled copper wire wound on bakelite spools, with soft iron cores. The windings on the coils are covered with epoxy resin to reduce deformity due to high current forces. The currents through the coils are controlled by five switching power amplifiers, capable of delivering a maximum of 30A continuous and 60A peak level. The amplifiers have a switching frequency of 22 kHz, and require a D.C. supply of 150V. The amplifiers function in a voltage-to-current converter mode and are set in a gain of 3 A/V to have a flat response. From the Bode plot of the current, it is found that the -3dB frequency is about 200 Hz. The coils cannot adequately dissipate the thermal energy generated in them due to their internal resistances. To protect against thermal runaway, each coil has been equipped with a temperature sensing device, which is monitored by a set of five digital temperature controllers. The temperature controllers are set to disable the power amplifiers at 160° F.

5.4 Position Sensors

The detection of the suspended cylinder's position is performed by five sets of infrared LEDs and photo detectors. These LED-photodetector pairs are installed in two perpendicular planes (vertical and horizontal), which allow detection of five degrees-of-freedom of the cylinder (see Figure 5.2). The beams from the infrared LEDs, which are

incident on the photo detectors, would be partially blocked by the cylinder. The relative position of the cylinder can then be determined from the amount of light received by the photo detectors. This method is common in wind tunnel magnetic suspension applications and has been quite successful. From Figure 5.2, one can realize that pairs 1 and 3 are used to detect the pitch angular and z displacements. Pair 2 is used to detect the x displacement. Pairs 4 and 5 are used to detect the yaw angular and y displacements. The linear range of the sensors is found to be about ±1° for pitch and yaw and ±0.5 mm for x, y, and z axes.

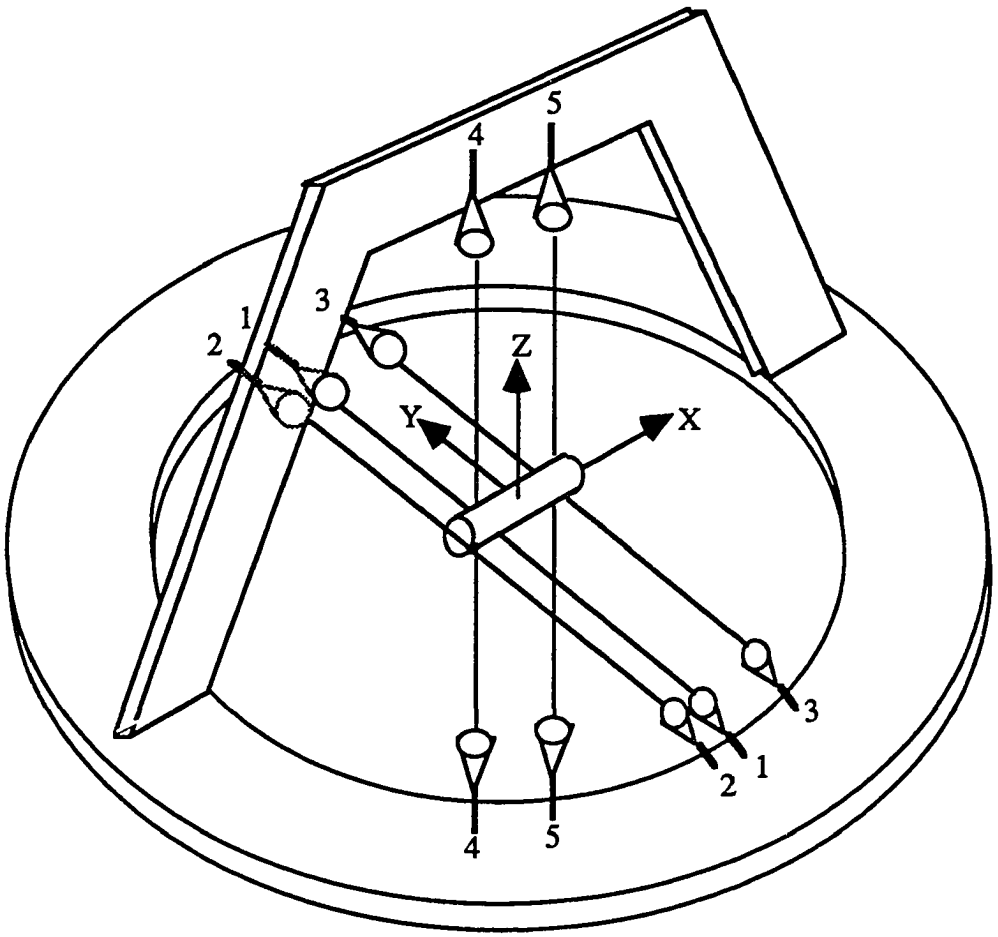

Figure 5.2 Position sensors of the cylinder.

5.5 System Modeling

The analytical model of this system has been derived in detail in References 39 and 40. This model can be obtained by combining two equations. One is the equation of motion for the cylinder dynamics. The other is the equation which relates the magnetic force and torque on the cylinder generated by the currents of the coils. Both equations are non-linear. After linearizing both equations and excluding the bias inputs for overcoming the weight of the cylinder, one has the state-space model:

$$\dot{x} = A_m x + B_m u \tag{5.1}$$

$$y = C_m x \tag{5.2}$$

where $x = \begin{Bmatrix} x_p \\ \dot{x}_p \end{Bmatrix}$, $A_m = \begin{bmatrix} 0_{5\times5} & I_{5\times5} \\ A_{21} & A_{22} \end{bmatrix}$, $B_m = \begin{bmatrix} 0_{5\times5} \\ B_2 \end{bmatrix}$ and $C_m = [C_1 \quad 0_{5\times5}]$. The state variable x_p includes pitch and yaw angles and three linear displacements of the cylinder's centroid. The matrices A_{21}, A_{22}, B_2 and C_1 are

$$A_{21} = \begin{bmatrix} 3341.5 & 0 & -39392 & 0.0000 & 0.0000 \\ 0 & 3341.5 & -0.0000 & 0.0000 & -0.0000 \\ -9.8070 & -0.0000 & 49.937 & 0.0000 & -0.0251 \\ -0.0000 & 0.0000 & 0.0000 & 95.577 & -0.0000 \\ -0.0000 & -0.0000 & -0.0251 & -0.0000 & -0.9132 \end{bmatrix},$$

$$A_{22} = 0_{5\times5},$$

$$B_2 = \begin{bmatrix} 38.370 & 38.370 & 38.370 & 38.370 & 38.370 \\ 0 & 89.802 & 55.514 & -55.514 & -89.802 \\ 0.2214 & -0.1527 & 0.0785 & 0.0785 & -0.1527 \\ 0 & 0.1215 & -0.1967 & 0.1967 & -0.1215 \\ -0.2767 & -0.0855 & 0.2239 & 0.2239 & -0.0855 \end{bmatrix}$$

$$C_1 = \begin{bmatrix} 89.024 & 0 & 0 & 0 & 6097.6 \\ 0 & 0 & 7874.0 & 0 & 0 \\ -116.25 & 0 & 0 & 0 & 6250.0 \\ 0 & 95.425 & 0 & -6535.9 & 0 \\ 0 & -107.25 & 0 & -5181.3 & 0 \end{bmatrix}.$$

The eigenvalues of the system matrix A_m are listed in Table 5.1. The corresponding mode shapes are shown in Figure 5.3. As shown, three modes are unstable, and the other two are marginally stable. The matrix C_1 which relates the sensor output voltage to the displacement can be obtained from calibration and is assumed to be deterministic. To recover the displacement from the sensor output voltage, one can use $x_p = C_1^{-1} y$.

5.6 Concluding Remarks

The NASA LAMSTF configuration has been described. The analytical model has been derived in detail in References 39 and 40. From open-loop eigenvalues, it has been found that there are three unstable modes and two stable oscillatory modes. Because it is difficult to accurately model the magnetic field and its gradients, the analytical model contains some modeling errors. Since the system is unstable, bounded input/output data can be obtained only from closed-loop operation. Closed-loop identification is thus required to validate this model and is presented in the next chapter. The process noise may include temperature effects on the coils, inevitable electrical noise, and error of the bias inputs used to overcome the gravity of the cylinder. The measurement noise is caused by the non-linearity and saturation of the sensors and inevitable electrical noise. The existence of the modeling errors, process noise, and measurement noise motivates the use of the iterative LQG controller design presented in Chapter 7.

Table 5.1 Open loop modes of the suspended cylinder.

mode #	eigenvalues	stability	degree of freedom
1	±58.78	unstable	x, θ_y (axial, pitch)
2	$\pm j7.97$	stable oscillatory	x, θ_y (axial, pitch)
3	±57.81	unstable	θ_z (yaw)
4	$\pm j0.96$	stable oscillatory	z (vertical)
5	±9.78	unstable	y (lateral)

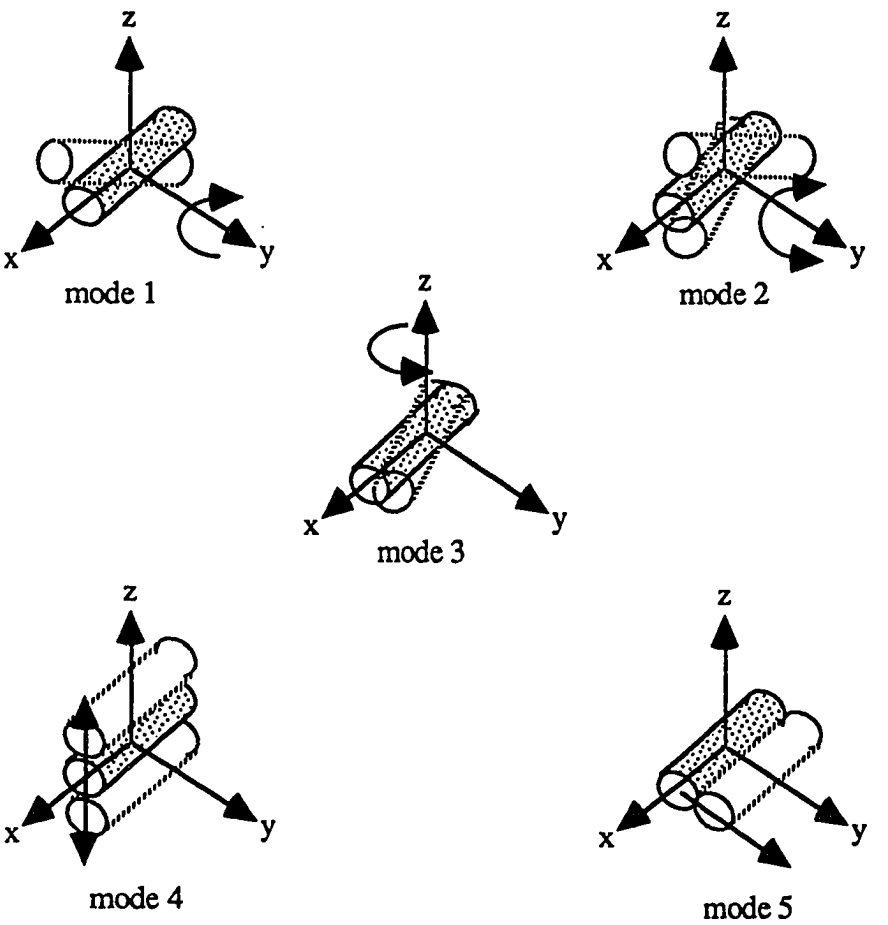

Figure 5.3 Mode shapes of LAMSTF configuration from analytical model.

Chapter 6

CLOSED-LOOP IDENTIFICATION

6.1 Introduction

In this chapter the derivation of the closed-loop identification is given. The closed-loop identification can simultaneously identify the open-loop state-space model of a system and the corresponding Kalman filter when the system is under closed-loop operation. To accomplish this, the relation between closed-loop state-space and AutoRegressive with eXogeneous (ARX) models for stochastic systems is first derived. From the derivation, it can be seen that a state-space model can be represented by an ARX model if the order of the ARX model is chosen large enough. Since the relation between the input/output data and the system parameters of an ARX model is linear, a linear programming approach such as least-square methods can be used for the ARX model parameter estimation. Second, an algorithm is derived to compute the open-loop system and Kalman filter Markov parameters from the estimated ARX model parameters. In this step, the closed-loop system and Kalman filter Markov parameters are first computed from the estimated ARX model parameters, and the open-loop system and Kalman filter Markov parameters are then computed from the closed-loop system and Kalman filter Markov parameters with known

controller Markov parameters. Third, the state-space model for the open-loop system is realized from the open-loop Markov parameters through the singular value decomposition method. Finally, the Kalman filter for the open-loop system can be estimated from the realized state-space model and the open-loop Kalman filter Markov parameters through a least-square approach.

Most existing system identification methods[6-12] apply for stable systems without requiring feedback control for identification purpose. For identifying marginally stable or unstable systems, feedback control is required to ensure overall system stability. These methods still can be applied by using the bounded *open-loop* input/output data obtained during closed-loop operation. However, it is generally harder to identify the open-loop system from the open-loop input/output data because it is difficult to ensure that the input signal to the plant has sufficient frequency richness to excite all of the system's dynamics. The method developed in this dissertation can identify a linear open-loop stochastic system from *closed-loop* input-output data in the time domain without recording feedback signals. This method can be applied to some other cases when a system, although stable, is operated in closed-loop and when it is impossible to remove the existing feedback controller for open-loop identification. Additionally, whether the system is stable or not, the feedback controller can be used as a design parameter for system identification. One may choose a controller to enhance the damping and thus shorten the closed-loop input/output data required for identification.

In the proposed method, the identification of an open-loop stochastic system by using a known dynamic output feedback controller is formulated. A similar approach was presented in References 16 and 17. However, it applied to *deterministic* systems only, and thus the optimal Kalman filter gain used for an estimator could not be identified. In Reference 16, no recursive form was derived for computing open-loop system dynamics. In Reference 17, the approach is based on system pulse response. In the proposed method, the

recursive form for computing the open-loop system and Kalman filter Markov parameters from the closed-loop system Markov parameters, the closed-loop Kalman filter Markov parameters, and the known controller Markov parameters is derived for *stochastic* systems with *random* excitation. Generally speaking, random excitation provides better result of identification than pulse input because part of noise from random excitation response can be removed through the least-squares method. The open-loop system can be realized from the calculated open-loop system Markov parameters. The method can also estimate the Kalman filter gain directly without estimating noise covariances. Like other direct approaches[41], it is simple in theory, has fewer parameters to estimate, and can prevent the problem of non-uniqueness in estimating process noise covariance.

Next, a special case with constant-gain full-state feedback controller is presented. A simpler identification procedure is described. Then a matrix is introduced to transform the identified state-space model from any arbitrary coordinate to the physical coordinate so that the identified system parameters can be compared to the analytical one. Finally, the example of identifying NASA LAMSTF system is provided with numerical simulations and experimental data to illustrate the proposed closed-loop identification method. There are several adjustable parameters in the closed-loop identification, the effect of these parameters to the identification accuracy is also discussed.

6.2 Closed-loop State-space and ARX Models Relationship

Since the relation between the input/output data and the model parameters of a state-space model is nonlinear, parameter estimation of a state-space model from input/output data is a nonlinear programming problem. Nonlinear programming is difficult to solve in general and involves complex iterative numerical methods. The convergence and uniqueness of the solution are also not guaranteed. Unlike a state-space model, the

AutoRegressive with eXogeneous input (ARX) model has a linear relationship between its model parameters and input/output data. Therefore, linear programming can be used for identifying the ARX model in a short time. After obtaining the ARX model, the state-space model can be computed based on the relation between these two models. In this section, the relation between a closed-loop state-space and an ARX model is derived by using z-transforms.

A finite-dimensional, linear, discrete-time, time-invariant system can be modeled as:

$$x_{k+1} = Ax_k + Bu_k + w_k \tag{6.1}$$

$$y_k = Cx_k + v_k. \tag{6.2}$$

where $x \in R^{n\times 1}$, $u \in R^{s\times 1}$, $y \in R^{m\times 1}$ are state, input and output vectors, respectively; w_k is the process noise, v_k the measurement noise; $[A,\ B,\ C]$ are the state-space parameters. Sequences w_k and v_k are assumed gaussian, white, zero-mean, and stationary with covariance matrices W and V respectively. One can derive a steady-state filter innovation model[42] presented in Section 2.4:

$$\hat{x}_{k+1} = A\hat{x}_k + Bu_k + AK\varepsilon_k \tag{6.3}$$

$$y_k = C\hat{x}_k + \varepsilon_k. \tag{6.4}$$

where $\hat{x}_k$ is the a priori estimated state, K is the steady-state Kalman filter gain and ε_k is the residual after filtering: $\varepsilon_k = y_k - C\hat{x}_k$. The existence of K is guaranteed if the system is detectable and $(A, W^{1/2})$ is stabilizable[43].

On the other hand, any kind of dynamic output feedback controller can be modeled as:

$$p_{k+1} = A_d p_k + B_d y_k \tag{6.5}$$

$$u_k = C_d p_k + D_d y_k + r_k, \tag{6.6}$$

where A_d, B_d, C_d, and D_d are the system matrices of the dynamic output feedback controller, p_k the controller state and r_k the reference input to the closed-loop system. Combining (6.3) to (6.6), the augmented closed-loop system dynamics becomes

$$\eta_{k+1} = A_c\eta_k + B_c r_k + A_c K_c \varepsilon_k \tag{6.7}$$

$$y_k = C_c\eta_k + \varepsilon_k, \tag{6.8}$$

where

$$\eta_k = \begin{bmatrix} \hat{x}_k \\ p_k \end{bmatrix}, A_c = \begin{bmatrix} A + BD_dC & BC_d \\ B_dC & A_d \end{bmatrix}, B_c = \begin{bmatrix} B \\ 0 \end{bmatrix},$$

$$A_cK_c = \begin{bmatrix} AK + BD_d \\ B_d \end{bmatrix}, \text{and } C_c = [C \quad 0]. \tag{6.9}$$

It is noted that K_c can be considered as the Kalman filter gain for the closed-loop system and the existence of the steady-state K_c is guaranteed when the closed-loop system matrix A_c is nonsingular. The advantage of using the filter innovation model (6.3) and (6.4) instead of the realistic model (6.1) and (6.2) in the closed-loop identification is that one can directly identify the Kalman filter gain without estimating the covariance matrices of both process and measurement noise which usually are difficult to obtain from test data. Substituting (6.8) into (6.7) yields

$$\eta_{k+1} = \bar{A}\eta_k + B_c r_k + A_c K_c y_k, \tag{6.10}$$

where $\bar{A} = A_c - A_cK_cC_c$ and is guaranteed to be asymptotically stable because the steady-state Kalman filter gain K_c exists. The z-transform of (6.10) and (6.8) yields

$$\eta(z) = (z - \bar{A})^{-1}(A_cK_cy(z) + B_cr(z)) \tag{6.11}$$

$$y(z) = C_c\eta(z) + \varepsilon(z). \tag{6.12}$$

Substituting (6.11) into (6.12), one has

$$y(z) = C_c(z - \bar{A})^{-1}(A_cK_cy(z) + B_cr(z)) + \varepsilon(z). \tag{6.13}$$

The inverse z-transform of (6.13) with $(z-\overline{A})^{-1} = \sum_{i=1}^{\infty} \overline{A}^{i-1} z^{-i}$ yields

$$y_k = \sum_{i=1}^{\infty} C_c \overline{A}^{i-1} A_c K_c y_{k-i} + \sum_{i=1}^{\infty} C_c \overline{A}^{i-1} B_c r_{k-i} + \varepsilon_k. \tag{6.14}$$

Since $\overline{A}$ is asymptotically stable, $\overline{A}^i \approx 0$ if $i > q$ for a sufficient large number q (discussed in Ref. 8). Thus (6.14) becomes

$$y_k \approx \sum_{i=1}^{q} a_i y_{k-i} + \sum_{i=1}^{q} b_i r_{k-i} + \varepsilon_k,$$

or in matrix form

$$y_k \approx \begin{bmatrix} a_1 & b_1 & \cdots & a_q & b_q \end{bmatrix} \begin{bmatrix} y_{k-1} \\ r_{k-1} \\ \vdots \\ y_{k-q} \\ r_{k-q} \end{bmatrix} + \varepsilon_k,$$

or

$$y_k^T \approx \begin{bmatrix} y_{k-1}^T & r_{k-1}^T & \cdots & y_{k-q}^T & r_{k-q}^T \end{bmatrix} \begin{bmatrix} a_1 & b_1 & \cdots & a_q & b_q \end{bmatrix}^T + \varepsilon_k, \tag{6.15}$$

where

$$a_i = C_c \overline{A}^{i-1} A_c K_c,\ b_i = C_c \overline{A}^{i-1} B_c. \tag{6.16}$$

The model described by (6.15) is the so called ARX model.

6.3 Parameter Estimation of ARX Model

The model described by (6.15) is the ARX model which directly represents the relationship between the input and output of the closed-loop system. The coefficient matrices a_i and b_i can be estimated through least-squares methods from random excitation input r_k and the corresponding output y_k. The least-squares methods include the batch type and the recursive type. For a large number of the closed-loop input/output data, the

recursive least-square method is required to avoid memory problems. From (6.15), one can form the least-squares problem $\xi = \Phi\theta$ for l data points by neglecting the residual ε_k, where

$$\Phi = \begin{bmatrix} y_q^T & r_q^T & y_{q-1}^T & r_{q-1}^T & \cdots & y_1^T & r_1^T \\ y_{q+1}^T & r_{q+1}^T & y_q^T & r_q^T & \cdots & y_2^T & r_2^T \\ \vdots & \vdots & \vdots & \vdots & \ddots & \vdots & \vdots \\ y_{l-1}^T & r_{l-1}^T & y_{l-2}^T & r_{l-2}^T & \cdots & y_{l-q}^T & r_{l-q}^T \end{bmatrix},$$

$$\xi = [y_{q+1} \quad y_{q+2} \quad \cdots \quad y_l]^T,$$

$$\theta = [a_1 \quad b_1 \quad a_2 \quad b_2 \quad \cdots \quad a_q \quad b_q]^T.$$

The integer l has to be chosen large enough so that the matrix Φ has more rows than columns. The batch least-square solution is

$$\theta = (\Phi^T\Phi)^{-1}\Phi^T\xi. \tag{6.17}$$

From (6.17) it can be seen that parameters of the ARX model are linearly related to the closed-loop input-output data. Therefore, solving for an ARX model involves solving a linear programming problem involving an over determined set of equations.

6.4 Markov Parameters

In the previous section, an ARX model, which represents a closed-loop system, is identified from the closed-loop input/output data through the least-squares method. With the known controller dynamics, the estimated ARX model can be transformed to an open-loop state-space model by the following steps. First, the closed-loop system and Kalman filter Markov parameters are calculated from the estimated coefficient matrices of the ARX model. Second, the open-loop system and Kalman filter Markov parameters are derived from the closed-loop system Markov parameters, the closed-loop Kalman filter Markov parameters, and the known controller Markov parameters. Third, the open-loop state-space

model is realized by using singular-value decomposition for a Hankel matrix formed by the open-loop system Markov parameters. Finally, an open-loop Kalman filter gain is calculated from the realized state-space model and the open-loop Kalman filter Markov parameters through least-squares.

The z-transform of the open-loop state-space model (6.3) yields

$$\hat{x}(z) = (z - A)^{-1}(Bu(z) + AK\varepsilon(z)). \tag{6.18}$$

Substituting (6.18) to the z-transform of (6.4), one has

$$y(z) = C(z - A)^{-1}(Bu(z) + AK\varepsilon(z)) + \varepsilon(z) = \sum_{k=1}^{\infty} Y(k)z^{-k}u(z) + \sum_{k=0}^{\infty} N(k)z^{-k}\varepsilon(z), \tag{6.19}$$

where $Y(k) = CA^{k-1}B$ is the open-loop system Markov parameter, $N(k) = CA^{k-1}AK$ open-loop Kalman filter Markov parameter, and $N(0) = I$ which is an identity matrix. Similarly, for the dynamic output feedback controller (6.5) and (6.6) and the closed-loop state-space model (6.7) and (6.8), one can derive

$$u(z) = \sum_{k=0}^{\infty} Y_d(k)z^{-k}y(z) + r(z) \tag{6.20}$$

$$y(z) = \sum_{k=1}^{\infty} Y_c(k)z^{-k}r(z) + \sum_{k=0}^{\infty} N_c(k)z^{-k}\varepsilon(z), \tag{6.21}$$

where $Y_d(0) = D_d$ and $Y_d(k) = C_d A_d^{k-1} B_d$ are the controller Markov parameters, $Y_c(k) = C_c A_c^{k-1} B_c$ the closed-loop system Markov parameter, and $N_c(k) = C_c A_c^{k-1} A_c K_c$ the closed-loop Kalman filter Markov parameters ($k = 1,2,\cdots,\infty$). It is also noted that $N_c(0) = I$.

6.4.1 Closed-loop System and Kalman Filter Markov Parameters

The z-transform of the ARX model (6.15) yields

$$\left(I-\sum_{i=1}^{q}a_i z^{-i}\right)y(z)=\sum_{i=1}^{q}b_i z^{-i}r(z)+\varepsilon(z). \tag{6.22}$$

Applying long division to (6.22), one has

$$\begin{aligned}y(z)=&[b_1z^{-1}+(b_2+a_1b_1)z^{-2}+(b_3+a_1(b_2+a_1b_1)+a_2b_1)z^{-3}+\ldots]r(z)\\&+[I+a_1z^{-1}+(a_1a_1+a_2)z^{-2}+(a_1(a_1a_1+a_2)+a_2a_1+a_3)z^{-3}+\ldots]\varepsilon(z).\end{aligned}$$

After comparing with (6.21), the closed-loop system and Kalman filter Markov parameters can be recursively calculated from the estimated coefficient matrices of the ARX model,

$$Y_c(k)=b_k+\sum_{i=1}^{k}a_iY_c(k-i),\quad k=1,2,\cdots,\infty \tag{6.23}$$

$$N_c(k)=\sum_{i=1}^{k}a_iN_c(k-i),\qquad k=1,2,\cdots,\infty. \tag{6.24}$$

It is noted that $Y_c(0)=0$, $N_c(0)=I$, and $a_i=b_i=0$, when $i>q$. One may obtain (6.23) and (6.24) from (6.16) and the definition of the Markov parameters.[9,10] However, the derivation is much more complex.

6.4.2 Open-loop System and Kalman Filter Markov Parameters

Next, the open-loop system and Kalman filter Markov parameters can be derived from the closed-loop system Markov parameters, the closed-loop Kalman filter Markov parameters, and the known controller Markov parameters. Substituting (6.20) into (6.19) yields

$$y(z)=\left(\sum_{k=1}^{\infty}Y(k)z^{-k}\right)\left(\sum_{k=0}^{\infty}Y_d(k)z^{-k}y(z)\right)+\sum_{k=1}^{\infty}Y(k)z^{-k}r(z)+\sum_{k=0}^{\infty}N(k)z^{-k}\varepsilon(z)$$

$$= \sum_{k=1}^{\infty} \alpha_k z^{-k} y(z) + \sum_{k=1}^{\infty} Y(k) z^{-k} r(z) + \sum_{k=0}^{\infty} N(k) z^{-k} \varepsilon(z), \tag{6.25}$$

where $\alpha_k = \sum_{i=1}^{k} Y(i) Y_d(k-i)$. Rearranging (6.25), one has

$$\left(I - \sum_{k=1}^{\infty} \alpha_k z^{-k} \right) y(z) = \sum_{k=1}^{\infty} Y(k) z^{-k} r(z) + \sum_{k=0}^{\infty} N(k) z^{-k} \varepsilon(z). \tag{6.26}$$

Similarly, one can apply long division to (6.26), and then compare it with (6.21), to describe the closed-loop system Markov parameters recursively in terms of the open-loop system and the controller Markov parameters,

$$Y_c(j) = Y(j) + \sum_{k=1}^{j} \alpha_k Y_c(j-k) = Y(j) + \sum_{k=1}^{j} \sum_{i=1}^{k} Y(i) Y_d(k-i) Y_c(j-k). \tag{6.27}$$

Similarly, the closed-loop Kalman filter Markov parameters can be recursively expressed in terms of the open-loop system Markov parameters, the open-loop Kalman filter Markov parameters, and the controller Markov parameters,

$$N_c(j) = N(j) + \sum_{k=1}^{j} \alpha_k N_c(j-k) = N(j) + \sum_{k=1}^{j} \sum_{i=1}^{k} Y(i) Y_d(k-i) N_c(j-k). \tag{6.28}$$

Rearranging (6.27) and (6.28), one has

$$Y(j) = Y_c(j) - \sum_{k=1}^{j} \sum_{i=1}^{k} Y(i) Y_d(k-i) Y_c(j-k) \tag{6.29}$$

$$N(j) = N_c(j) - \sum_{k=1}^{j} \sum_{i=1}^{k} Y(i) Y_d(k-i) N_c(j-k). \tag{6.30}$$

Equations (6.29) and (6.30) show that one can recursively calculate the open-loop system and Kalman filter Markov parameters from the closed-loop system Markov parameters (from (6.23)), the closed-loop Kalman filter Markov parameters (from (6.24)), and the known controller Markov parameters $Y_d(k) = C_d A_d^{k-1} B_d$. It is noted that $Y_c(0) = 0$ and $N_c(0) = I$. One can easily verify (6.29) and (6.30) from (6.9), and also from the definition of the Markov parameters.

6.5 State-space Realization

The open-loop state-space model can be realized from the open-loop system Markov parameters through the Singular Value Decomposition (SVD) method[44,45]. The first step is to form a Hankel matrix from the open-loop system Markov parameters,

$$H(j)=\begin{bmatrix} Y(j) & Y(j+1) & \cdots & Y(j+\beta) \\ Y(j+1) & Y(j+2) & \cdots & Y(j+\beta+1) \\ \vdots & \vdots & \ddots & \vdots \\ Y(j+\gamma) & Y(j+\gamma+1) & \cdots & Y(j+\gamma+\beta) \end{bmatrix}, \tag{6.31}$$

where $Y(j)$ is the j-th Markov parameter. From the measurement Hankel matrix, the realization uses the SVD of $H(1)$, $H(1)=U\Sigma V^T$, to identify a n-th order discrete state-space model as

$$A=\Sigma_n^{-1/2}U_n^T H(2)V_n\Sigma_n^{-1/2},\ B=\Sigma_n^{1/2}V_n^T E_s,\ C=E_m^T U_n\Sigma_n^{1/2}, \tag{6.32}$$

where matrix Σ_n is the upper left hand $n\times n$ partition of Σ containing the n largest singular values along the diagonal. Matrices U_n and V_n are obtained from U and V by retaining only the n columns of singular vectors associated with the n singular values. Matrix E_m is a matrix of appropriate dimension having m columns, all zero except that the top $m\times m$ partition is an identity matrix. E_s is defined similarly.

6.6 Open-loop Kalman Filter Gain

Once the open-loop A and C are obtained, one can easily calculate the open-loop Kalman filter gain from the open-loop Kalman filter Markov parameters $N(k)$ in a least-squares sense as follows

$$K=(O^TO)^{-1}O^T\begin{bmatrix} N(1) \\ : \\ N(k) \end{bmatrix},\ \text{where } O=\begin{bmatrix} CA \\ : \\ CA^k \end{bmatrix}. \tag{6.33}$$

The integer k has to be chosen large enough so that the matrix O has more rows that columns. The identified Kalman filter gain can be used directly for state estimation.

6.7 Identification with Output Feedback

This section summarizes the procedure for identifying an open-loop state-space model from closed-loop input/output data with a known dynamic output feedback controller.

1. Estimate the coefficient matrices of the ARX model from closed-loop input/output data by using (6.17).
2. Compute the closed-loop system and Kalman filter Markov parameters from the estimated coefficient matrices of the ARX model by using (6.23) and (6.24), respectively.
3. Compute the open-loop system and Kalman filter Markov parameters from the closed-loop system Markov parameters, the closed-loop Kalman filter Markov parameters, and the controller Markov parameters calculated from the known controller dynamics, by using (6.29) and (6.30), respectively.
4. Realize the open-loop system matrices from the open-loop system Markov parameters by using (6.31) and (6.32).
5. Estimate the open-loop Kalman filter gain from the open-loop Kalman filter Markov parameters and the realized system matrices by using (6.33).

6.8 Identification with Full-state Feedback

In this section, the above closed-loop identification problem is considered for a particular case. If a constant-gain full-state feedback controller is used, the open-loop system can be identified by following a simpler procedure. An open-loop system with a full-state sensor and a constant gain full-state feedback controller can be modeled as:

$$x_{k+1} = Ax_k + Bu_k + w_k \tag{6.34}$$

$$y_k = x_k + v_k \tag{6.35}$$

$$u_k = -Fy_k + r_k, \tag{6.36}$$

where F is the known constant feedback gain and r_k is the reference input to the closed-loop system. After applying filter innovation model[42] to the open-loop system and eliminating control input u_k, the closed-loop system becomes

$$\hat{x}_{k+1} = (A - BF)\hat{x}_k + Br_k + (AK - BF)\varepsilon_k \tag{6.37}$$

$$y_k = \hat{x}_k + \varepsilon_k. \tag{6.38}$$

Comparing (6.37) and (6.38) with (6.7) and (6.8), one can have $\eta_k = \hat{x}_k$, $A_c = A - BF$, $B_c = B$, $A_cK_c = AK - BF$, and $C_c = I$. Then one can use (6.17), (6.23), (6.24), (6.31), (6.32) and (6.33) to identify the *closed-loop* system matrices and Kalman filter gain. If the *identified* closed-loop system matrices and Kalman filter gain are described by a quadruplet, $[\hat{A}_c, \hat{B}_c, \hat{C}_c, \hat{A}_c\hat{K}_c]$, one needs to transform it to the same coordinate used in (6.37) and (6.38), so that the controller dynamics can be removed from the closed-loop system. Since full-state feedback is used, the identified output matrix $\hat{C}_c$ is a square matrix, and is generally invertable. Then one may use $\hat{C}_c^{-1}$ as the transformation matrix to transform the identified quadruplet to be $[\hat{C}_c\hat{A}_c\hat{C}_c^{-1}, \hat{C}_c\hat{B}_c, I, \hat{C}_c\hat{A}_c\hat{K}_c]$ where I is an identity matrix. Comparing the transformed quadruplet with (6.37) and (6.38), on can easily obtain

$$A - BF = \hat{C}_c\hat{A}_c\hat{C}_c^{-1},\ B = \hat{C}_c\hat{B}_c,\ AK - BF = \hat{C}_c\hat{A}_c\hat{K}_c. \tag{6.39}$$

The identified open-loop system matrices and Kalman filter gain become

$$A = \hat{C}_c \hat{A}_c \hat{C}_c^{-1} + \hat{C}_c \hat{B}_c F,\ B = \hat{C}_c \hat{B}_c, C = I,\ K = A^{-1}(\hat{C}_c \hat{A}_c \hat{K}_c + BF). \tag{6.40}$$

If sensors are available to provide all the state information, one can choose a constant-gain controller (e.g. a pole-placement controller or a Linear Quadratic Regulator (LQR)) so that the closed-loop system has the same dimension as the open-loop system. This controller can be designed (e.g. by adjusting the weighting matrices in the LQR controller) so that the closed-loop system is very easy to identify. For example, a closed-loop system with poles located evenly within a desired frequency range with similar damping ratios between 0.4 to 0.7 may be easily identified.

6.9 Coordinate Transformation

For any dynamic system, although its system Markov parameter is unique, the realized state-space model is not unique. If one needs to compare the identified state-space model with the analytical model, both models have to be in the same coordinate. In this section, a unique transformation matrix is derived to transform any realized state-space model to be in a form usually used for a structural dynamic system, so that any identified system parameter can be compared with the corresponding analytical one. This unique transformation matrix exists only when one half of the states can be measured directly. If this condition is not satisfied, other transformation matrices may exist, but they usually are not unique.

Consider a structural dynamic system

$$M\ddot{p} + D\dot{p} + Kp = Gu \tag{6.41}$$

where p is the displacement, u the control force, G the control influence matrix and M, D and K are the mass, damping, and stiffness matrices, respectively. One can have the state-space equation and output equation,

$$\dot{x} = A_m x + B_m u, \text{ and } y = C_m x, \tag{6.42}$$

where $A_m = \begin{bmatrix} 0 & I \\ -M^{-1}K & -M^{-1}D \end{bmatrix}$, $B_m = \begin{bmatrix} 0 \\ M^{-1}G \end{bmatrix}$, C_m is the output matrix and $x = \begin{Bmatrix} p \\ \dot{p} \end{Bmatrix}$. If it is assumed that the displacement can be measured, one can have $C_m = [I \quad 0]$. Now, one may first convert the realized discrete-time system $[A,B,C]$ to a continuous-time system $[A_s,B_s,C]$. If A is diagonalized by matrix Φ, then

$$\Phi^{-1}A\Phi = \Lambda \tag{6.43}$$

$$A_s = \Phi \frac{\ln(\Lambda)}{T} \Phi^{-1} \tag{6.44}$$

$$B_s = (A - I)^{-1} A_s B \tag{6.45}$$

where T is the sampling time. It is assumed that the matrix $\begin{bmatrix} C \\ CA_s \end{bmatrix}$ is full rank. Let the transformation matrix

$$P = [P_1 \quad P_2] = \begin{bmatrix} C \\ CA_s \end{bmatrix}^{-1}, \tag{6.46}$$

then

$$P^{-1}P = \begin{bmatrix} C \\ CA_s \end{bmatrix} [P_1 \quad P_2] = \begin{bmatrix} CP_1 & CP_2 \\ CA_sP_1 & CA_sP_2 \end{bmatrix} = \begin{bmatrix} I & 0 \\ 0 & I \end{bmatrix}, \tag{6.47}$$

$$P^{-1}A_sP = \begin{bmatrix} CA_sP_1 & CA_sP_2 \\ CA_s^2P_1 & CA_s^2P_2 \end{bmatrix} = \begin{bmatrix} 0 & I \\ X & X \end{bmatrix}, \tag{6.48}$$

$$P^{-1}B_s = \begin{bmatrix} CB_s \\ CA_sB_s \end{bmatrix} = \begin{bmatrix} C_mB_m \\ CA_sB_s \end{bmatrix} = \begin{bmatrix} 0 \\ X \end{bmatrix}, \tag{6.49}$$

$$CP = [CP_1 \quad CP_2] = [I \quad 0]. \tag{6.50}$$

where 0 is a null matrix, I a identity matrix, and X neither null nor identity matrix. Note that $CP = C_m$. As a result, the identified continuous-time model $[A_s,B_s,C]$ can be

transformed to be $\left[P^{-1}A_s P, P^{-1}B_s, CP\right]$ which is in the form of (6.42). Then both identified and analytical model are in the same coordinate, and can be compared.

6.10 Numerical Simulations and Experimental Results

In this section the closed-loop identification is investigated through numerical simulations and experiments by using the LAMSTF as an example. The adjustable parameters of the closed-loop identification include the number of data points, the order of ARX model, and the number of Markov parameters for realization. Those parameters to the accuracy of the identified result are studied. The optimal parameters to acquire an accurate result are then determined and used in the iterative LQG control design.

The analytical model of the LAMSTF system includes two highly unstable modes in about 10 Hz and two low-frequency oscillatory modes in about 1.27 and 0.16 Hz (see Table 6.1). To avoid the aliasing problem, the sampling rate has to be more than two times of the highest frequency (about 10 Hz) of the system. Due to modeling error, however, it is more difficult to design a controller to stabilize the system in a lower sampling rate. One output feedback controller has been tested to be able to stabilize the system in the sampling rate of 400 Hz. This controller is used in both numerical simulations and experiments, being in the form of (6.5) and (6.6) where

$$A_d = 0.2850 I_{5\times 5}$$

$$B_d = \begin{bmatrix} 7.0490e-6 & 0 & -6.8771e-6 & 0 & 0 \\ 0 & 0 & 0 & 6.1850e-6 & -7.8020e-6 \\ 0 & 1.8123e-7 & 0 & 0 & 0 \\ 0 & 0 & 0 & -1.2803e-7 & -1.1391e-7 \\ 1.3111e-7 & 0 & 1.0041e-7 & 0 & 0 \end{bmatrix},$$

$$C_d = \begin{bmatrix} 2.2693e4 & 0 & 2.3448e6 & 0 & -1.6433e6 \\ 2.9422e4 & 1.8450e4 & -1.8973e6 & 1.3099e6 & -5.0817e5 \\ 2.5256e4 & 1.1398e4 & 7.2486e5 & -2.1190e6 & 1.3298e6 \\ 3.5256e4 & -1.1398e4 & 7.2486e5 & 2.1190e6 & 1.3298e6 \\ 2.9422e4 & -1.8450e4 & -1.8973e6 & -1.3099e6 & -5.0817e5 \end{bmatrix},$$

$$D_d = \begin{bmatrix} 9.9724e-2 & -1.1052e0 & 7.1206e-1 & 0 & 0 \\ -3.2968e-1 & 8.9423e-1 & 5.7182e-1 & 1.4605e-1 & 6.9344e-1 \\ -7.8239e-1 & -3.4164e-1 & 1.0836e-1 & -8.2183e-1 & -3.8308e-1 \\ -7.8239e-1 & -3.4164e-1 & 1.0836e-1 & 8.2183e-1 & 3.8303e-1 \\ -3.2958e-1 & 8.9423e-1 & 5.7182e-1 & -1.4605e-1 & -6.9344e-1 \end{bmatrix}.$$

In numerical simulations the noise to signal ratios of the system process and measurement noise are 2% and 1%, respectively. The number of input/output data points is 4000. After the closed-loop identification is performed, the open-loop Markov parameters of the identified model are reconstructed. To evaluate the accuracy of the identified result, the reconstructed Markov parameters are compared with the true ones. Because there are five inputs and five outputs in this system, each open-loop system Markov parameter or each Kalman filter Markov parameter is a five-by-five matrix. To compare two matrices, 2-norm is usually used. Therefore, the error between the first 60 true and reconstructed open-loop system Markov parameters is defined as $\sum_{i=1}^{60} \frac{\left\| \hat{C}\hat{A}^{i-1}\hat{B} - CA^{i-1}B \right\|_2}{\left\| CA^{i-1}B \right\|_2}$ where the head $\wedge$ denotes the reconstructed ones. Similarly, the error between the first 60 true and reconstructed open-loop Kalman filter Markov parameters is defined as $\sum_{i=1}^{60} \frac{\left\| \hat{C}\hat{A}^{i-1}\hat{A}\hat{K} - CA^{i-1}AK \right\|_2}{\left\| CA^{i-1}AK \right\|_2}$ where the head $\wedge$ denotes the reconstructed ones. Figure 6.1 shows the error percentage of the open-loop system and Kalman Markov parameters versus the order of the ARX model. As shown, the error for both open-loop system and Kalman filter Markov parameters remains about the same after the order is 30. For this system, therefore, 30 is the minimum order of the ARX model to reduce the infinite-order input-output representation shown in (6.14) to the finite-order ARX model shown in (6.15).

Moreover, at the order of 30 the error of the Kalman filter Markov parameters (about 13.82%) is much more than the error of the system Markov parameter (about 1.97%). The reason is that finite number of data points will not provide the complete accurate information of the noise statistics. When the number of data points is increased to 10000, the error is reduced to about 8.47%. It is found that with more data points, the more accurate the identified result. However, more data points require more computational time and more memory in the least-squares algorithm. The number of the Markov parameters for the state-space realization is found to provide an insignificant effect on the accuracy as long as it is more than the order of the ARX model. Figure 6.2 shows the comparison of the (1,1) element of the true and reconstructed Markov parameters.

The identified model is further transformed to the form of (6.42) where

$$A_{21} = \begin{bmatrix} 3302.5 & 24.350 & -33432 & 4299.4 & -1381.4 \\ 79.675 & 3349.1 & -6222.8 & -213.38 & 199.24 \\ -9.7047 & -0.0083 & 28.8832 & -15.281 & -9.5271 \\ 0.0655 & 0.1014 & -13.276 & 115.49 & 10.600 \\ -0.7503 & 0.0669 & 89.081 & -81.865 & -6.8598 \end{bmatrix},$$

$$A_{22} = \begin{bmatrix} -0.1745 & -0.0446 & 6.5531 & -181.65 & 66.626 \\ -1.0665 & -0.2778 & 169.48 & 140.58 & 53.252 \\ -0.0003 & -0.0016 & 1.7437 & 0.7986 & 0.0718 \\ -0.0002 & 0.0016 & 0.3609 & -0.5261 & -0.5126 \\ 0.0030 & -0.0056 & -2.0860 & -2.7257 & -0.1475 \end{bmatrix},$$

$$B_2 = \begin{bmatrix} 39.009 & 38.642 & 37.481 & 37.995 & 37.181 \\ -0.8611 & 91.163 & 55.068 & -56.150 & -89.335 \\ 0.2208 & -0.1535 & 0.0761 & 0.0751 & -0.1504 \\ -0.0060 & 0.1241 & -0.1927 & 0.1994 & -0.1234 \\ -0.2664 & -0.0880 & 0.2153 & 0.2312 & -0.0978 \end{bmatrix}.$$

As compared with the true model shown in (5.1), the identified model is fairly accurate. The eigenvalues of the identified model are listed in Table 6.1. As shown, the three unstable modes are fairly accurate, but the two oscillatory modes are not. The reason is that the three positive real poles are the dominant poles but the two complex poles are not.

Experiments are also performed for closed-loop identification with the same controller. The number of data points is 6000 which is the maximum limitation of the memory. The constructed Markov parameters are reconstructed after the closed-loop identification. Figure 6.3 shows the (1,1) element of the reconstructed Markov parameters. As shown, the curves are similar to those shown in Figure 6.2. The identified model is further transformed to the form of (5.1) where

$$A_{21} = \begin{bmatrix} 3766.6 & 70.325 & -75117 & 1924.3 & -27136 \\ -117.61 & 3923.4 & -1077.2 & -29312 & -3690.0 \\ -3.2179 & 5.7394 & 136.28 & -22.192 & 64.823 \\ -0.9768 & 12.871 & -11.237 & -88.650 & 7.9619 \\ 9.8282 & 0.1383 & 51.006 & -7.8415 & -66.471 \end{bmatrix},$$

$$A_{22} = \begin{bmatrix} -0.3676 & 0.2909 & -149.27 & -6.4746 & -82.993 \\ 1.8430 & 1.5609 & 176.17 & 9.8511 & 66.933 \\ -0.0034 & 0.0042 & -5.1229 & -0.4162 & -0.5839 \\ 0.0075 & 0.0084 & 0.0980 & -0.1222 & -0.0837 \\ -0.0317 & 0.0083 & -3.7143 & 0.1091 & -2.1338 \end{bmatrix},$$

$$B_2 = \begin{bmatrix} 65.913 & 47.979 & 61.979 & 71.050 & 56.621 \\ 0.0156 & 106.93 & 69.132 & -73.363 & -116.88 \\ 0.2137 & 0.0706 & 0.2005 & -0.0056 & -0.2459 \\ 0.0074 & 0.4595 & 0.0311 & -0.0398 & -0.5191 \\ -0.2163 & 0.0157 & 0.4482 & 0.4931 & 0.0137 \end{bmatrix}.$$

The eigenvalues of the identified model are also listed in Table 6.1. There are also three unstable modes and two flexible modes.

Table 6.1 Comparison of eigenvalues of analytical and identified model.

analytical model	simulation	testing
±58.78	58.25, -58.82	62.78, -62.07
±57.81	57.71, -57.58	61.23, -60.20
±9.78	10.60, -11.64	9.84, -16.05
±7.97i	-0.95± 6.66i	1.06± 8.02i
±0.96i	1.99± 6.40i	0.21± 1.64i

Because the true Markov parameters are not available from experiments, step responses are compared in order to evaluate the identified model. Five step commands in pitch, yaw, x, y, and z are performed individually. Figures 6.4 to 6.7 show the corresponding five step responses from test data, simulation via the analytical model, simulation via the identified model only, and simulation via the identified model with the identified Kalman filter, respectively. As shown, the step responses simulated via the identified model only are closer to the test data than the step responses via the analytical model. The actual cause for the errors of the analytical model has not yet been confirmed. However, some inaccuracies are discovered in the hardware which may contribute to the errors. It is found that the core suspends slightly above its designed operation point due to the position of the sensor frame. The fields and the field gradients, used in the system analysis, have been calculated on the designed operating point. This may cause noticeable error in more unstable modes such as the pitch. Another hardware inaccuracy was found in the position of the coils in the array. The radius of the coil array is about 1/8" larger than the actual design. This would result in lower field intensity at the operating point. The eddy currents in the base plate used to support the sensor devices are another potential source of error in the results. Some study of the effect of the eddy current induced on the base plate directly under each coil suggested negligible effect on the system. However, more investigation should be done on the eddy currents generated by combination of coils, and their effects on the system response. The

ignorance of the dynamics of the power amplifiers is another source of the error. The bandwidth of the power amplifiers is about 200Hz which is lower than the sampling rate of 400Hz. Through the closed-loop identification, the system model can be updated to take into account the sources of the error. The step responses simulated via the identified model with the identified Kalman filter are much closer to the test data than the step responses via the identified model only. The reason is that the error of the state will not propagate with the correction of the measurement through the Kalman filter. Figure 6.8 shows the comparison of the dominant axis for each step response to provide better observation.

6.11 Concluding Remarks

Closed-loop identification has been derived for a stochastic system operating under closed-loop conditions. A matrix is also derived to transform the identified state-space model from any arbitrary coordinates to the physical coordinates so that the identified system parameters can be compared to analytical parameters. The main contribution is that a *recursive* form for computing the open-loop system and Kalman filter Markov parameters from the closed-loop system Markov parameters, the closed-loop Kalman filter Markov parameters, and the known controller Markov parameters is derived for *stochastic* systems with *closed-loop random* excitation. This method also provides physical interpretation of mapping from closed-loop input/output data to the open-loop state-space model and the explicit meaning of the ARX parameters. It can also estimate the Kalman filter gain directly without estimating noise covariances.

The effect of the adjustable parameters, in the closed-loop identification, to the identification accuracy is also investigated through numerical simulations. To evaluate the accuracy of the identification, the error between true and reconstructed Markov parameters based on 2-norm is defined. To obtain a sufficiently accurate result, the minimum order of

the ARX model for the LAMSTF system is found to be 30. Therefore, this order will be used in the iterative LQG control design presented in the next chapter. The number of Markov parameters for the realization algorithm is found to provide insignificant effect on the accuracy as long as the number is more than the order of the ARX model. Furthermore, more data points provide more accurate result but need more computational time in solving least squares. To completely simulate a gaussian white noise, the number of data points has to be infinity, which is not available in a realistic situation. When a finite set of data is used, the identified Kalman filter satisfies an optimality condition indicating that it is the best filter that can be obtained with the data length available. Therefore, the identified Kalman filter gain is found to be quite different from the steady state Kalman filter gain form Riccati equation, as one compares those Markov parameters. In the experiments, as one compares the closed-loop step responses, it is found that the behavior of the identified model is closer to the test data than that of the analytical model. It is also found that the simulated step response from the identified model with the identified Kalman filter almost coincide with the test data. It can be concluded that the identified model and Kalman filter can be used for control design.

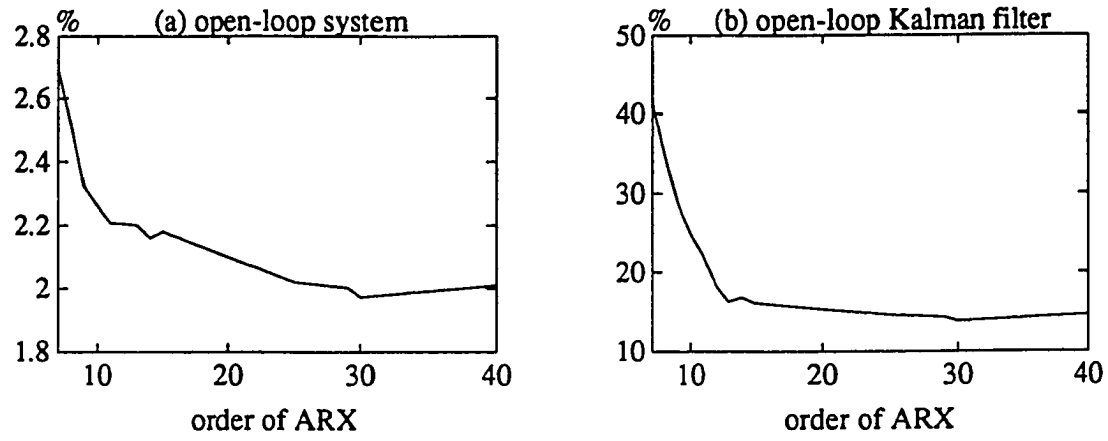

Figure 6.1 Error percentage between true and reconstructed Markov parameters.

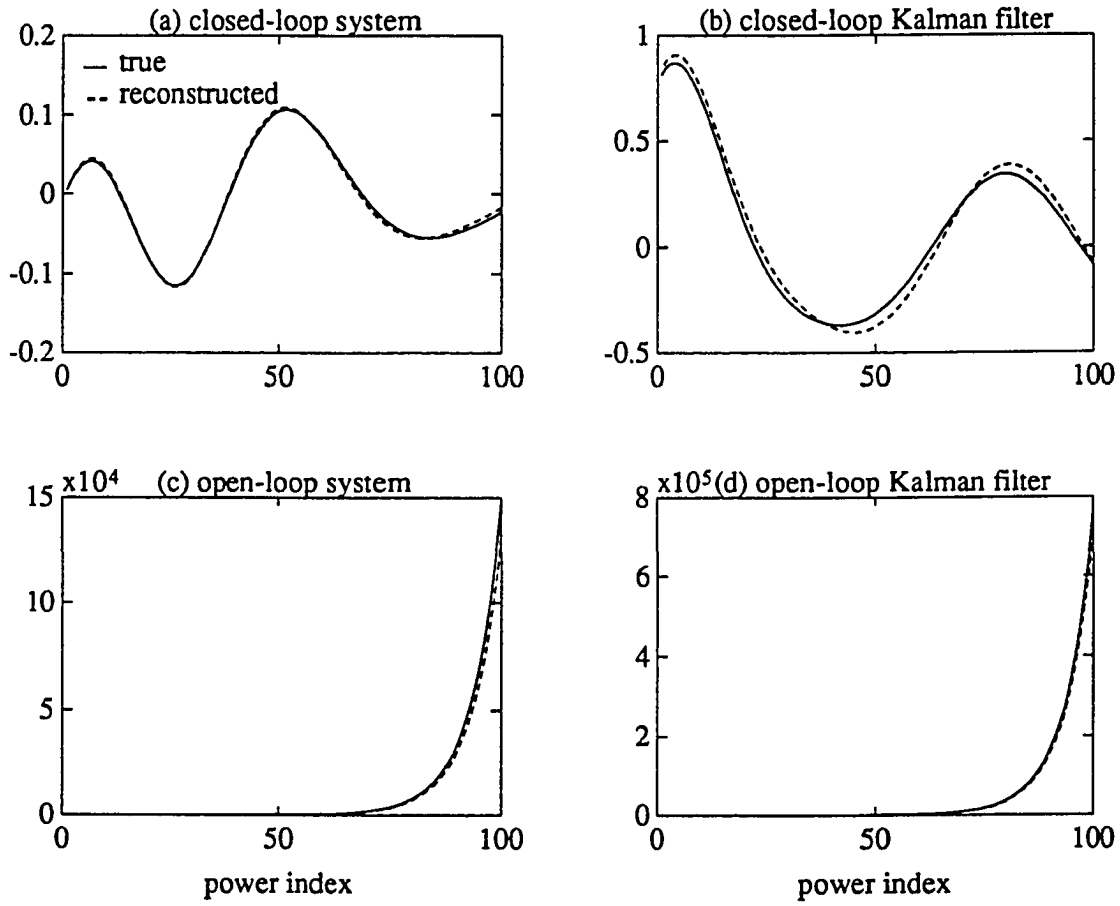

Figure 6.2 Comparison of (1,1) element of true and reconstructed Markov parameters.

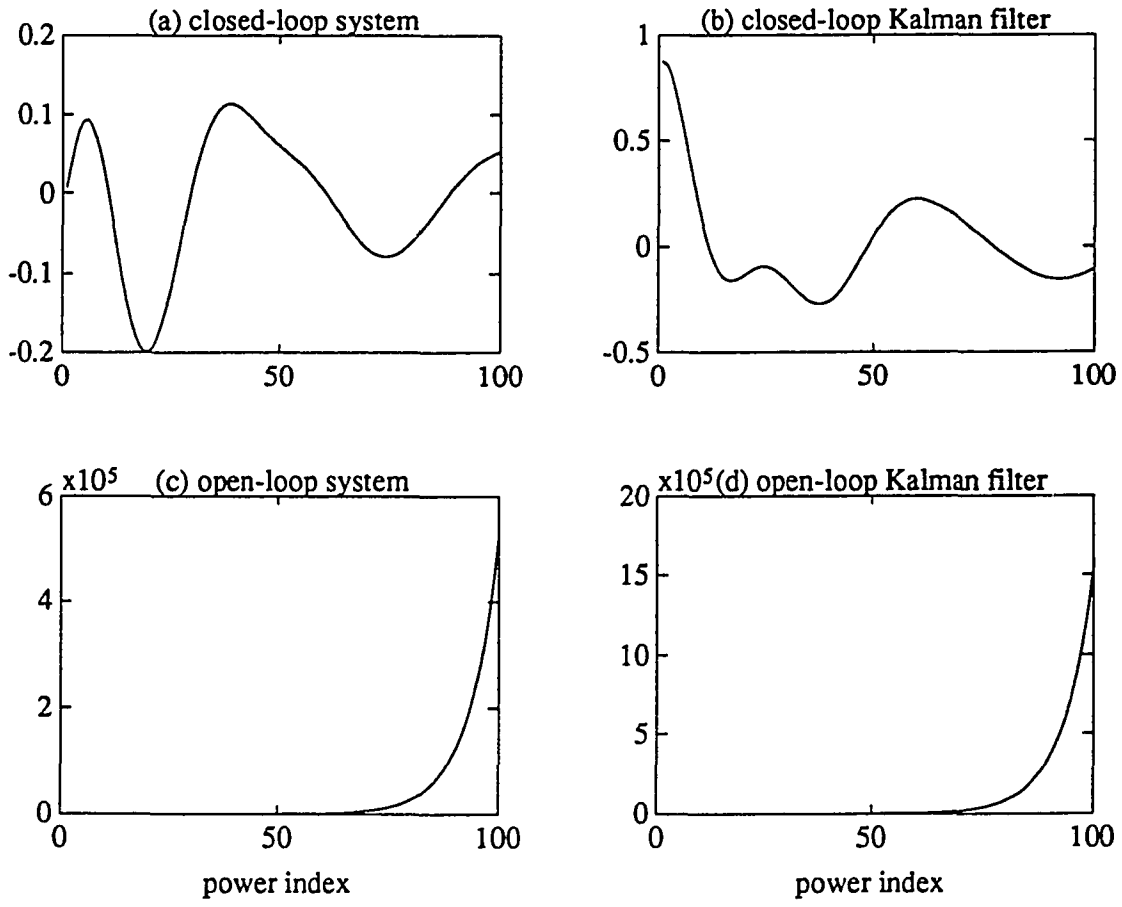

Figure 6.3 Markov parameters from testing.

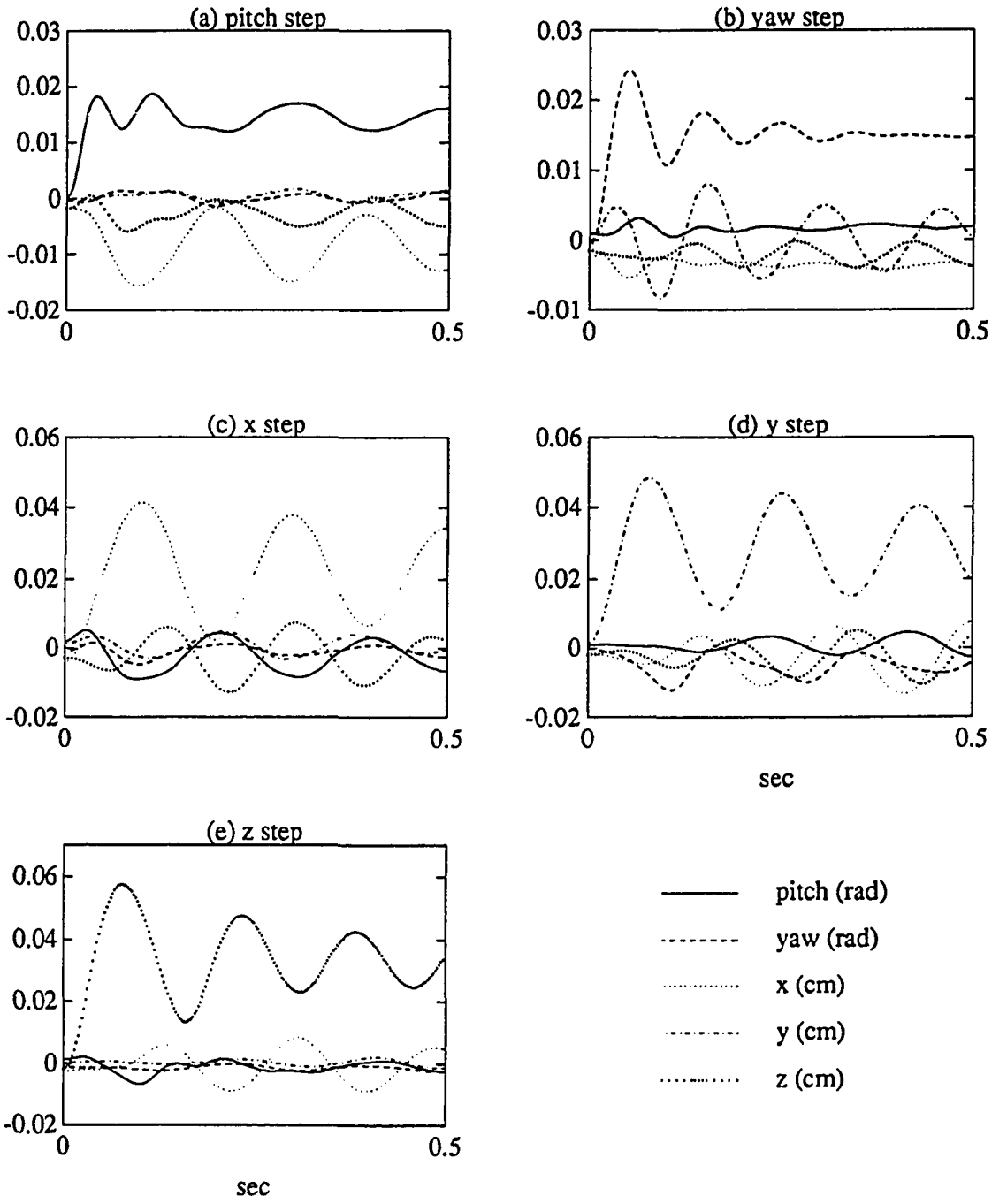

Figure 6.4 Step responses from testing.

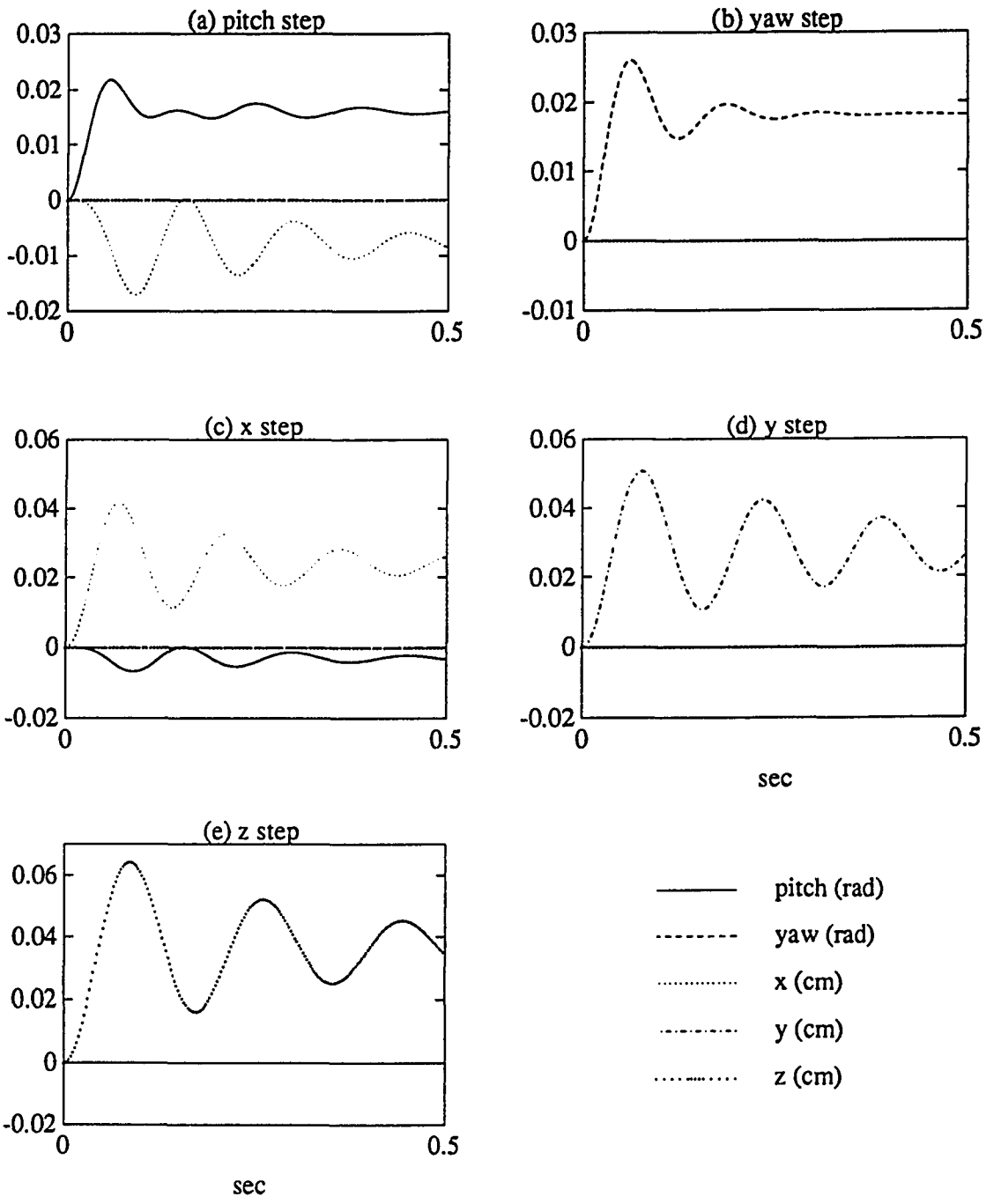

Figure 6.5 Step responses from the analytical model.

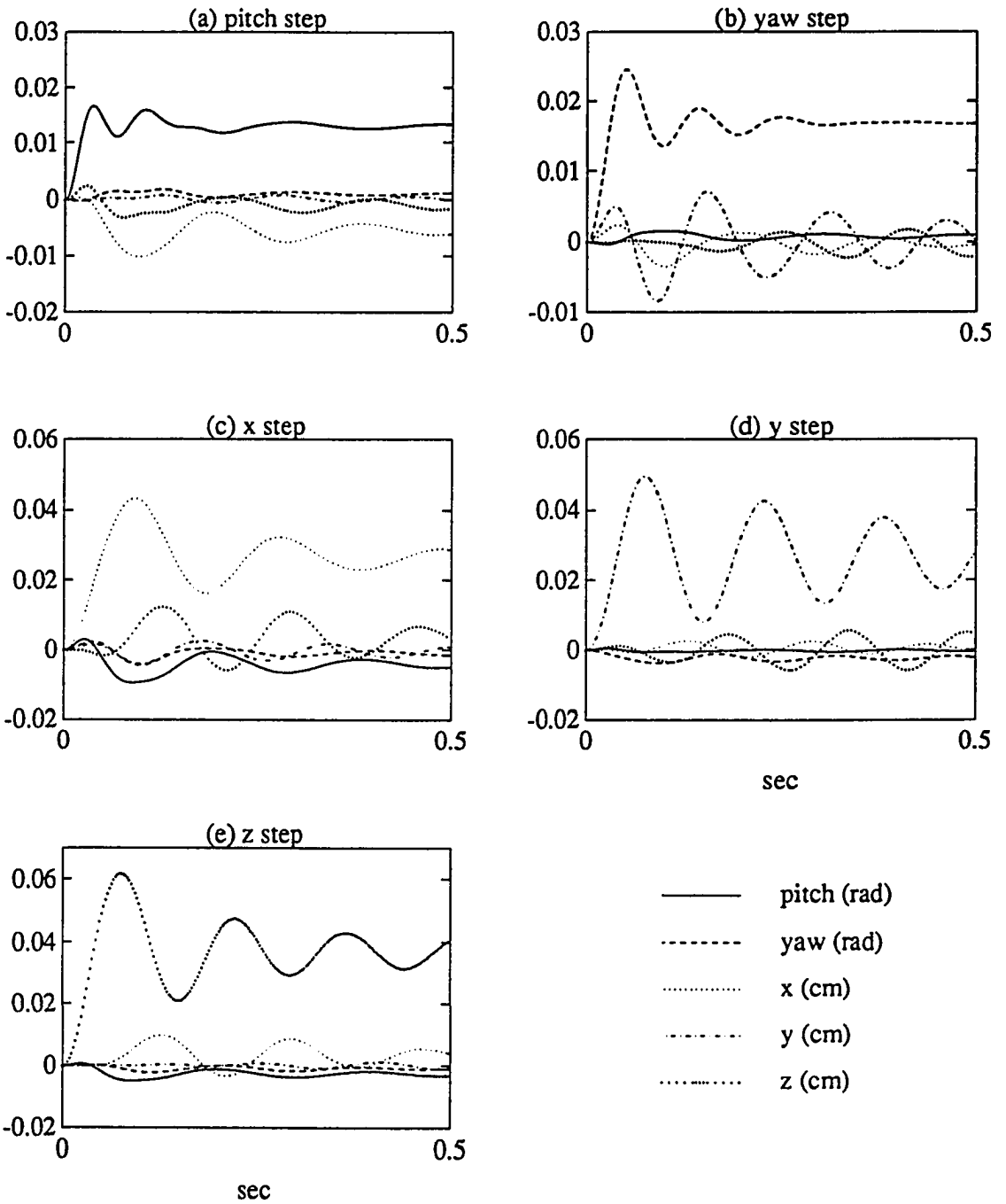

Figure 6.6 Step responses from the identified model without Kalman filter.

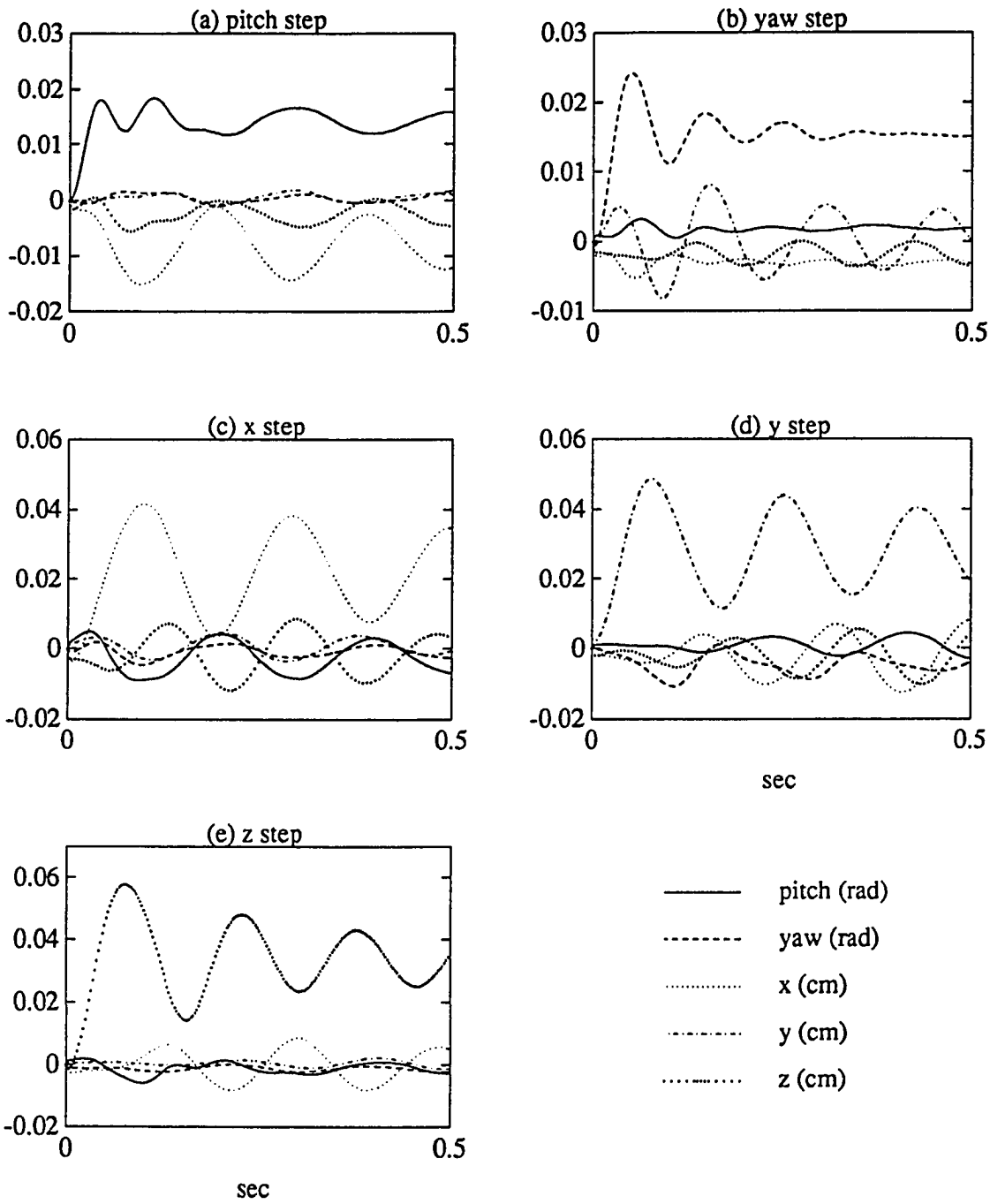

Figure 6.7 Step responses from the identified model with Kalman filter.

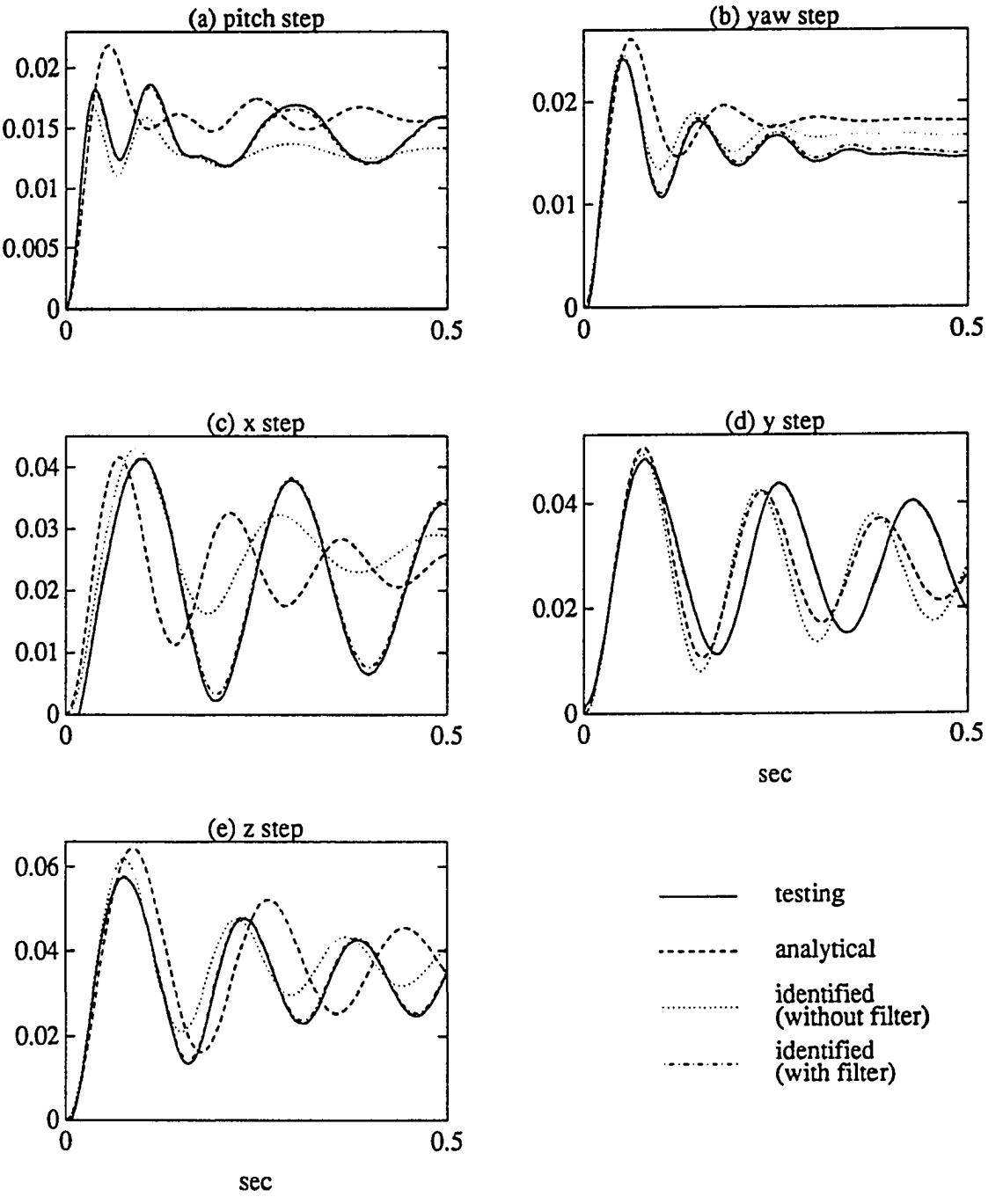

Figure 6.8 Comparison of step responses in dominant axis.

Chapter 7

ITERATIVE LQG CONTROLLER DESIGN

7.1 Introduction

This chapter demonstrates the iterative LQG control design through the closed-loop identification presented in the previous chapter. Numerical simulations and experiments for the NASA LAMSTF are provided to illustrate and validate this controller design. An algorithm for computing covariance matrices of system process and measurement noise is derived. The computed covariance matrices can be used to simulate noise in numerical simulations. The computation of reference input for a desired step output is also derived.

Existing LQG controllers are designed by solving two separate, but dual problems: the state-feedback design and state-estimation design. The performance of the controllers relies on an accurate open-loop model for the state feedback and an accurate estimate of the measurement and process noise statistics for the state estimation. It is very difficult to obtain an accurate model through analysis for some systems and an accurate estimate of the noise statistics through testing for most systems. Especially for the NASA LAMSTF, it is very difficult to accurately model the magnetic field and its gradients. Furthermore, the

noise statistics may be related to the controller if part of the measurement and process noise are generated by the sensor and actuator amplifiers, respectively. Therefore, an iterative control design is required.

Reference 17 proposed an iterative design which combined a closed-loop identification and a output covariance control. However, there are two shortcomings. First, the closed-loop identification is based on system pulse response. General speaking, random excitation provides better result of identification than pulse input because part of noise from random excitation response can be removed through least squares method. Second, Kalman filter can not be identified because the derivation is based on deterministic. Since no Kalman filter can be used to estimate state, the control becomes output feedback. Usually, state feedback provides better performance than output feedback. In our approach, the closed-loop identification is based on random excitation data and the Kalman filter gain can also identified. Thus, the closed-loop identification and the state feedback can be combined to achieve the iterative control design. Another approach can be found in Reference 46. Basically, a frequency-response identification and a robust control design were used to set up the iterative design. However, the example was a stable system. Our approach can apply to an unstable system.

The iterative LQG control design consists of closed-loop identification and state feedback redesign cycles. The closed-loop identification method can simultaneously identify the open-loop model and the Kalman gain when a system is under closed-loop operation with a known dynamic controller. Then the identified open-loop model is used for the state-feedback design. The state feedback and the identified Kalman filter are used to form an updated LQG controller for next closed-loop identification. The process continues until the updated LQG controller converges. The state feedback tends to reject the process noise and the Kalman filter tends to filter out the measurement noise. Therefore, the closed-loop identification can improve the LQG design and an updated LQG

controller can enhance the closed-loop identification in the next cycle. This is the reason for the convergence of the controller.

7.2 Procedure

This section summarizes the steps of the iterative LQG controller design through closed-loop identification. Existing LQG controllers are designed by solving two separate, but dual problems: the state-feedback design and Kalman filter design. Here, the Kalman gain can be simultaneously obtained with the open-loop state-space model through the closed-loop identification. Only the state-feedback design based on the identified open-loop model needs to be solved. The performance index for the state feedback is defined as

$$P.I.=\sum_{k=1}^{\infty} y_k^T Q y_k + u_k^T R u_k = \sum_{k=1}^{\infty} x_k^T C^T Q C x_k + u_k^T R u_k \tag{7.1}$$

where weighting matrices Q and R are design parameters. The iterative LQG controller design is summarized as follows:

1. Use the a priori open-loop model and arbitrary covariance matrices of the measurement and process noise to design the state feedback and Kalman filter. Then, calculate the controller Markov parameters. The weighting matrices Q and R for the state feedback chosen here will remain the same in the following iterations.
2. Apply random excitation input to the closed-loop system and record the closed-loop input/output data.
3. Perform closed-loop identification presented in Section 6.7 to obtain the identified system matrices $\hat{A}$, $\hat{B}$, and $\hat{C}$ and Kalman filter $\hat{K}$.
4. Obtain the state feedback gain F by solving the corresponding Riccati equation based on the identified open-loop model.
5. Form the updated LQG controller in (6.5) and (6.6) by using $A_d = \hat{A} - \hat{B}F - \hat{A}\hat{K}\hat{C}$, $B_d = \hat{A}\hat{K}$, $C_d = -F$, and $D_d = 0$.

6. Calculate the updated controller Markov parameters and check the convergence of the controller by

$$\delta = \sum_{k=0}^{n} \left\| Y_d(k)_{updated} - Y_d(k)_{previous} \right\|_2 . \tag{7.2}$$

If δ is greater than a desired value, go back to step 2, otherwise stop.

7.3 Covariances of State and Output

To simulate the noise in computer programming, an algorithm for computing covariance matrices of process and measurement noises is derived. Recall an open-loop system without any noise

$$x_{k+1} = Ax_k + Bu_k \tag{7.3}$$

$$y_k = Cx_k, \tag{7.4}$$

and a controller

$$p_{k+1} = A_d p_k + B_d y_k \tag{7.5}$$

$$u_k = C_d p_k + D_d y_k + r_k . \tag{7.6}$$

Combining (7.3) to (7.5) yields the augmented closed-loop system dynamics

$$\eta_{k+1} = A_c \eta_k + B_c r_k \tag{7.7}$$

$$y_k = C_c \eta_k, \tag{7.8}$$

where

$$\eta_k = \begin{bmatrix} x_k \\ p_k \end{bmatrix}, A_c = \begin{bmatrix} A + BD_d C & BC_d \\ B_d C & A_d \end{bmatrix}, B_c = \begin{bmatrix} B \\ 0 \end{bmatrix}, \text{ and } C_c = [C \quad 0]. \tag{7.9}$$

From (7.7), one can derive

$$E[\eta_k \eta_k^T] = E[\eta_{k+1} \eta_{k+1}^T] = E[(A_c \eta_k + B_c r_k)(A_c \eta_k + B_c r_k)^T]. \tag{7.10}$$

Since the reference input r_k can be chosen to be uncorrelated with the augmented state η_k,

$E[\eta_k r_k^T] = E[r_k \eta_k^T] = 0$. Let $\Xi = E[\eta_k \eta_k^T]$, $\Re = E[r_k r_k^T]$, one can have

$$\Xi = A_c \Xi A_c^T + B_c \Re B_c^T. \tag{7.11}$$

This equation is well known as discrete Lyapunov equation[25]. Since $\Xi = E[\eta_k \eta_k^T]$ $= E\begin{bmatrix} x_k x_k^T & x_k p_k^T \\ p_k x_k^T & p_k p_k^T \end{bmatrix}$, one can partition this matrix to get the covariance of the open-loop state $X = E[x_k x_k^T]$. From (7.8), one can obtain the covariance of the output $Y = E[y_k y_k^T]$ $C_c \Re C_c^T$.

In the numerical simulations presented in Section 7.5, it is assumed that the covariances of the process and measurement noises are proportional to the covariances of the open-loop state and the output, respectively. According to this and an open-loop system with noise

$$x_{k+1} = Ax_k + Bu_k + w_k \tag{7.12}$$

$$y_k = Cx_k + v_k, \tag{7.13}$$

the covariances of the process and measurement noises, W and V, are $k_p X$ and $k_m Y$, respectively (k_p and k_m are given constants).

7.4 Reference Input for Desired Step Output

From (7.7) and (7.8), one can derive the relation between the steady-state output y_{ss} and the step reference r_d

$$y_{ss} = C_c (I - A_c)^{-1} B_c r_d, \tag{7.14}$$

by using the fact $\eta_{k+1} = \eta_k$, $k \to \infty$. If the number of the outputs equals the number of the inputs, one can have

$$r_d = (C_c (I - A_c)^{-1} B_c)^{-1} y_{ss} \tag{7.15}$$

This equation can be used to calculate the reference input for the desired output.

7.5 Numerical Simulations and Experimental Results

To validate the proposed iterative LQG control design, numerical simulations and experiments for the NASA LAMSTF system will be performed. For both numerical simulation and experiment, the sampling rate is 250 Hz rather than 400 Hz to allow more time for the digital computer in the experiments to process data. The performance index used for the state feedback is

$$P.I.=\sum_{k=1}^{\infty} y_k^T Q y_k + u_k^T R u_k \tag{7.16}$$

where $Q=(C_1^{-1})^T diag[1.e3 \quad 1.e3 \quad 2.e8 \quad 2.e8 \quad 2.e8]C_1^{-1}$ and $R=I_{5\times5}$. The step command for all simulations and experiments is 0.02 radian for pitch and yaw, and 0.02 cm for x, y, and z. The corresponding reference input varies with the applied controller, and can be computed by using (7.15).

In the numerical simulation, the analytical model is used as the true model. The ratios of the process and measurement noise to the corresponding signal are 2% and 1%, respectively. The corresponding covariance matrices of the process noise and measurement noise will vary with the applied controller. They can be computed from the corresponding Lyapunov equation presented in Section 7.3. According to the computed covariance, the random number generator in MATLAB is used to simulate the process and measurement noises. To simulate modeling error and unknown noise statistics, the initial LQG controller is designed by using a guessed model of which each parameter is 5% greater than the corresponding parameter of the analytical model and guessed covariance matrices of noise $W=10I_{10\times10}$ and $V=I_{5\times5}$. The simulated step response with this initial controller for the pitch, yaw, x, y, and z is shown in Figure 7.1. It is clear that the result is very poor.

Usually, one can use overshoot and settling time to evaluate the performance of a closed-loop system. The overshoot is defined as the deference of the maximum output and the steady-state output. The settling time is defined as the time when the difference of the output and the steady-state output begins to fall into certain bound, usually, 2% of the steady-state output. Large overshoot is not desired. the settling time indicates how quick response of the system is. The initial controller makes the closed-loop system provide large overshoot in pitch and long settling time in y and z. After performing the first iteration of the proposed iterative LQG controller design, the step response shown in Figure 7.2 is greatly improved. However, the overshoot of the x step is still large and its settling time is still long. The performance is further improved slightly in the following iterations. The controller after the third iteration provides settling time of about 0.05 sec for pitch and yaw, and about 0.08 sec for x, y, and z. The overshoot for any step is very little. Figure 7.3 shows how the controller converges by comparing the (1,1) element of the controller Markov parameters.

For a noise free system, the exact open-loop model can be obtained after the first closed-loop identification and no further iteration is required. In this case, the identified Kalman gain becomes the dead-beat observer gain.[9,10] For a noise corrupted system, iterations are required to update the open-loop model and the Kalman gain until the iterative LQG controller converges. Although the numerical simulations show that the iterative controller can converge quickly, the required conditions to guarantee the convergence need further study.

In the experiments, the analytical model and guessed covariance matrices of noise $W = 10I_{10\times10}$ and $V = I_{5\times5}$. are used to design the initial LQG controller. The experimental step responses for the initial controller and the first two iterations are compared in Figure 7.4 to demonstrate how the step response is improved with iteration. In each iteration, the open-loop system model and the Kalman filter gain are update through the closed-loop

identification from experimental data. From Figure 7.4, in the initial controller the steady-state error for pitch and yaw is very large. The steady-state error means the difference between the actual output and the desired output. In the first iteration steady-state error is greatly improved. However, the overshoot of x and y steps is still large. In the second iteration the overshoot is improved. The results show that the proposed iterative LQG controller design is very effective for controlling this highly unstable magnetic suspension system.

7.6 Concluding Remarks

In contrast to most existing LQG control design of which the great majority solve two separate, but dual problems: the state-feedback and state-estimation design, an iterative LQG control design is proposed. The closed-loop identification developed in the previous chapter is used to update the open-loop state-space model and the Kalman filter gain simultaneously from the closed-loop input/output test data. For a noise free system, the exact open-loop model can be obtained after the first closed-loop identification and the identified Kalman gain becomes the dead-beat observer gain. For a noise corrupted system, iterations are required to update the open-loop model and the Kalman filter gain from testing until the iterative LQG controller converges. In each iteration, since the Kalman filter gain is identified directly from test data, the LQG design is simplified to be state-feedback design. Because the identified Kalman filter is directly used as state estimation, the knowledge of the noise statistics is no longer required. Furthermore, since the open-loop system is identified under the closed-loop operation with the previous controller, the interdependence between the modeling and the controller is automatically taken into account. For the NASA LAMSTF system, both numerical simulations and test data show that the controller converges after two iterations and is very effective when the system is subjected to modeling error and unknown noise statistics.

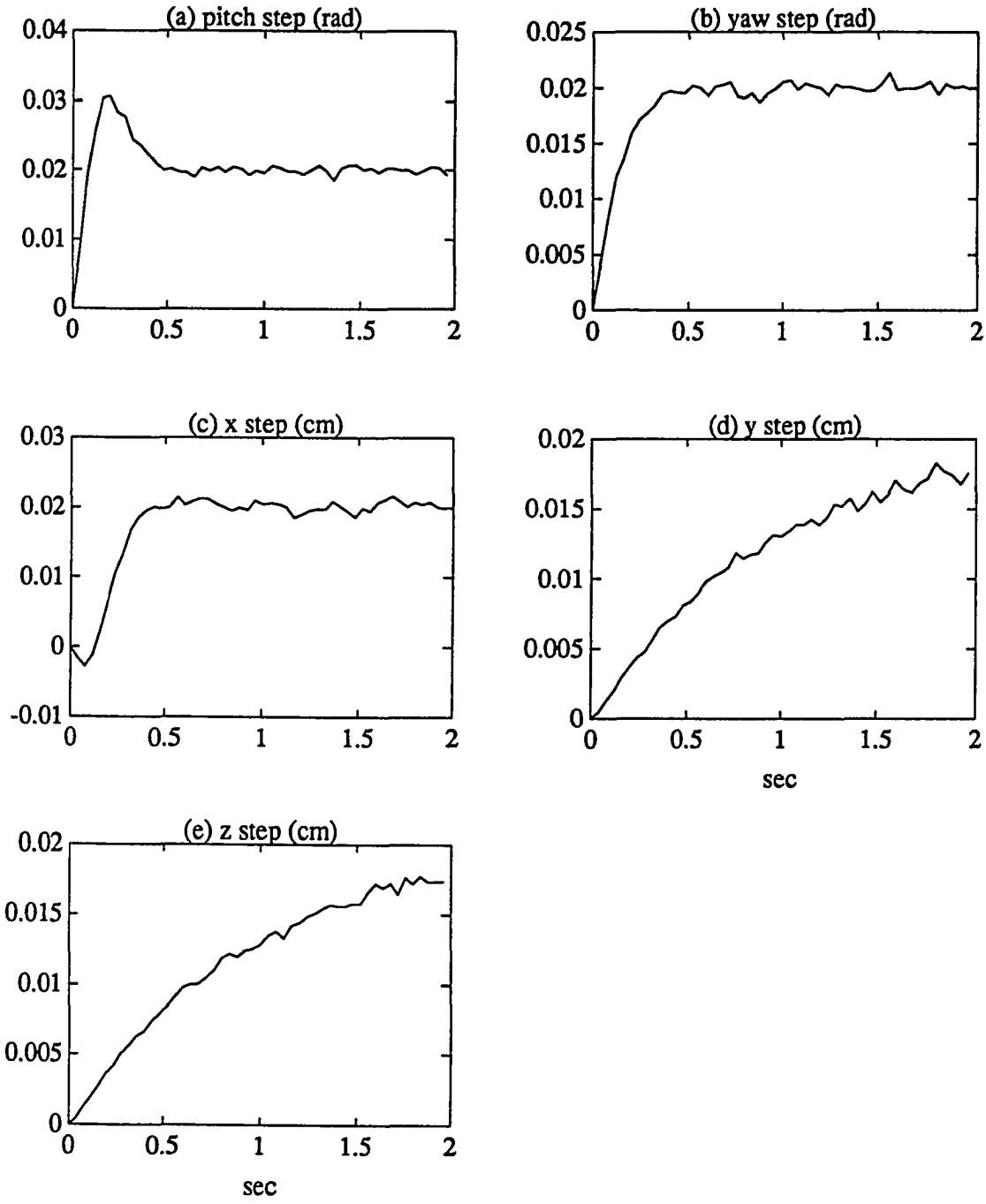

Figure 7.1 Simulated step responses with the initial LQG controller.

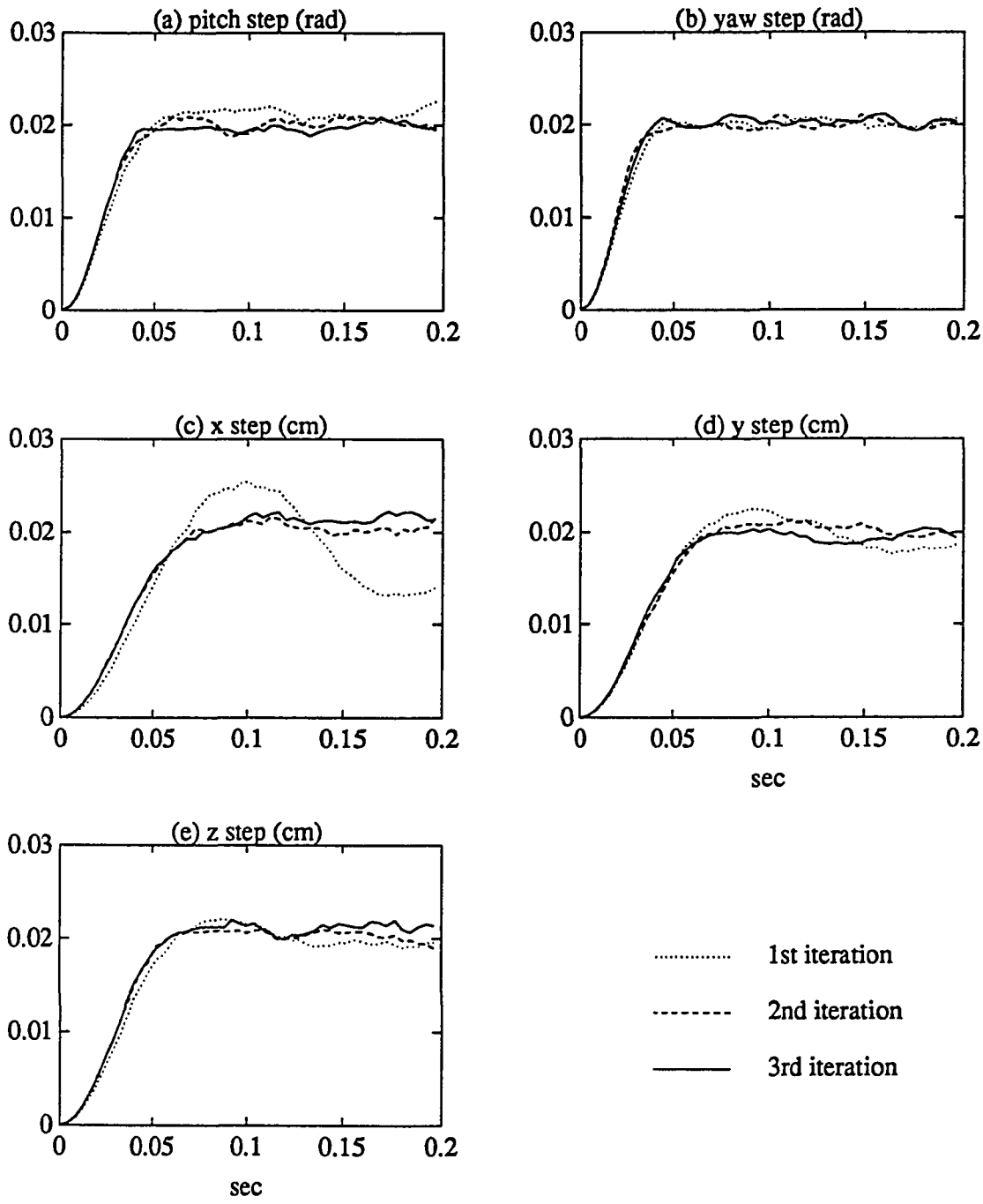

Figure 7.2 Comparison of simulated step responses with the iterative LQG controller.

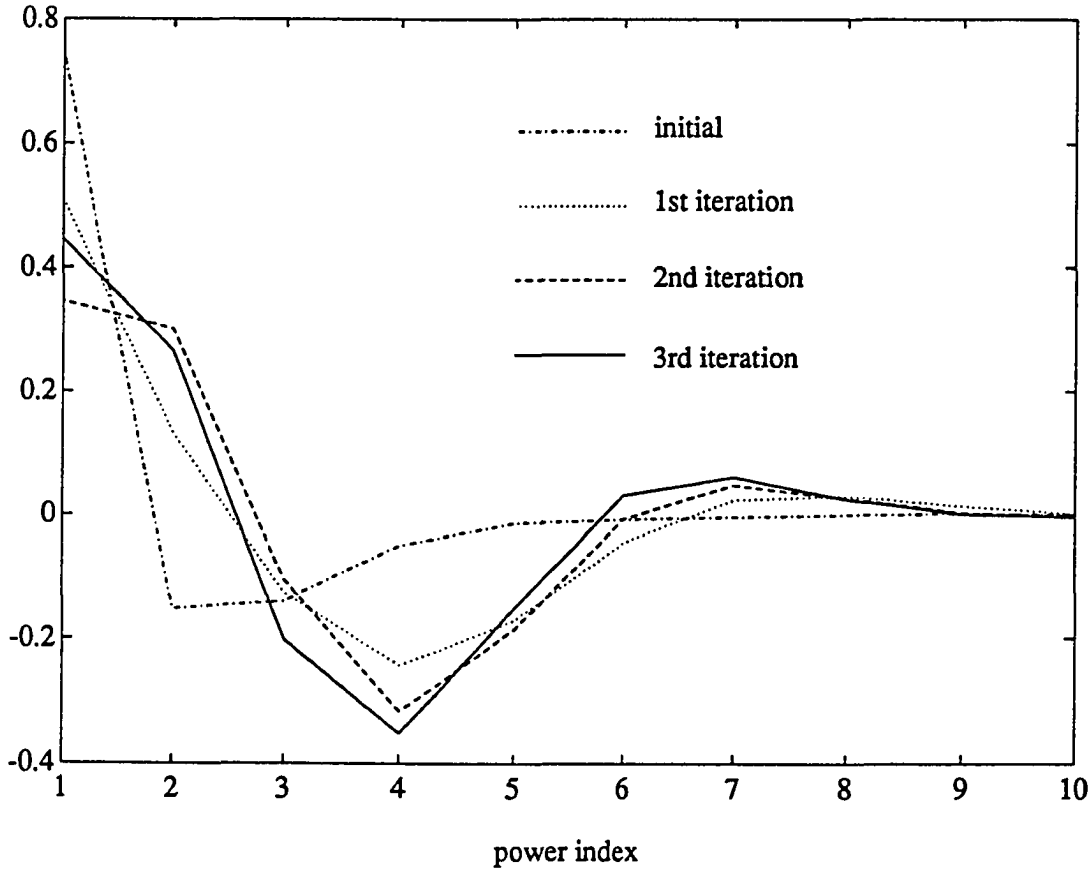

Figure 7.3 Comparison of the (1,1) element of the controller Markov parameters.

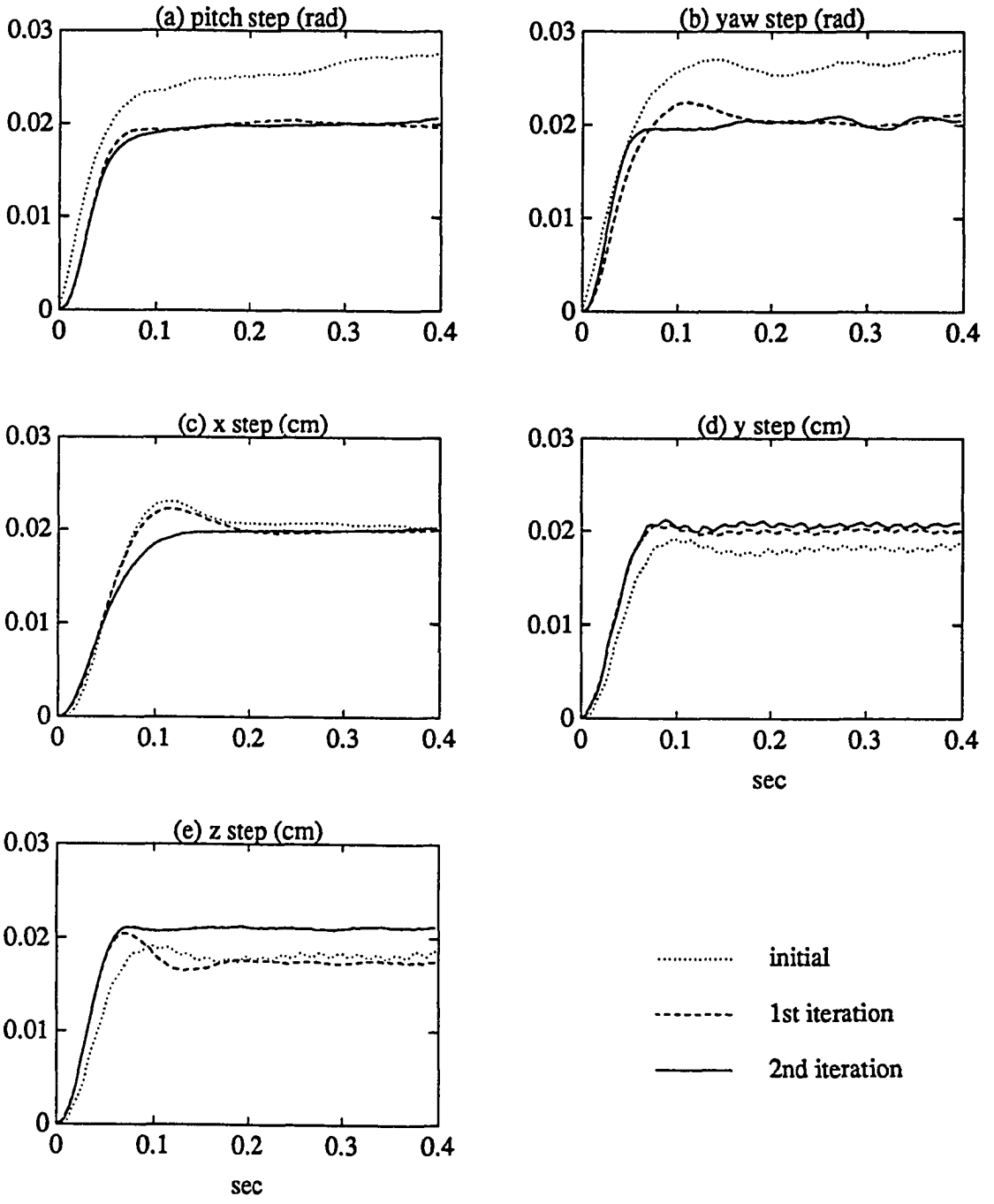

Figure 7.4 Comparison of testing step responses with the iterative LQG controller.

Chapter 8

CONCLUSIONS

8.1 Contributions

Two novel approaches have been proposed for the LQG controller design for linear stochastic systems. If the system model is known with collocated rate sensors and actuators, one may use the explicit LQG controller design approach. If the system model is unknown, the iterative LQG controller design approach is presented.

Existing LQG controllers are designed by solving two separate, but dual problems: the state-feedback design and state-estimation design. The performance of the controller relies on an accurate model and proper design parameters. Thus, there are several shortcomings. First, numerically solving Riccati equations needs a lot of computational time when the system is very large. Second, choosing the weighting matrices for the state-feedback design may need try-and-error approach. Third, detecting the covariance matrices for the state-estimation design is usually difficult. Fourth, the system model from system analysis usually contains some errors. Fifth, the statistics of the noise may vary with the controller.

For a large flexible structure, the order of the system is usually large. An explicit LQG controller design based on a modal space for a large flexible structures with collocated rate sensors and actuators is developed. The explicit solutions to the corresponding Riccati equations for state feedback and state estimation are found so that numerical calculation for solving the Riccati equations is no longer required. Furthermore, the number of the design parameter for either state feedback or state estimation equals the number of the controlled modes. Thus, the design parameters can be easily adjusted to enhance the damping of each controlled mode. Both numerical simulations and experiments for the NASA SCOLE configuration show that the explicit LQG controller can suppress vibration effectively for large flexible structures.

For some systems, it is difficult to accurately model the system through system analysis. System identification is required to update the system model. Most of existing identification methods apply for a system under open-loop operation. For an unstable system, feedback control is required to ensure overall system stability. Thus, closed-loop identification is may become important for identifying an open-loop model from closed-loop input/output data. Several methods has been proposed for closed-loop identification. However, the derivation is based on deterministic systems. Kalman filter gain, therefore, can not be identified. In this dissertation a closed-loop identification, which can simultaneously identify an open-loop model and Kalman filter by using closed-loop input/output data from closed-loop random excitation, is derived. The identified Kalman filter can be directly used for state estimation. Hence, the noise statistics is no longer required to be detected and state-estimation design is no longer needed. Both numerical simulations and experiments for the NASA LAMSTF system show that the identified model with the identified Kalman filter can accurately predict the behavior of the closed-loop system.

To take into account the effect of a controller on noise statistics, an iterative LQG controller design is proposed. The design consists of the closed-loop identification and

state-feedback redesign cycles. In each cycle, the closed-loop identification is used to identify the open-loop model and Kalman filter. The identified Kalman filter is used for state estimation so that LQG controller design reduced to state-feedback design only. Then the identified model is used to redesign the state feedback. The state feedback and the identified Kalman filter form an updated LQG controller for next cycle. This iterative process continues until the updated controller converges. The state feedback tends to reject the process noise and the Kalman filter tends to filter out the measurement noise. Therefore, the closed-loop identification can improve the LQG design and an updated LQG controller can enhance the closed-loop identification in the next cycle. Since the updated model is identified under the previous controller, the effect of the controller on noise statistics is automatically taken into account. Both numerical simulations and experiments for the NASA LAMSTF system show that the controller converges quickly and is very effective for a system subjected to modeling error and unknown noise statistics.

8.2 Further Extension of the Research

The theories derived in this dissertation can be applied or extended further to other areas. For the explicit LQG controller design, one can easily apply it to more complex flexible structures, for example, the Middeck Active Control Experiment (MACE)[47] and Controls-Structures Interaction (CSI) Phase-Zero Evolutionary Model Test Bed[48] at NASA Langley Research Center. For both examples, collocated rate sensors and actuators are available. In both systems there are more than 20 modes below 10 Hz. As compared with the NASA SCOLE which includes 5 modes below 10 Hz, they are much larger and more complex.

For the iterative controller design, one nature extension is to apply it for closed-loop frequency response data. For some dynamic systems, analysis and design in the frequency

domain is preferred. Another natural extension is to apply it for adaptive control design[43] or robust control design[49]. In general, a physical system is time-varying or nonlinear. Adaptive control and robust control are commonly used for such a system. For adaptive control, the system model has to be updated every certain period during control. To accomplish on-line identification in short period, one may use the closed-loop identification to develop an algorithm for parallel processing. Unlike adaptive control, robust control utilizes system uncertainty to design controller to avoid on-line system identification. The system uncertainty means the bound of the system matrices within the operation range of the system. For robust control, one may extend the closed-loop identification to identify system uncertainty when the system is under closed-loop operation. With the identification of the system uncertainty model, an effective robust controller design can be naturally accomplished.

REFERENCES

1. Kalman, R. E., "A New Approach to Linear Filtering and Prediction Problem," *Trans. ASME Journal of Basic Engineering*, Vol. 82D, March, 1960, pp. 35-45.

2. Kalman, R. E., and Bucy, R. S., "New Results in Linear Filtering and Prediction Theory," *Trans. ASME J. Basic Eng.*, Vol. 83, 1961, pp. 95-108.

3. Balakrishnan, A. V., "Compensator Design for Stability Enhancement with Collocated Controllers," *IEEE Transactions on Automatic Control*, Vol. 36, No. 9, Sept. 1991, pp. 994-1007.

4. Joshi, S. M., and Maghami, P. G., "Robust Dissipative Compensators for Flexible Spacecraft Control," *IEEE Trans. on Aerospace & Electronic system.*, Vol. 28, No. 3, July 1992, pp. 769-774.

5. Juang, J. N., and Phan, M., "Robust Controller Designs for Second-Order Dynamic Systems: A Virtual Passive Approach," Paper No. 91-0983, *Proceedings of the AIAA Structural Dynamics & Materials Conference*, Baltimore, MD, April 8-10, 1991, and NASA TM-102666, May 1990.

6. Ljung, L., *System Identification —Theory for the User*, Prentice-Hall, Inc., Englewood Cliffs, New Jersey, 1987.

7. Juang, J.-N., *Applied System Identification*, PTR Prentice-Hall, Inc., Englewood Cliffs, New Jersey, 1994.

8. Chen, C. W., Huang, J. K., Phan, M., and Juang, J. N., "Integrated System Identification and Modal State Estimation for Control of Flexible Space Structures," *Journal of Guidance, Control and Dynamics*, Vol. 15, No.1, Jan.-Feb. 1992, pp. 88-95.

9. Phan, M., Horta, L. G., Juang, J.-N., and Longman, R. W., "Linear System Identification via an Asymptotically Stable Observer", *Proceedings of the AIAA Guidance, Navigation and Control Conference*, New Orleans, LA, Aug. 12-14, 1991, pp. 1180-1194., also to appear in *Journal of Optimization and Application.*

10. Juang, J.-N., Phan, M., Horta, L. G., and Longman, R. W., "Identification of Observer/Kalman Filter Markov Parameters: Theory and Experiments," *AIAA Journal of Guidance, Control and Dynamics*, Vol. 16, No. 2, March/April 1993, pp. 320-329.

11. Huang, J.-K, Juang, J.-N. and Chen, C. W., "Single-Mode Projection Filters for Modal Parameter Identification for Flexible Structures," *AIAA Journal of Guidance, Control and Dynamics*, Vol. 12, No. 4, July/August 1989, pp. 568-576.

12. Chen, C. W., Huang, J. K., and Juang, J.-N., "Identification of Linear Stochastic Systems Through Projection Filters", *Proceedings of the AIAA Structures, Structural Dynamics and Materials Conference,* Dallas, Texas, April 13-15, 1992, pp. 2330-2340.

13. Chen, C.-W., Juang, J.-N., and Huang, J.-K., "Adaptive Linear System Identification and State Estimation," in *Control and Dynamic Systems: Advances in Theory and Applications, Vol. 57, Multidisciplinary Engineering Systems: Design and Optimization Techniques and Their Application,* edited by C. T. Leondes, Academic Press, Inc., 1993, pp. 331-368.

14. Juang, J. -N., and Phan, M., "Identification of System, Observer, and Controller from Closed-Loop Experimental Data," *Proc. of the AIAA Guidance, Navigation, and Control Conference*, 1992.

15. Hu, A., and Martin, D., "System Identification of Unstable Manipulators Using ERA Methods", *Proc. of the AIAA Guidance, Navigation, and Control Conference*, 1993, pp. 1264-1270.

16. Phan, M., Juang, J.-N., Horta, L. G., and Longman, R. W., "System Identification from Closed-Loop Data with Known Output Feedback Dynamics," NASA TM-107604, April, 1992, also to appear in *AIAA Journal of Guidance, Control and Dynamics.*

17. Liu, K., and Skelton, R. E., "Closed-Loop Identification and Iterative Controller Design," *Proceedings of the IEEE Decision and Control,* Honolulu, Hawaii, Dec., 1990, pp. 482-487.

18. Schrama, R. J. P., "Control-oriented Approximate Closed-loop Identification via fractional representations," *Proc. of American Control Conf.*, Boston, MA, 1991, pp. 719-720.

19. Skelton, R. E., "Model error concepts in control design," *Int. Journal of Control,* Vol. 49, No. 5, 1989, pp. 1725-1753.

20. Skelton, R. E., "On the Structure of Modeling Errors and the Inseparability of the modeling and control problems," *Proc. IFAC Workshop*, Boston, MA, 1985, pp. 13-20.

21. Dolye, J. C. and Stein, G., "Robustness with Observers," *IEEE Trans. on Automatic Control,* Vol. 24, 1979, pp. 607-611.

22. Dolye, J. C. and Stein, G., "Multivariable Feedback Design: Concepts for a classical/Modern synthesis," *IEEE Trans. on Automatic Control,* Vol. 26, 1981, pp. 4-16.

23. Stein, G., and Athans, M., "The LQG/LQR Procedure for Multivariable Feedback Control Design," *IEEE Trans. on Automatic Control,* Vol. 32, 1987, pp. 105-114.

24. Kwakernaak, H., and Sivan, R., *Linear Optimal Control Systems,* John Wiley & Son, Inc., New York, 1972.

25. Franklin, G. F., Powell, J. D., and Workman, M. L., *Digital Control of Dynamic Systems,* Addison-Wesley Publishing Company, Reading, Massachusetts, 1990.

26. Gelb, A., *Applied Optimal Estimation*, The M.I.T. Press, Cambridge, Massachusetts, and London, England, 1974.

27. Balakrishnan, A. V., and Taylor, L. W. "A Mathematical Problem and Spacecraft Control Laboratory Experiment (SCOLE) Used to Evaluate Control Laws for Flexible Spacecraft... NASA/IEEE Design Challenge," *Proc. of the NASA SCOLE Workshop*, Hampton, Virginia, Dec. 6-7, 1984.

28. Shen, J. Y., Huang, J.-K., and Taylor, Jr., L. W., "Likelihood Estimation for Distributed Parameter Models of Large Beam-Like Structures," *Journal of Sound and Vibration*, Vol. 155, No. 3, 1992, pp. 467-480.

29. Shen, J. Y., Huang, J.-K. and Taylor, Jr., L. W., "Timoshenko Beam Modeling for Parameter Estimation of NASA Mini-Mast Truss," *ASME Journal of Vibration and Acoustics*, Vol. 115, No. 1, January 1993, pp. 19-24.

30. Lee, K. Y., and Hossain S. A., "Distributed Systems Approach to the Identification of Flexible Structures," *AIAA Journal of Guidance, Control and Dynamics*, Vol. 10, No. 6, Nov./Dec. 1987, pp. 540-548.

31. Taylor, Jr., L. W., "PDEMOD: Computer Software for Distributed Parameter Estimation for Flexible Spacecraft Applied to NASA Mini-Mast Truss Experiment," *2nd USAF/NASA Workshop on System Identification and Health Monitoring of Precision Space Structures*, Pasadena, CA, 1990.

32. Pestel, E. C., and Leckie, F. A., *Matrix Methods in Elastomechanics*, McGraw-Hill Book Company, Inc., New York, 1963.

33. Horner, G. C., "The Riccati Transfer Matrix Method," Ph.D. Dissertation, University of Virginia, Charlottesville, VA, May 1975.

34. Uhrig, R., "The Transfer Matrix Method Seen as One Method of Structural Analysis among Others," *Journal of Sound and Vibration*, Vol. 4, No. 2, Sept. 1966, pp. 136-148.

35. Balakrishnan, A. V., "Explicit LQG Optimized control Laws for Flexible Structures/Collocated Rate Sensor," *Proc. of the AIAA Structures, Structural Dynamics and Materials Conf.*, La Jolla, CA, April 19-22, 1993, pp. 3108-3114.

36. Balakrishnan, A. V., "An Explicit Solution to the Optimal LQG Problem for Flexible Structures with Collocated Rate Sensors," *Proceedings of the 5th NASA/DOD CSI Technology Conference*, Lake Tahoe, Nevada, March 3-5, 1992.

37. Groom, N. J., Britcher, C. P., "A Description of a Laboratory Model Magnetic Suspension Test Fixture with Large Angular Capability," *Proc. of the First IEEE Conference on Control Applications*, Vol. 1, pp. 454, 1992.

38. Ghofrani, M., "Approaches to Control of the Large Angle Magnetic Suspension Test Fixture," Master thesis, Old Dominion University, Norfolk, Virginia, Dec., 1992 and NASA CR-191890, Dec., 1992.

39. Groom, N. J., "Analytical Model of a Five Degree of Freedom Magnetic Suspension Systems using Electromagnets Mounted in a Planar Array," NASA CP-10066, Vol. 1, pp. 355-376, March 1991.

40. Groom, N. J., and Britcher, C. P., "Open-Loop Characteristics of Magnetic Suspension Systems Using Electromagnets Mounted in a Planar Array," NASA-TP 3229, November 1992.

41. Chen, C.-W., Huang, J.-K., "Estimation of Steady-State Optimal Filter Gain from Non-Optimal Kalman Filter Residuals," to appear in *ASME Journal of Dynamic Systems, Measurement, and Control.*

42. Haykin, S., *Adaptive Filter Theory*, Second edition, Prentice-Hall, Englewood Cliffs, New Jersey 07632, 1991.

43. Goodwin, G. C., and Sin K. S., *Adaptive Filtering, Prediction and Control*, Prentice-Hall, Englewood Cliffs, New Jersey 07632, 1984.

44. Chen, C. T., *Linear System Theory and Design*, Second Edition, Chapter 6, CBS College Publishing, New York, 1984.

45. Juang, J.-N., and Pappa, R. S., "An Eigensystem Realization Algorithm for Modal Parameter Identification and Model Reduction," *Journal of Guidance, Control, and Dynamics*, Vol. 8, Sept.-Oct. 1985, pp. 620-627.

46. Schrama, R. J. P., "Accurate Identification for Control: The Necessity of an Iterative Scheme," *IEEE Trans. on Automatic Control*, Vol. 37, No. 7, pp. 991-994, July, 1992.

47. Miller, D., Saarmaa, E., and Jacques, R., "Preliminary Structural Control Results from the Middeck Active Control Experiment (MACE)," *Proc. of the AIAA Dynamics Specialist Conference*, Dallas, Texas, pp. 566-576, April, 1992.

48. Belvin, W. K., Horta, L. G., and Elliott, K. E. "The LaRC CSI Phase-0 Evolutionary Model Test Bed: Design and Experimental Results," *Proc. of the 4th Annual NASA-DOD Conference on CSI Technology*, Orlando, Florida, November 5-7, 1990.

49. Maciejowski, J. M., *Multivariable Feedback Design*, Addison-Wesley Publishing Company, Reading, Massachusetts, 1989.